A Practitioner's Guide to Kolmogorov–Arnold Networks

Amir Noorizadegan[1,*], Sifan Wang[2], and Leevan Ling[1]

[1]Department of Mathematics, Hong Kong Baptist University, Hong Kong SAR, China
[2]Institution for Foundations of Data Science, Yale University, New Haven, CT 06520, USA

*Corresponding author: `amir_noori@hkbu.edu.hk`

December 11, 2025

Abstract

The so-called Kolmogorov–Arnold Networks (KANs), whose design is merely *inspired*, rather than dictated, by the Kolmogorov superposition theorem, have emerged as a promising alternative to traditional Multilayer Perceptrons (MLPs). This review provides a systematic and comprehensive overview of the rapidly expanding KAN landscape. By collecting and categorizing a large set of open-source implementations, we map the vibrant ecosystem supporting modern KAN development. We organize the review around four core themes:

(i) presenting a precise **history of Kolmogorov's superposition theory toward neural-network formulations** (Sec. 3);

(ii) establishing the **formal equivalence between KANs and MLPs** (Secs. 4,5);

(iii) analyzing the **critical role of basis functions** (Sec. 6); and

(iv) organizing recent advancements in **accuracy**, **efficiency**, **regularization**, and **convergence** (Secs. 7, 8, 9, 10).

Finally, we provide a practical **Choose-Your-KAN guide** (Sec. 11) to assist practitioners in selecting appropriate architectures, and we close by identifying **current research gaps and future directions** (Sec. 12). The associated GitHub repository (`https://github.com/AmirNoori68/kan-review`) complements this paper and serves as a structured reference for ongoing KAN research.

1 Introduction

Multilayer perceptrons are universal approximators and remain a standard building block for regression, function approximation, and pattern recognition across scientific and engineering applications. A major extension of this paradigm is the physics-informed neural network (PINN) framework of Raissi et al. [1], which has rapidly grown and enabled large-scale studies.

Since then, numerous advances have broadened the scope of MLP-based PINNs. Fractional operators were addressed by fPINNs [2], while uncertainty quantification for forward and inverse problems was introduced in [3]. Extensions such as VPINNs [4], XPINNs for domain decomposition [5], and multi-fidelity PINNs [6] improved accuracy and scalability. The framework also inspired convergence analyses [7], NTK-based diagnostics [8], and practical toolkits like DeepXDE [9]. More recent contributions include multi-stage training with near machine-precision accuracy [10], adaptive residual weighting [11], and distributed solvers for extreme-scale PDEs [12–15]. Collectively, these developments establish MLP–PINNs as a mature reference standard in scientific machine learning, many of which, as we show in Section 5, have directly inspired KAN development.

Despite their flexibility, MLPs face well-documented limitations. Fixed activation functions restrict adaptability [16]. Network behavior can be difficult to interpret [17] and to attribute causally [18]. Achieving high accuracy often entails large parameter counts, which can hinder efficient updates [19, 20]. Generalization robustness can degrade in challenging regimes [21, 261]. Optimization itself can be fragile or stiff, depending

on the task and scaling [22]. MLPs also exhibit spectral bias: a tendency to learn low frequencies faster than high frequencies [23, 24]. The effect slows convergence and reduces accuracy for oscillatory or sharp-gradient solutions [25]. This motivates investigations into alternatives with explicit basis control.

KANs [26] replace fixed activations with *learnable univariate functions* on edges, motivated by the Kolmogorov representation theorem. The original model uses B-spline bases [26], but the framework is modular: Chebyshev polynomials, Gaussian kernels, and other basis families can be substituted as needed. This flexibility is central, since the chosen basis controls smoothness, locality, and spectral behavior, directly affecting expressivity and interpretability. The combination of adaptive basis learning and interchangeable basis families is therefore a core advantage of KANs. KANs also include a growing set of architectural variants, optimization strategies, and theoretical developments.

A number of recent surveys have appeared on KANs, each highlighting different facets of this emerging architecture. Notable contributions include those by Andrade et al. [27], Basina et al. [28], Beatrize et al. [29], Faroughi et al. [30], Kilani et al. [31], Hou et al. [32], Dutta et al. [33], Essahraui et al. [34], and Somvanshi et al. [35], which together provide valuable entry points into the literature. Our review builds on these efforts by seeking to offer a more systematic and comprehensive perspective: rather than cataloguing studies in isolation, we integrate theoretical, architectural, optimization, and application viewpoints into a structured roadmap. By combining comparative analysis, methodological insights, and practical guidance, our goal is to provide a resource that complements existing surveys and serves readers aiming to both understand and apply KANs. Table 1 presents a structured roadmap of the paper's sections and themes.

Table 1: Paper roadmap (clickable links to sections).

When it comes to deciding whether MLP-PINNs or KAN-PIKANs are the better choice, the comparison is far from straightforward, with studies that emphasize fairness often reaching divergent or contradictory conclusions [36][1], [37, 38]. A key reason is that KANs are not a monolithic architecture; their performance is critically influenced by the choice of basis function. For example, a comprehensive comparison by Farea and Celebi [39][2] found that the optimal basis (e.g., B-spline, Fourier, Gaussian) varies significantly with the PDE being solved, making a simple "KAN vs. MLP" verdict insufficient.

Despite these complexities, Table 2 summarizes reported outcomes across regression, function approximation, and PDE-solving tasks. The entries reflect prevailing tendencies in the literature rather than definitive results for every case. A consistent pattern is that KANs—particularly when equipped with specialized basis functions—tend to match or outperform vanilla MLPs and PINNs in terms of accuracy and convergence speed.

---

[1] https://github.com/yu-rp/KANbeFair
[2] https://github.com/afrah/pinn_learnable_activation

Table 2: Representative performance trends comparing KAN-based models with MLPs. Results are aggregated from the literature and reflect general outcomes. *"Slower training" refers to higher per-iteration cost, though total wall-clock time can be different due to fewer epochs to convergence. All rows compare KANs to plain MLP/PINN baselines without advanced features.*

Ref.	Accuracy	Convergence/Time(per-iter.)	Basis Functions
Regression & Symbolic Representation			
[40]	BSRBF-KAN $\approx$ MLP	Faster convergence; slower training	B-spline + Gaussian
[41]	MLP-KAN > MLP	–	B-Spline
[42]	KAN < MLP	Slower training; less generalizable	B-Spline
[43]	DE-KAN > MLP	Faster convergence	B-spline
[44]	KAN-ODE > MLP-ODEs	Faster convergence; slower training	Gaussian
[45]	KAN-Therm > MLP	Faster convergence	B-spline
Function Approximation			
[26]	KAN $\geq$ MLP	Faster convergence; slower training	B-spline
[36]	KAN > MLP (symbolic)	Slower training	B-spline
[46]	KAN $\approx$ MLP	Faster training	Free-knot B-spline
[47]	KAN $\geq$ MLP (noisy)	Faster convergence; slower training	B-spline
[47]	KAN $\leq$ MLP (non-smooth)	Faster convergence; slower training	B-spline
[48]	PowerMLP > MLP	Slower training	Power-ReLU
[49]	SincKAN > MLP	Faster convergence; slower training	Sinc
[50]	ChebyKAN > MLP	Faster convergence; slower training	Shifted Chebyshev
[51]	QKAN > MLP	Faster convergence	Quantum variational
PDE Solving			
[52]	KKAN > PINN	Faster convergence	Various Basis
[53]	PIKAN $\gg$ PINN	Faster convergence; slower training	B-spline
[26]	PIKAN $\gg$ PINN	slower training (10×)	B-spline
[54]	DeepOKAN > DeepONet	Faster convergence; slower training	Gaussian
[55]	PIKAN > PINN	Faster convergence	B-Spline
[56]	KAN-MHA > PINN	Faster convergence; comparable time	B-spline + Attention
[57]	Res-KAN $\gg$ PINN	Faster convergence; better generalization	B-Spline + Residual
[58]	HPKM-PINN > PINN	Faster convergence; slower training	B-spline
[59]	PI-KAN $\gg$ PINN	Faster convergence	Spline
[60]	DPINN $\gg$ PINN	Faster convergence; slower training	B-spline + Fourier
[61]	PIKAN $\approx$ PINN	Slower training	B-spline
[37]	PIKAN $\approx$ PINN	slower training	Various Basis
[62]	EPi-cKAN $\gg$ PINN	Slower training; better generalization	Chebyshev
[63]	Scaled-cPIKAN $\gg$ PINN	Faster convergence	Chebyshev
[64]	PIKAN $\gg$ PINN	Faster convergence	Chebyshev
[65]	tanh-PIKAN > PINN	–	Chebyshev
[66]	AL-PKAN > PINN	Faster convergence	B-spline decoder
[67]	KANtrol > PINN	Slower training	B-spline
[68]	PIKAN > PINN	Slower training	B-spline
[69]	KINN > PINNs	Slower training	B-spline
[70]	PIKAN $\approx$ PINNs	Slower training	B-spline
[71]	PIKAN $\approx$ PINNs	Slower training	Fourier-based
[72]	MR-PIKAN $\gg$ PINN	Slower training	Chebyshev
[39]	PIKAN $\gtrless$ PINN (Prob-dep)	Faster convergence; slower training	Various Bases
[73]	J-PIKAN $\gg$ PINN	Faster convergence; slower training	Jacobi (orthogonal)
[74]	Legend-KINN > MLP, KAN	Faster convergence; slower training	Legendre

Table 3: GitHub repositories related to KANs for regression, function approximation, or PDEs.

Repository	Description	Ref.
.../pykan	Official PyKAN for "KAN" and "KAN 2.0".	[113]
.../Anant-Net	High-dimensional PDE solver with tensor sweeps.	[256]
.../RGA-KANs	Deep cPIKANs with variance-preserving initialization.	[262]
.../pinn_learnable_activation	Compares various KAN bases vs. MLP on PDEs	[39]
.../torchkan	Simplified PyTorch KAN with variants	[114]
.../awesome-kan	Curated list of KAN resources, projects, and papers.	[75]
.../Deep-KAN	Spline-KAN examples and a PyPI package.	[115]
.../RBF-KAN	RBF-KAN examples	[116]
.../KANbeFair	Fair benchmarking of KANs vs MLPs.	[36]
.../efficient-kan	Efficient PyTorch implementation of KAN.	[117]
.../spikans	Separable PIKAN (SPIKAN).	[190]
.../jaxKAN	JAX-based KAN package with grid extension support.	[259]
.../fast-kan	FastKAN using RBFs.	[119]
.../faster-kan	Using SWitch Activation Function	[120]
.../LKAN	Implementations of KAN variations.	[121]
.../neuromancer− >fbkans	Parametric constrained optimization.	[122]
.../relu_kan	Minimal ReLU-KAN.	[123]
.../MatrixKAN	Matrix-parallelized KAN.	[124]
.../PowerMLP	MLP-type network with KAN-level expressiveness.	[48]
.../FourierKAN	Fourier-based KAN layer.	[125]
.../FusedFourierKAN	Optimized FourierKAN with fused GPU kernels	[126]
.../fKAN	Fractional KAN using Jacobi functions.	[127]
.../rKAN	Rational KAN (Padé/Jacobi rational designs).	[128]
.../CVKAN	Complex-valued KANs.	[129]
.../SincKAN	Sinc-based KAN with PINN applications.	[49]
.../ChebyKAN	Chebyshev polynomial-based KAN variant.	[130]
.../OrthogPolyKANs	Orthogonal polynomial-based KAN implementations.	[131]
.../kaf_act	PyTorch activation combining with RFF.	[132]
.../KAF	Kolmogorov-Arnold Fourier Networks.	[71]
.../HRKAN	Higher-order ReLU-KANs.	[133]
.../KINN	PIKAN for solid mechanics PDEs.	[69]
.../KAN_PointNet_CFD	Jacobi-based network for CFD predictions.	[70]
.../FKAN-GCF	FourierKAN-GCF for graph filtering.	[134]
.../KKANs_PIML	Kurkova-KANs combining MLP with basis functions.	[52]
.../MLP-KAN	MLP-augmented KAN activations.	[135]
.../kat	Kolmogorov-Arnold Transformer.	[136]
.../FAN	Fourier Analysis Network (FAN).	[137]
.../Basis_Functions	Polynomial bases for KANs (comparative study).	[138]
.../Wav-KAN	Wav-KAN: wavelet-based KANs.	[139]
.../qkan	Quantum variational activations and pruning tools.	[51]
.../KAN-Converge	Additive & hybrid KANs for convergence-rate experiments	[140]
.../BSRBF_KAN	Combines B-splines and radial basis functions.	[40]
.../Bayesian-HR-KAN	Introduces Bayesian higher-order ReLU-KANs.	[141]
.../Legend-KINN	Legendre polynomial–based KAN.	[74]
.../DeepOKAN	Deep Operator Network based on KAN.	[54]
.../LeanKAN	A memory-efficient Kolmogorov–Arnold Network.	[142]
.../KANQAS_code	KANQAS: KAN for Quantum Architecture Search.	[257]
.../pkan	Probabilistic KAN via divisive data re-sorting.	[258]
.../pihnn	Holomorphic KAN/PIHNN framework for solving PDEs.	[255]

.../lmkan	Lookup-based KAN for fast high-dim mappings.	[268]
.../KAN_Initialization_Schemes	Initialization schemes for spline-based KANs.	[276]
.../mlp-kan	KAN vs. MLP for PDEs in DeepONet/GNS frameworks.	[267]

KANs are rapidly expanding on open-access platforms, with diverse implementations and variants shared by the community. Curated repositories such as [75][3] track the latest developments across different fields, making this growth more accessible to readers. Table 3 summarizes representative GitHub repositories that illustrate this fast-growing ecosystem in regression, function approximation, and PDE solving. These resources are also referenced in footnotes throughout this study when further details of specific methods are discussed.

Organization (Table 1). Section 2 reviews MLP basics. Section 3 introduces Kolmogorov Superposition Theory and its refinements. Section 4 connects KANs to classical neural networks. Section 6 surveys basis families and computational trade-offs. Section 7 covers accuracy-improvement strategies, and Section 8 addresses efficiency via parallelism/GPU/JAX and matrix optimization. Section 9 treats sparsity, regularization, and Bayesian variants, while Section 10 discusses scaling laws and convergence. Section 11 presents the practical "Choose–Your–KAN" guide. We conclude with final remarks in Section 13.

2 MLP Basics

MLPs are feedforward neural networks composed of stacked affine layers followed by element-wise nonlinear activations. Given an input vector $\mathbf{x} \in [0,1]^n$, an MLP with L layers produces an output $\hat{f}(\mathbf{x}; \boldsymbol{\theta}) \in \mathbb{R}$ via

$$\mathbf{z}^{(0)} = \mathbf{x}, \tag{1}$$

$$\mathbf{z}^{(\ell)} = \sigma\left(\mathbf{W}^{(\ell)}\mathbf{z}^{(\ell-1)} + \mathbf{b}^{(\ell)}\right), \quad \ell = 1, \ldots, L-1, \tag{2}$$

$$\hat{f}(\mathbf{x}; \boldsymbol{\theta}) = \mathbf{W}^{(L)}\mathbf{z}^{(L-1)} + \mathbf{b}^{(L)}, \tag{3}$$

where

- $\sigma(\cdot)$ is a nonlinear activation function (e.g., ReLU, tanh),

- $\mathbf{W}^{(\ell)} \in \mathbb{R}^{n_\ell \times n_{\ell-1}}$ and $\mathbf{b}^{(\ell)} \in \mathbb{R}^{n_\ell}$ are the weights and biases at layer ℓ,

- $\mathbf{z}^{(\ell)} \in \mathbb{R}^{n_\ell}$ is the hidden representation at layer ℓ,

- n_ℓ is the width (number of neurons) of layer ℓ,

- $\boldsymbol{\theta} = \{\mathbf{W}^{(\ell)}, \mathbf{b}^{(\ell)}\}_{\ell=1}^L$ collects all trainable parameters.

3 KST Toward Neural Networks

Superpositions and Hilbert's Question. A *superposition* is any function obtained by repeatedly composing simpler functions. Lorentz [82] illustrates this idea with the example

$$F(x, y, z) = f\big(g(x, y),\, h(x,\, k(y, z))\big),$$

for scalar inputs $x, y, z \in \mathbb{R}$, showing how a multivariate mapping can be built from bivariate ones. Even the elementary identity

$$x_1 + \cdots + x_n = x_1 + \big(x_2 + \cdots + (x_{n-1} + x_n) \cdots\big)$$

is a superposition of binary additions.

---

[3] https://github.com/mintisan/awesome-kan

Hilbert's 13th Problem [76], posed at the 1900 International Congress of Mathematicians, asked whether every continuous function of three variables

$$f : [0,1]^3 \to \mathbb{R}$$

can be represented as a finite superposition of continuous bivariate functions. Hilbert conjectured that such a representation was impossible. However, the later work of Kolmogorov and Arnol'd overturned this view, showing that *every* continuous function of s variables can be expressed using only sums and superpositions of univariate functions—a result that fundamentally reshaped the theory of functional representation.

Kolmogorov and Arnol'd: resolving the 13th Problem. Kolmogorov's 1956 note [77] introduced the idea that multivariate functions might be representable via functions of fewer variables. Arnol'd, his student, confirmed this for the three–variable case in 1957 [78], giving an explicit decomposition of a general $f(x, y, z)$ into superpositions of continuous bivariate functions. Later that year, Kolmogorov published his full and elementary solution [79]: any continuous function of $n > 2$ variables can be written using only univariate functions and addition. Thus Hilbert's conjecture was disproved.

The Kolmogorov Superposition Theorem (KST). Let $E_1 = [0,1]$ and $E_n = [0,1]^n$. Kolmogorov proved that for every $n > 2$ there exist continuous *universal* inner functions

$$\phi_{q,p} : E_1 \to \mathbb{R}, \qquad p = 1, \ldots, n, \ \ q = 0, \ldots, 2n,$$

independent of the target function f, such that every $f \in C(E_n)$ admits the representation

$$f(x_1, \ldots, x_n) = \sum_{q=0}^{2n} \Phi_q \left(\sum_{p=1}^{n} \phi_{q,p}(x_p) \right), \qquad (x_1, \ldots, x_n) \in E_n, \tag{4}$$

where each $\Phi_q : \mathbb{R} \to \mathbb{R}$ is continuous and depends on f, while the inner functions $\phi_{q,p}$ are universal. KST shows that multivariate continuity can be synthesized entirely from univariate nonlinearities, a structural insight that later motivated two–layer interpretations and neural–network analogies.

Proof strategies and later refinements. Two major approaches emerged in the decades following Kolmogorov's work:

(i) *Baire–category proofs*: Kahane [80] and Hedberg [81] showed that for generic tuples of continuous increasing functions, the superposition operator is surjective. Their arguments reveal that KST is not only true but *abundant*: for almost all choices of inner functions, an appropriate outer function exists.

(ii) *Constructive proofs*: Lorentz [82], Sprecher [83], Arnol'd [84], and others developed explicit (though highly involved) constructions. These proofs follow a common pattern: partition E_n into subcubes, map each subcube into a disjoint real interval via the inner functions, and build the outer functions iteratively to approximate the target f. Kolmogorov's original paper left several analytic details unstated; these were filled in by Arnol'd [84] and later authors, making the constructive picture complete.

This classical theory forms the starting point for the refinements described next: reductions in the number of unique functions, improvements in regularity, and the development of computationally usable versions that ultimately connect the superposition viewpoint to modern KAN architectures.

Refinements to KST. Kolmogorov's constructive formulation (4) established the universality of the inner functions $\phi_{q,p}$, but it did so at considerable structural cost: the representation requires $2n^2 + n$ distinct inner functions and $2n+1$ outer functions. While theoretically elegant, this level of redundancy makes the original form far too complex for computation or numerical approximation. The decades following Kolmogorov's work therefore focused on two goals: (i) reducing the number of *unique* functions needed, and (ii) improving their regularity. These efforts produced the modern, compressed form of KST that underlies computational constructions and later neural interpretations.

(i) Reducing the number of functions. Sternfeld [85] proved that the number of *summands* $2n + 1$ in the Kolmogorov superposition formula is optimal and cannot be reduced. However, his functional–analytic

framework shows that these $2n+1$ summands do *not* require $2n+1$ different inner or outer functions: the same small collection of functions can be reused repeatedly. Thus the number of *distinct* functions can be much smaller, even though the number of summands is fixed.

Lorentz' reduction of outer functions. Lorentz's 1962 exposition [82] clarified Kolmogorov's argument and showed that the $2n+1$ outer functions Φ_q can be replaced by a single continuous function Φ. In the bivariate case ($s = 2$), with inputs $(x_1, x_2) \in [0, 1]^2$, he derived the canonical representation

$$f(x_1, x_2) = \sum_{q=1}^{5} \Phi\big(\phi_{1,q}(x_1) + \phi_{2,q}(x_2)\big),$$

where the ten inner functions $\phi_{1,q}$ and $\phi_{2,q}$ are universal, but the outer function Φ depends on f. More generally, for s variables he obtained

$$f(x_1, \ldots, x_s) = \sum_{q=1}^{2s+1} \Phi\left(\sum_{p=1}^{s} \phi_{p,q}(x_p)\right), \tag{5}$$

demonstrating that the dependence on f enters only through a single continuous outer function Φ.

Sprecher's reduction of inner functions. Sprecher [83] achieved the corresponding simplification for the inner layer. He showed that the entire family $\{\phi_{q,p}\}$ can be generated from a *single* monotone universal function $\psi : E_1 \to \mathbb{R}$, together with fixed positive weights $\{\lambda_p\}_{p=1}^{n}$ and uniform shifts $x \mapsto x + \varepsilon q$, where $\varepsilon > 0$ is a small constant. In modern notation,

$$\phi_{q,p}(x) = \lambda_p \, \psi(x + \varepsilon q), \tag{6}$$

where the weights $\lambda_p > 0$ depend only on the dimension and satisfy a rational independence condition. Sprecher also proved that ψ may be chosen with an explicit Hölder–Lipschitz exponent.

By combining Lorentz' outer-function reduction and Sprecher's inner-function compression, one obtains the modern compressed version of the superposition theorem:

$$f(x_1, \ldots, x_n) = \sum_{q=0}^{2n} \Phi\left(\sum_{p=1}^{n} \lambda_p \, \psi(x_p + \varepsilon q) + \delta q\right), \tag{7}$$

where $\psi : E_1 \to \mathbb{R}$ is a single universal inner function, $\Phi : \mathbb{R} \to \mathbb{R}$ is a continuous outer function depending on f, the constants $\{\lambda_p\}$ are positive and rationally independent, $\varepsilon > 0$ is a uniform shift, and $\delta \in \mathbb{R}$ is an offset introduced for separation of summands.

(ii) Improving regularity. The inner functions in Kolmogorov's original proof are highly irregular—Hölder but non-differentiable. A function $u : E_1 \to \mathbb{R}$ is Hölder continuous with exponent $\alpha \in (0, 1]$ if

$$|u(x) - u(y)| \le L|x - y|^\alpha, \qquad x, y \in E_1,$$

for some $L > 0$. The case $\alpha = 1$ corresponds to Lipschitz continuity.

Vitushkin and Henkin [86–88] proved that no universal inner family can possess C^1 (or C^s with $s > 1$) smoothness. Within the theoretical development of KST itself, Fridman [92] constructed universal inner maps in Lip^1, the maximal regularity consistent with these impossibility results. Sprecher [93] further demonstrated that his compressed formulation (6) can also be realized with Lipschitz inner functions. More recently, Actor and Knepley introduced the first explicit algorithm aimed at computing Lipschitz universal inner functions, refining the earlier Hölder-type constructions of Köppen and Braun–Griebel [94, 95].

Computational KST. Algorithmic approaches fall into three categories:

- *Exact constructive KST*: compute the universal inner map and the outer functions exactly.

- *Approximate KST (outer-only)*: fix the universal inner map and approximate or learn only the outer function.

- *Approximate KST (inner–and–outer)*: approximate both inner and outer maps within a superposition-type architecture.

Exact constructions. Sprecher's digit-based inner function and outer correction schemes were made fully computable and later corrected by Köppen and rigorously validated by Braun–Griebel, who established continuity and monotonicity of the corrected recursion [96–99]. Constructive and guaranteed versions include Nakamura et al., who provide algorithmic constructions of the universal inner map ψ and outer map χ with certified error bounds [101].

Approximate KST (outer-only; inner fixed). This line of work preserves the universal inner map and reduces learning to a one-dimensional outer problem.

- De Figueiredo (1980): fixes Sprecher's universal inner function ψ and learns the outer function g using a Chebyshev basis—the first data-driven outer-fitting scheme in a KST layout [104].

- Frisch et al. (1989): retain Lorentz's universal inner maps and iteratively refine a single outer function g [111].

- Braun–Griebel inner + RKHS outer (2009): uses the corrected universal inner function ψ and replaces constructive outer windows by spline/Fourier RKHS approximants [100].

- Lai–Shen (2025): again fix the Lorentz–Sprecher inner maps and reconstruct the outer function using linear B–splines with $O(n^{-2})$ accuracy [265, 266].

Outer-only methods preserve inner universality and thus avoid the curse of dimensionality: all problem dependence flows through a univariate outer approximation.

Approximate KST (inner–and–outer; controversial). These approaches approximate or entirely replace the universal inner functions, thereby departing from the exact Kolmogorov formulation.

- **Kurková (1991–1992):** replaces the universal inner staircase by sigmoidal staircase approximants and learns the outer coefficients within a two-hidden-layer sigmoidal architecture [90, 91].

- **Nees (1994, 1996):** constructs explicit recursive piecewise-linear approximations of the inner maps ϕ_q^k together with data-driven outer corrections g_r that achieve geometric error decay [102, 103].

- **Spline-based architectures:** The KSN model of Igelnik and Parikh (2003) [106] uses cubic splines for *both* inner and outer functions, while Coppejans (2005) [107] introduces monotone inner splines for statistical identifiability. Related spline-based superpositional models, including ExSpliNet [108], KASAM [109], and the Urysohn-operator framework of Polar and Poluektov [110], adopt additive or hierarchical structures reminiscent of KST but do not enforce universality of the inner layer. These methods yield practical spline architectures but are not constructive realizations of the Kolmogorov superposition theorem.

Caveat. Exact KST requires a universal (target-independent) inner function; approximating or smoothing this function breaks universality and may violate separation. Classical results of Vitushkin and Henkin, and the modern analysis of Actor–Knepley, show that no C^1 or overly smooth inner functions can satisfy the Kolmogorov separation property [86–88, 95]. Thus inner approximations are meaningful only in the *approximation-theoretic* sense, not as exact KST.

Neural interpretations. De Figueiredo (1980) [104] was the first to view the Kolmogorov–Sprecher representation as a computational architecture, expressing it in block-diagram form and proposing a data-driven procedure for learning the outer function g using Chebyshev bases. Hecht–Nielsen (1987) [105] interprets

Sprecher's representation as a three-stage mapping network with a fixed universal hidden layer and learned outer functions. Kurková's approximation framework (1991–1992) [90, 91] provides compatibility with standard trainable neural networks by replacing the inner staircase with smooth sigmoidal combinations while learning the outer layer. Spline-based models such as KSN (2003) [106] and the shape-constrained variant of Coppejans (2005) [107] train both inner and outer functions within spline families, yielding practical but non-KST architectures. See Table 4 for a chronological overview of these developments, tracing the progression from the original KST theory to its computational and neural interpretations.

Table 4: Development of Kolmogorov's Superposition Theorem towards Kolmogorov-inspired networks (1900–2024).

Year	Author(s)	Key Contribution	Focus on
1900	Hilbert [76]	Poses Hilbert's 13th problem	Theory
1956	Kolmogorov [77]	Preliminary idea of superpositions; first hint toward the theorem.	Theory
1957	Arnol'd [78]	First explicit 3-variable construction with 9 terms; provides concrete counterexample to Hilbert 13.	Theory
1957	Kolmogorov [79]	Full Kolmogorov Superposition Theorem; first general n-D proof,	Theory
1958	Arnol'd [84]	Supplies missing lemmas; first to complete Kolmogorov's proof.	Theory
1962	Lorentz [82]	Gives simplified canonical form with *one* outer function.	Theory
1965	Sprecher [83]	First single universal inner function; reduces many $\phi_{p,q}$ to one ψ with shifts; major structural simplification over Kolmogorov.	Theory
1967	Fridman [92]	Shows universal inner functions may be taken Lip(1); first optimal smoothness result; strengthens Sprecher–Kolmogorov scheme.	Theory
1980	de Figueiredo [104]	First network-like interpretation; introduces block diagram + data-driven outer fitting; operationalizes Sprecher's form.	Theory
1987	Hecht–Nielsen [105]	First explicit neural mapping theorem; views KST as two-hidden-layer network.	Network
1989	Girosi–Poggio [89]	First critical analysis of learnability; shows inner function must be non-smooth + outer non-parametric.	Theory
1989	Frisch et al. [111]	First computational implementation of Lorentz form; iterative learning of single outer function.	Network
1991	Kurková [90]	First approximation-theoretic reinterpretation; ties network size to modulus of continuity.	Network
1992	Kurková [91]	Two-hidden-layer sigmoidal approximants; universal inner parameters.	Both
1993	Sprecher [112]	Single universal ψ for *all* n.	Both
1993	Nakamura et al. [101]	First fully constructive + guaranteed-accuracy version.	Theory
1994	Nees [102]	First use of spline (piecewise-linear) inner maps, introducing geometric error decay and a fully constructive, algorithmic approximation of KST with explicit error bounds;	Both
1996	Sprecher [96]	First executable version of ψ with separation guarantees.	Both
1997	Sprecher [97]	Explicit algorithm for outer functions.	Both
2002	Köppen [98]	Corrected continuous monotone inner function of Sprecher [96]; first training-ready inner map.	Network
2003	Igelnik–Parikh [106]	First fully trainable Kolmogorov Spline Network; replaces fractal inner functions with smooth cubic splines and provides learnable inner and outer maps.	Network
2009	Braun–Griebel [99]	First correct constructive KST; fixes Sprecher's errors [96]; modern constructive foundation.	Theory
2019	Actor–Knepley [95]	Proves C^1 inner functions impossible; first rigorous smoothness obstruction.	Theory
2024	Liu *et al.* [26]	First deep network architecture inspired by the Kolmogorov–Arnold representation (KAN).	Network

2024: Liu et al. — Kolmogorov–Arnold Network

Liu et al. [26] introduce the *Kolmogorov–Arnold Network*, a neural architecture explicitly *motivated* by the structure of the KST (4), though not intended as a mathematical realization of it. The authors emphasize that KAN is *not* an exact implementation of the Kolmogorov Superposition Theorem, but rather a computational architecture "inspired by" the Kolmogorov–Arnold representation.

Because the Kolmogorov Superposition Theorem prescribes only a two-layer structure (universal inner functions $\phi_{q,p}$ followed by outer maps Φ_q), Liu et al. generalize the idea by redefining the basic computational block. A *KAN layer* is introduced as a matrix of univariate functions,

$$\mathbf{\Phi}_\ell = \{\phi_{\ell,j,i}\}, \qquad i = 1, \ldots, n_\ell, \ \ j = 1, \ldots, n_{\ell+1},$$

where n_ℓ and $n_{\ell+1}$ denote the widths of layers ℓ and $\ell + 1$, respectively, and where each edge $(i \to j)$ carries a trainable B-spline activation $\phi_{\ell,j,i} : \mathbb{R} \to \mathbb{R}$. Within a layer, the forward computation is purely Kolmogorov-like aggregation:

$$x_{\ell+1,j} = \sum_{i=1}^{n_\ell} \phi_{\ell,j,i}(x_{\ell,i}), \tag{8}$$

so each layer performs only "inner-type" operations: univariate nonlinearities followed by summation.

In the deep setting, the outputs of one collection of inner-type functions become the inputs to the next. No separate outer function Φ_q is introduced: the final layer plays the role of an outer map only in the trivial sense that it produces the scalar output. Thus a deep KAN is simply the composition of its inner-type layers,

$$\text{KAN}(\mathbf{x}) = \big(\mathbf{\Phi}_{L-1} \circ \cdots \circ \mathbf{\Phi}_0\big)(\mathbf{x}), \tag{9}$$

with "outer-like" effects distributed across all layers rather than concentrated in a single KST-style stage.

Why KANs should not be viewed as exact realizations of the Kolmogorov Superposition Theorem. Although Liu et al. describe KANs as *inspired* by the Kolmogorov superposition theorem, it is helpful to distinguish KST and KAN as follows:

- *Inner functions are learned, not universal.* In KST the inner maps are universal and fixed for all target functions [79,83], whereas in KANs every edge function is trained from data. This points to a structural analogy rather than an exact correspondence.

- *Regularity properties differ.* Classical KST inner functions are only Hölder or Lipschitz continuous [86, 88, 92], whereas KANs use smooth B–splines. This indicates that KANs operate within an approximation framework rather than reproducing the exact KST construction.

- *Separation constraints are not enforced.* Constructive proofs of KST rely on fixed shifts and integrally independent weights to separate subcube images [82,83]. KANs do not impose these geometric constraints, so they do not replicate the mechanism underlying the theorem.

- *Width and depth do not follow KST.* Sternfeld's optimal width $2n+1$ applies to the shallow superposition setting [85]. KANs allow arbitrary widths and depths, reflecting modern deep-learning practice rather than KST optimality.

- *No final one-dimensional outer function.* KST reduces approximation to a single univariate outer map [82,83]. Deep KANs distribute nonlinearity across multiple layers and do not preserve this one-dimensional reduction.

4 Bridging KANs and MLPs

KANs and MLPs are both hierarchical function approximators, yet they differ fundamentally in *where* and *how* nonlinearities are applied. In a conventional MLP, inputs are first *linearly mixed* and then passed through a fixed activation function (mix → activate). In contrast, a KAN applies a (typically trainable) univariate transformation to each input coordinate before aggregation (activate → mix). This reversal of operations produces more localized, interpretable, and adaptable mappings.

This structure closely parallels *Sprecher's* constructive version of the Kolmogorov superposition theorem (7), where inner univariate functions act independently on shifted coordinates:

$$f(x_1, \ldots, x_n) = \sum_q \Phi\bigg(\underbrace{\sum_p \lambda_p\, \phi(x_p + \eta_q)}_{\substack{\lambda_p:\ \text{weights} \\ \eta_q:\ \text{shifts}}} + \underbrace{c_q}_{\text{offset}}\bigg),$$

with positive weights $\lambda_p > 0$, shifts η_q, and offsets c_q. The KAN formulation operationalizes this constructive principle within a neural architecture, turning theoretical decomposition into a learnable process.

Formal Equivalence. Wang et al. [53] establish a bidirectional correspondence between MLPs and KANs. Any MLP with ReLU^k activations,

$$\sigma_k(x) = \max(0, x)^k,$$

can be represented by an equivalent KAN parameterization using B-spline bases of order k and grid size $G=2$. For an MLP approximating a target function $f : \mathbb{R}^d \to \mathbb{R}$,

$$f(\mathbf{x}) = \sum_{i=1}^{W} \underbrace{\alpha_i}_{\text{output weight}} \sigma_k \Big(\underbrace{\sum_{j=1}^{d} w_{ij} x_j}_{\text{linear mix}} + \underbrace{b_i}_{\text{bias}} \Big),$$

there exists an equivalent KAN representation,

$$f(\mathbf{x}) = \sum_{i=1}^{W} \underbrace{\Phi_i}_{\text{outer map}} \Big(\underbrace{\sum_{j=1}^{d} \varphi_{ij}(x_j)}_{\substack{\text{sum of 1D transforms} \\ \varphi_{ij}: \text{ edge-wise univariate}}} \Big),$$

where each univariate function $\varphi_{ij} : \mathbb{R} \to \mathbb{R}$ is a learned B-spline that approximates $\sigma_k(w_{ij} x_j + b_i)$. In essence, KANs replace the fixed nonlinearities of MLPs with learnable one-dimensional functions, enabling richer local adaptation without increasing architectural depth.

The reverse direction also holds under mild constraints. If a KAN layer employs polynomial-type univariate functions (e.g., B-splines of order k) and excludes non-polynomial activations such as SiLU, the model can be reformulated as an equivalent MLP with ReLU^k activations. In this conversion, a KAN of width W, grid size G, and depth L induces an MLP whose effective width grows as $(G + 2k + 1)W^2$, resulting in a parameter complexity of $\mathcal{O}(G^2 W^4 L)$. By comparison, the original KAN requires only $\mathcal{O}(G W^2 L)$ parameters—highlighting its superior parameter efficiency, especially for fine grids or high-order spline bases. This equivalence creates a bridge through which approximation and convergence results from MLP theory can be transferred directly to KANs (see Section 10).

Special Case: Piecewise-Linear Functions. Schoots et al. [164] demonstrate that KANs using piecewise-linear univariate functions are functionally identical to ReLU-based MLPs. Any piecewise-linear $\varphi : \mathbb{R} \to \mathbb{R}$ with k breakpoints admits the expansion

$$\varphi(x) = \underbrace{a_0}_{\text{bias}} + \underbrace{a_1 x}_{\text{linear term}} + \sum_{j=1}^{k} \underbrace{\alpha_j}_{\text{coeff.}} \text{ReLU}(x - b_j),$$

where $a_0, a_1, \alpha_j, b_j \in \mathbb{R}$. Thus, each KAN univariate map can be embedded into a compact ReLU subnetwork, reinforcing the view of KANs as structured and interpretable MLPs.

Actor et al. [46] and Gao et al. [165] reach similar conclusions: KANs can emulate MLP behavior while introducing task-adaptive nonlinearities—such as spline, Fourier, or Chebyshev bases—that improve inductive bias and generalization for structured data.

Summary. KANs and MLPs are expressively equivalent but structurally distinct. KANs achieve localized, interpretable representations by applying learnable univariate transformations before aggregation, whereas MLPs rely on fixed activations after linear mixing. This reversal leads to substantial parameter savings and smoother function representations, while maintaining theoretical consistency with the Kolmogorov–Arnold superposition principle. In practice, KANs can thus be viewed as structured, efficient, and interpretable extensions of MLPs.

5 How KANs Extend the MLP Landscape

KAN layers are increasingly adopted as *drop-in replacements* for traditional MLP blocks across convolutional, transformer, graph, and physics-informed models. They enhance expressivity, interpretability, and parameter efficiency—often with minimal architectural or training changes.

Vision and Representation Learning. In computer vision, *Convolutional KANs* embed spline-based activations directly within convolutional kernels, producing more expressive yet lightweight CNNs [166][4]. Residual KAN modules integrate into ResNet backbones to improve gradient flow and generalization [171][5], while *U-KAN* extends U-Nets for image segmentation and diffusion models [173][6]. Similarly, the *KAN-Mixer* adapts MLP-Mixer architectures for image classification [186][7]. Additional applications include remote sensing [175], hyperspectral imaging via *Wav-KAN* [174], medical image classification [176], and autoencoding tasks [172][8].

Sequential and Temporal Modeling. For time-series and sequential tasks, *KAN-AD* employs Fourier expansions for efficient anomaly detection [177][9], while *T-KAN* and *MT-KAN* enhance forecasting under concept drift and multivariate dependencies [179]. Other extensions include satellite-traffic forecasting [178], recurrent temporal KANs (*TKANs*) [180], and the transformer-based *TKAT* model [181][10], which integrates learnable univariate mappings within self-attention layers.

Graph and Structured Data. KAN layers have also been incorporated into graph learning frameworks, where replacing MLPs in GNN message-passing blocks improves numerical stability and feature smoothness. Implementations such as *GraphKAN* [182][11] and *KAN4Graph* [183][12] achieve consistent accuracy gains. *GKAN* integrates spline-based kernels directly into graph convolutions [184], while general-purpose variants like *S-KAN* and *S-ConvKAN* enable task-dependent activation selection across architectures [38].

Physics-Informed and Operator Learning. In scientific computing, *Physics-Informed KANs* preserve the original PINN objective but replace fixed activations with learnable basis functions, improving locality and interpretability. This modularity enables direct architectural transfers—e.g., *DeepONet* → *DeepOKAN*, separable *PINNs* → separable *PIKANs*, and even *NTK* analyses in PINNs → corresponding analyses in PIKANs. Moreover, existing advances such as variational losses, residual reweighting, and adaptive sampling naturally carry over, bridging traditional PINN frameworks with modern kernel-based representations. Representative examples are summarized in Table 5.

Table 5: Representative advanced PINN baselines [145, 146] and corresponding KAN/PIKAN counterparts.

PINN contribution	KAN/PIKAN counterpart
2017— [1] Foundational PINN for data-driven PDE solutions	[26]
2018— [3] Uncertainty quantification for forward/inverse PINNs	[141]
2019— [168] Neural ordinary differential equations (Neural ODEs)	[44]
2019— [149] Neural operators for PDE solution maps (DeepONet)	[54]
2020— [230] PINN for symbolic regression via recursive decomposition	[231]
2020— [6] Multi-fidelity PINNs (low/high-fidelity correlation)	[189]
2020— [152] Fourier-feature embeddings for multiscale structure	[71]
2020— [238] Fourier Neural Operator (FNO)	[237]
2021— [9] DeepXDE library (resampling strategies and benchmarks)	[26]
2022— [8] NTK-based analysis explaining PINN training pathologies	[63, 165]
2023— [158] Adaptive PINN (moving collocation points)	[118]
2023— [211] Finite-basis PINNs with overlapping subdomains	[122]
2023— [154] Separable PINN architectures	[190]
2023— [167] Surrogate + PDE-constrained optimization	[56]
2023— [169] Surrogate modeling in elasto-plasticity	[62]
2025— [170] Multigrid and multi-resolution training strategy	[72]

---

[4] https://github.com/AntonioTepsich/Convolutional-KANs
[5] https://github.com/withray/residualKAN
[6] https://github.com/CUHK-AIM-Group/U-KAN
[7] https://github.com/engichang1467/KAN-Mixer
[8] https://github.com/SekiroRong/KAN-AutoEncoder
[9] https://github.com/issaccv/KAN-AD
[10] https://github.com/remigenet/TKAT
[11] https://github.com/WillHua127/GraphKAN-Graph-Kolmogorov-Arnold-Networks
[12] https://github.com/yueliu1999/KAN4Graph

6 Basis Functions

This section reviews commonly used bases in KANs: B-splines, Chebyshev and Jacobi polynomials, ReLU compositions, Fourier series, Gaussian kernels, wavelets, finite-basis partitions, and Sinc functions. We begin with an overview (Table 6) to orient the reader. Subsequent subsections expand on each family, beginning with B-splines.

Table 6: Comparison of Basis Functions in KANs

Name	Support	Equation Form	Grid Required	Basis/Activation Type	Ref.
B-spline	Local	$\sum_n c_n B_n(x)$	Yes	B-spline	[26]
Chebyshev	Global	$\sum_k c_k T_k(\tanh x)$	No	Chebyshev + Tanh	[196]
Stabilized Chebyshev	Global	$\tanh\left(\sum_k c_k\, T_k(\tanh x)\right)$	No	Chebyshev + linear head	[65]
Chebyshev (grid)	Global	$\sum_k c_k T_k\left(\frac{1}{m}\sum_i \tanh(w_i x + b_i)\right)$	Yes	Chebyshev + Tanh	[52]
ReLU-KAN	Local	$\sum_i w_i R_i(x)$	Yes	Squared ReLU	[123]
HRKAN	Local	$\sum_i w_i[\mathrm{ReLU}(x)]^m$	Yes	Polynomial ReLU	[133]
Adaptive ReLU-KAN	Local	$\sum_i w_i v_i(x)$	Yes	Adaptive ReLU	[118]
fKAN (Jacobi)	Global	$\sum_n c_n P_n(x)$	No	Jacobi	[127]
rKAN (Padé/Jacobi)	Global	$\frac{\sum_i a_i P_i(x)}{\sum_j b_j P_j(x)}$	No	Rational + Jacobi	[128]
Jacobi-KAN	Global	$\sum_i c_i P_i(\tanh x)$	No	Jacobi + Tanh	[70]
FourierKAN	Global	$\sum_k a_k \cos(kx) + b_k \sin(kx)$	No	Fourier	[134]
KAF	Global	$\alpha\, \mathrm{GELU}(x) + \sum_j \beta_j \psi_j(x)$	No	RFF + GELU	[71]
Gaussian	Local	$\sum_i w_i \exp\left(-\left(\frac{x-g_i}{\varepsilon}\right)^2\right)$	Yes	Gaussian RBF	[119]
RSWAF-KAN	Local	$\sum_i w_i\left(s_i - \tanh^2\left(\frac{x-c_i}{h_i}\right)\right)$	Yes	Reflectional Switch	[120]
CVKAN	Local	$\sum_{u,v} w_{uv} \exp\left(-|z - g_{uv}|^2\right)$	Yes	Complex Gaussian	[129]
BSRBF-KAN	Local	$\sum_i a_i B_i(x) + \sum_j b_j \exp\left(-\frac{(x-g_j)^2}{\varepsilon^2}\right)$	Yes	B-spline + Gaussian	[40]
Wav-KAN	Local	$\sum_{j,k} c_{j,k}\, \psi\left(\frac{x-u_{j,k}}{s_j}\right)$	No	Wavelet	[139]
FBKAN	Local	$\sum_j \omega_j(x) K_j(x)$	Yes	PU + B-spline	[122]
SincKAN	Global	$\sum_i c_i \, \mathrm{Sinc}\left(\frac{\pi}{h}(x - ih)\right)$	Yes	Sinc	[49]
Poly-KAN	Global	$\sum_i w_i P_i(x)$	No	Polynomial	[138]

6.1 B-spline

B-spline bases are among the most widely adopted in KANs due to their compact support, smoothness, local control, and piecewise–polynomial structure [42, 43, 45–47, 53, 56–61, 66–69, 115, 118, 122, 124, 164, 165, 187–195, 206, 237, 239, 244]. Their locality and flexibility make them expressive, numerically stable, and particularly well suited for interpretable representations. The original KAN formulation [26] and its accompanying software package further contributed to their early adoption and widespread use.

Each univariate KAN map $\varphi : \mathbb{R} \to \mathbb{R}$ is represented as a linear combination of fixed–knot B-spline basis functions:

$$\varphi(x) \;=\; \sum_{n=0}^{N-1} c_n\, B_n^{(k)}(x), \tag{10}$$

where N is the number of basis functions, $B_n^{(k)}(x)$ denotes the n-th B-spline of polynomial degree k defined on a knot vector $\mathbf{t} = (t_0, \ldots, t_{N+k})$, and $c_n \in \mathbb{R}$ are trainable coefficients. The Cox–de Boor recursion yields C^{k-1} continuity, and open–uniform knot choices give well–behaved boundary conditions.

To match boundary and interior regularity/support, the knot vector is often *extended* by k points on each side. This padding allows the model to progressively capture finer details [53]. As illustrated in Figure 1, the number of active basis functions grows from $G - k$ to $G + k$, where G is the number of internal intervals in the original, non–extended grid.

Subfigures 1(a) and 1(b) visualize cubic (k=3) B-spline bases on non–extended and extended grids, respectively. Without extension, boundary bases are truncated and lose symmetry; with extension, added knots outside the domain restore full polynomial support (gray bands). To compare expressivity, subfigures 1(c) and 1(d) synthesize univariate maps

$$\varphi(x) \;=\; \sum_{n=0}^{N-1} c_n B_n^{(k)}(x),$$

using the *same* coefficient vector across the two grids (truncated in the non–extended case). Differences in φ thus arise solely from the basis itself: the extended grid yields richer boundary behavior and overall smoother maps, while the non–extended grid flattens near edges. This highlights the practical benefit of grid extension for boundary–sensitive tasks (e.g., PDEs).

(a) Non–extended cubic B-spline basis

(b) Extended cubic B-spline basis

(c) Learned map $\varphi(x)$ on non–extended grid

(d) Learned map $\varphi(x)$ on extended grid
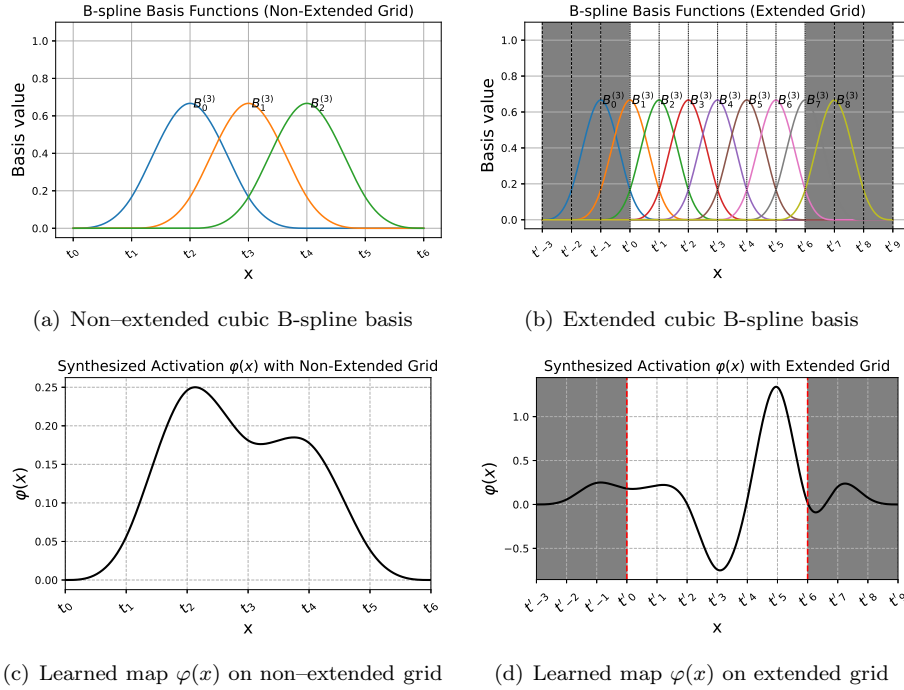
Figure 1: Comparison of B-spline bases and synthesized univariate maps with/without grid extension. (a,b) Cubic (k=3) bases on non–extended vs. extended grids. (c,d) Learned maps $\varphi(x)$ using identical random coefficients c_n. Gray regions mark padded boundary intervals.

In the original KAN [26] and KAN 2 [113][13], each univariate activation uses uniformly spaced cubic B-splines ($k = 3$) together with a smooth residual term to aid gradients and enhance expressivity in flat regions:

$$\tilde{\varphi}(x) \;=\; \sum_{n=0}^{N-1} c_n \, B_n^{(k)}(x) \;+\; \frac{x}{1 + e^{-x}}.$$

A global `tanh` is applied after each hidden layer (but not the output) to keep activations within the spline domain. KAN 2 further supports post–training grid refinement, which increases knot resolution without reinitializing parameters, thereby improving fidelity with minimal overhead.

Convergence implications. Recent theory gives spline-KANs some of the strongest guarantees in the KAN family. Wang [53] proves accelerated Sobolev approximation rates; Kratsios et al. [271] show optimal Besov performance on Lipschitz and even fractal domains; and Liu et al. [140] establish minimax-optimal regression

rates together with optimal spline–knot scaling. These results place B-splines on the firmest theoretical footing among KAN bases. (See Sec. 10.)

Spectral bias and NTK conditioning. Spline grids control frequency reach: finer grids reduce spectral bias but may worsen conditioning [39, 53]. Initialization also matters—Rigas et al. [276][14] show that Glorot-style and power-law initializations yield more stable NTKs and faster early convergence. (See Secs. 10.2 and 10.3.)

6.2 Chebyshev Polynomials

Chebyshev polynomials offer a clean and theoretically grounded alternative to B-splines for KAN univariate mappings—especially in PIKANs—due to their global orthogonality, excellent spectral approximation properties, and simple recursive structure suited for smooth or oscillatory targets.

Definition and Recurrence. Let $T_k(x)$ denote the Chebyshev polynomials of the first kind, defined recursively as

$$T_0(x) = 1, \qquad T_1(x) = x, \qquad T_k(x) = 2x\,T_{k-1}(x) - T_{k-2}(x) \quad (k \geq 2), \tag{11}$$

which form an orthogonal basis on $[-1, 1]$ with weight $w(x) = (1 - x^2)^{-1/2}$.

ChebyKAN Formulation. The *ChebyKAN* model [130][15] represents each univariate map as

$$\varphi_{q,p}^{(\ell)}(x) \; = \; \sum_{k=0}^{K} c_{q,p,k}^{(\ell)}\, T_k(\tilde{x}), \qquad \tilde{x} = \tanh(x) \;\; \text{(per-layer input normalization)},$$

with trainable coefficients $c_{q,p,k}^{(\ell)} \in \mathbb{R}$. Each layer thus evaluates T_k on normalized inputs $\tilde{x} \in [-1, 1]$ for numerical stability, producing the output

$$x_q^{(\ell+1)} \; = \; \sum_{p=1}^{P} \varphi_{q,p}^{(\ell)}\big(x_p^{(\ell)}\big),$$

consistent with the generic KAN layer formulation.

Efficient Evaluation. In practice, most implementations (e.g., [72]) compute T_k via

$$T_k(z) = \cos(k \arccos z),$$

which vectorizes efficiently on GPUs. Alternatively, the recurrence relation (11) or Clenshaw's algorithm provides equivalent, numerically stable computation—particularly advantageous for high-degree expansions where repeated arccos calls become costly. Mahmoud et al. [50] further employ *shifted Chebyshev polynomials* on $[0, 1]$, defined as

$$T_n(x) = \cos\big(n \arccos(2x - 1)\big),$$

to align the domain with the standard Kolmogorov–Arnold representation on non-symmetric intervals.

Normalization and Stability. Figure 2 illustrates how per-layer tanh normalization stabilizes Chebyshev activations. Panel (a) shows the standard basis $T_k(x)$ on $[-1, 1]$ for degree $K=8$, where extrema occur at $T_k(\pm 1) = \pm 1$, forcing steep slopes near the boundaries. Panel (b) instead evaluates $T_k(\tanh x)$, compressing the effective range to $\tanh(\pm 1) \approx \pm 0.762$, which moderates endpoint slopes while preserving interior structure. This compression prevents saturation at ± 1 and keeps features in a well-conditioned range, critical for deep stacks of Chebyshev layers.

---

[14]https://github.com/srigas/KAN_Initialization_Schemes
[15]https://github.com/SynodicMonth/ChebyKAN

The difference becomes clearer in Panel (c), comparing the deep composite maps

$$\sum_{k=0}^{K} c_k\, T_k(\tanh x) \quad \text{and} \quad \sum_{k=0}^{K} c_k\, T_k(x)$$

with identical coefficients c_k. Both are bounded, but by the chain rule,

$$\frac{d}{dx}\left[\sum_{k=0}^{K} c_k\, T_k(\tanh x)\right] = \left(1 - \tanh^2 x\right) \sum_{k=0}^{K} c_k\, T_k'\!\left(\tanh x\right),$$

the tanh-normalized version suppresses slope growth near $|x| \approx 1$, removing the synchronized oscillations visible in the unnormalized case. Even without training, this normalization yields smoother and better-conditioned responses.

(a) Chebyshev basis without tanh normalization

(b) Chebyshev basis with tanh normalization

(c) Deep Chebyshev KAN map: with vs. without tanh normalization
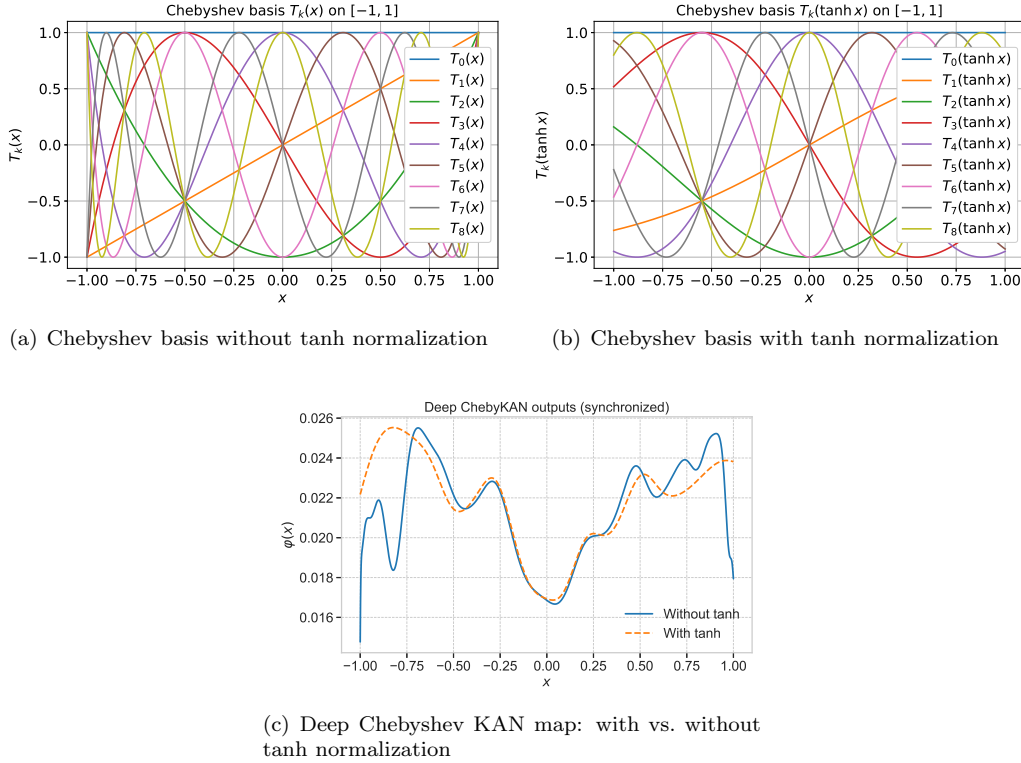
Figure 2: (a) Standard Chebyshev basis functions without per-layer tanh normalization. (b) Same basis with tanh normalization, showing compressed input range and moderated edge slopes. (c) Deep Chebyshev KAN map ($K{=}8$) comparing $\sum c_k T_k(\tanh x)$ (blue) vs. $\sum c_k T_k(x)$ (orange); the normalized version exhibits smoother behavior and smaller endpoint gradients, indicating improved conditioning.

Grid-Averaged Variant. Following Toscano et al. [52], a practical enhancement introduces grid before evaluating the Chebyshev expansion. For a univariate input x,

$$g(x) = \frac{1}{m} \sum_{i=1}^{m} \tanh\!\left(w_i x + b_i\right), \qquad \varphi_{q,p}^{(\ell)}(x) = \sum_{k=0}^{K} c_{q,p,k}^{(\ell)}\, T_k\!\left(g(x)\right),$$

where m denotes the number of centers, b_i are uniformly spaced biases within $[\beta_{\min}, \beta_{\max}]$ (e.g., -0.1 to 0.1), and w_i control local slope. The coefficients $c_{q,p,k}^{(\ell)}$ can follow the stable initialization proposed in [196]. This averaged-tanh grid constrains $g(x) \in (-1, 1)$, introduces mild spatial warping, improves numerical conditioning, and as reported in [52], supports stable training even with higher polynomial degrees.

Spectral Properties and Efficiency. The spectral parameterization of Chebyshev-based KANs was first formalized in Sidharth et al. [196], while Guo et al [197] demonstrated superior parameter efficiency and generalization in data-scarce regimes. From a theoretical perspective, Faroughi and Mostajeran [64] showed that Chebyshev PIKANs (cPIKANs) yield better-conditioned NTKs with slower spectral decay, accelerating convergence for PDEs such as diffusion and Helmholtz equations.

Stabilization and Hybrid Designs. Yu et al. [49] confirmed these advantages for function approximation and PDE learning but also highlighted failure modes of raw polynomial stacks at high depth, motivating stabilizers such as domain normalization, nested nonlinearities, and contractive mappings. Building on these insights, Daryakenari et al. [65] proposed a stabilized Chebyshev stack by inserting an additional tanh between layers and replacing the Chebyshev head with a linear readout:

$$x_q^{(\ell+1)} = \tanh\left(\sum_{p=1}^{P}\sum_{k=0}^{K} c_{q,p,k}^{(\ell)} T_k\big(\tanh(x_p^{(\ell)})\big)\right), \qquad \ell = 0,\ldots,L-1, \tag{12}$$

with the network output

$$\hat{f}(\mathbf{x}) = \mathbf{W}^{\mathrm{out}}\,\mathbf{x}^{(L)} + \mathbf{b}^{\mathrm{out}}, \tag{13}$$

where $\mathbf{x}^{(L)} = [x_1^{(L)},\ldots,x_{H_L}^{(L)}]^\top$. The inter-layer tanh in (12) acts as a contraction, curbing gradient growth [49], while the linear head (13) isolates the final mapping from additional polynomial expansions, improving stability in inverse and PDE learning tasks [65].

Depth Stabilization. Deep Chebyshev KANs often become unstable. Rigas et al. [262][16] mitigate this with a *basis-agnostic Glorot-style initialization* that preserves activation variance, and a *Residual–Gated Adaptive (RGA) KAN* block that stabilizes deep cPIKANs on PDEs. *One-liner: variance-preserving init + residual gating enable deep Chebyshev KANs to train without divergence.*

Summary. Chebyshev-based KANs combine spectral approximation theory with practical stability mechanisms. Their global orthogonality and efficient recursion yield compact and interpretable representations, while nested nonlinearities and grid-averaged normalization ensure stable deep training. These features make them particularly well suited for scientific computing, operator learning, and inverse problems—complementing and often surpassing spline-based KANs within the broader KAN framework.

6.3 ReLU

ReLU–based KANs (ReLU-KANs) were introduced by Qiu et al. [123][17] as a hardware–efficient alternative to B-spline KANs. The key idea is to replace spline activations with compactly supported, bell–shaped functions constructed from ReLU compositions. This preserves the localized, compositional spirit of Kolmogorov–Arnold models while enabling fast, GPU–friendly primitives.

Local ReLU bases and univariate maps. In ReLU-KANs, each univariate map $\varphi : \mathbb{R} \to \mathbb{R}$ is a weighted sum of compact local bases:

$$\varphi(x) = \sum_{i=0}^{G+k-1} w_i\, R_i(x),$$

where $w_i \in \mathbb{R}$ are trainable weights, G is the number of grid intervals, and k controls overlap among neighboring bases. Each R_i is supported on $[s_i, e_i]$ with uniformly spaced endpoints

$$s_i = \frac{i-k}{G}, \qquad e_i = s_i + \frac{k+1}{G}, \quad i = 0,\ldots,G+k-1.$$
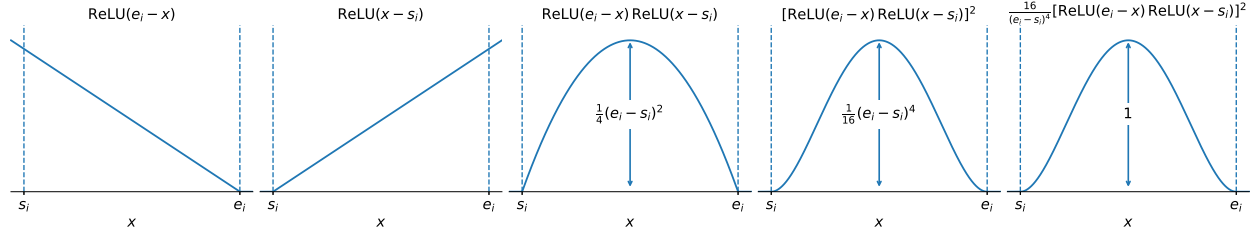
---

[16]https://github.com/srigas/RGA-KANs
[17]https://github.com/quiqi/relu_kan

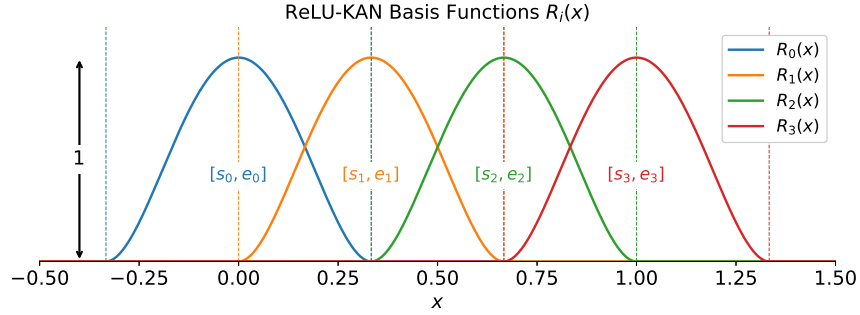Inside its support, R_i has a smooth bell shape (Figure 3):

$$R_i(x) = \begin{cases} 0, & x < s_i, \\ \left((x - s_i)(e_i - x)\right)^2 \dfrac{16}{(e_i - s_i)^4}, & s_i \le x \le e_i, \\ 0, & x > e_i, \end{cases}$$

which can be written equivalently using squared ReLUs:

$$R_i(x) = \left[\mathrm{ReLU}(e_i - x)\, \mathrm{ReLU}(x - s_i) \right]^2 \cdot \frac{16}{(e_i - s_i)^4}, \qquad \mathrm{ReLU}(x) = \max(0, x).$$

(a) Step-by-step construction of ReLU basis

(b) Complete set of normalized ReLU–KAN basis functions

Figure 3: (a) Step-by-step construction of the normalized ReLU-based local basis function from its constituent $\mathrm{ReLU}(e_i - x)$ and $\mathrm{ReLU}(x - s_i)$ terms. (b) Complete set of normalized ReLU–KAN basis functions $R_i(x)$ with supports $[s_i, e_i]$ [123].

Speed and a smoothness caveat. ReLU-KANs often train 5–20× faster than spline variants in practice [123], but the squared–ReLU construction has limited smoothness, which can hinder PDE tasks requiring higher–order derivatives.

Higher–order ReLU KAN (HRKAN). So et al. [133] generalize the squared–ReLU basis by introducing *local* powers of ReLU. For a finite interval $[s_i, e_i]$, the basis function of order m is

$$v_{m,i}(x) = \left[\mathrm{ReLU}(x - s_i)\, \mathrm{ReLU}(e_i - x) \right]^m \cdot \left(\frac{2}{e_i - s_i} \right)^{2m},$$

where $\mathrm{ReLU}(x) = \max(0, x)$ and $m \in \mathbb{Z}_+$ controls the interior smoothness: $v_{m,i} \in C^{m-1}$. Larger m produces lobes that are more peaked in the interior and decay more smoothly to zero at the boundaries, leading to higher continuity of derivatives and potentially better performance for PDEs that require smooth high-order derivatives.

Figure 4 compares individual basis functions $v_{m,i^\star}$ over $[s_{i^\star}, e_{i^\star}]$. Panel (a) shows the squared–ReLU case ($m = 2$), which is C^1 but exhibits visible jumps in the second derivative at the boundaries. Panel (b)

18

shows a higher–order ReLU with $m = 4$, which is C^3 and decays smoothly to zero, eliminating derivative discontinuities. This single-basis view makes clear how increasing m improves both interior smoothness and boundary regularity.
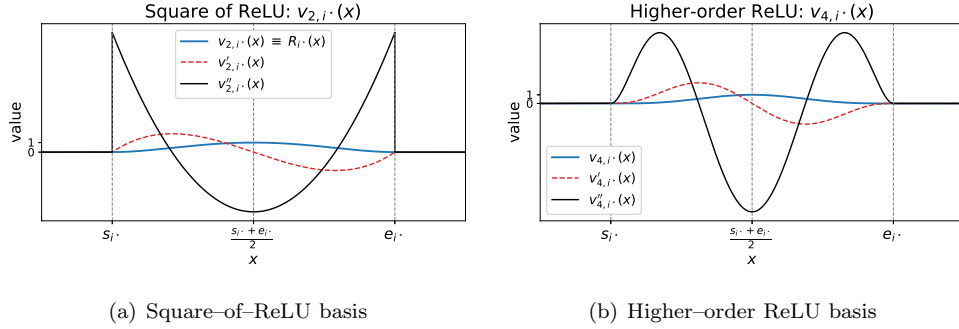

(a) Square–of–ReLU basis

(b) Higher–order ReLU basis

Figure 4: Symbolic basis on $[s_{i^\star}, e_{i^\star}]$: (a) $v_{2,i^\star}(x)$ with first and second derivatives; (b) $v_{4,i^\star}(x)$ with first and second derivatives. Observation: $v_{m,i}$ is globally C^{m-1} (with the m-th derivative discontinuous at $s_{i^\star}, e_{i^\star}$); hence $v_{4,i^\star}$ (C^3) offers smoother higher-order derivatives than $v_{2,i^\star}$ (C^1) [133].

Figure 5 compares synthesized activations

$$\varphi(x) \;=\; \sum_i c_i\, v_{m,i}(x),$$

constructed from the two basis types using *identical random coefficients* ($G = 3$, $k = 1$) over support of $[s_{i^\star}, e_{i^\star}] = [-0.6, 1]$. Because the coefficients are shared, differences between the dashed ($m = 2$) and solid ($m = 4$) curves arise solely from the change in m. The higher-order case produces narrower, more sharply peaked bumps with smoother interior derivatives, while the squared–ReLU case yields broader lobes with lower differentiability. Together with Figure 4, this demonstrates both the *local* and *global* effects of the order parameter m in HRKAN.
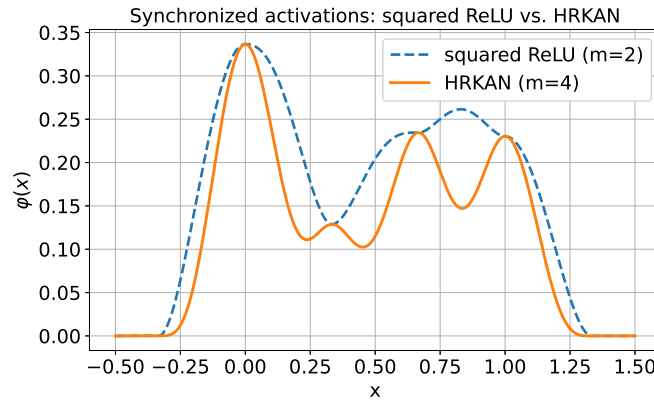

Figure 5: Synthesized activation $\varphi(x)$ from ReLU-KAN bases using shared random coefficients. Dashed: squared–ReLU basis ($m = 2$), Solid: higher–order ReLU basis ($m = 4$). Higher order yields sharper, smoother lobes while preserving the same coefficient structure.

Both ReLU-KAN and HRKAN originally used fixed, uniformly spaced grids. To add adaptivity, Rigas et al. [118][18] define bases over a nonuniform, data–dependent grid $\mathcal{G} = \{x_0, \ldots, x_G\}$. With neighborhood

---

[18]https://github.com/srigas/jaxKAN

19

parameter p,
$$s_i = \mathcal{G}[i] - \tfrac{1}{2}\big(\mathcal{G}[i+p] - \mathcal{G}[i-p]\big), \qquad e_i = 2\mathcal{G}[i] - s_i.$$

Adaptive widths and centers improve resolution in regions with singularities, steep gradients, or boundary layers; their `jaxKAN` implementation also uses resampling and loss reweighting for heterogeneous PDEs.

6.4 Jacobi and General Polynomials

Polynomial families constitute one of the most general and historically established classes of basis functions in KANs. Beyond splines and Chebyshev polynomials, a comprehensive benchmark by Seydi [138][19] systematically evaluated *eighteen* distinct polynomial families as KAN activation functions, offering a unified comparison across orthogonal, recurrence-based, and rational constructions. Among all tested variants, the *Gottlieb* polynomial achieved the highest accuracy and stability metrics on the MNIST benchmark. The surveyed families can be grouped according to their mathematical origin:

- **Classical and General Orthogonal Polynomials:** Charlier and Gottlieb (discrete orthogonal), Boas–Buck and Boubaker (generalized continuous families encompassing Hermite, Laguerre, and related forms).

- **Advanced Orthogonal Polynomials (Askey Scheme & Related):** Askey–Wilson and Al–Salam–Carlitz (q-orthogonal series), Bannai–Ito (Racah generalization).

- **Recurrence-Based and Number-Theoretic Polynomials:** Tribonacci, Tetranacci, Pentanacci, Hexanacci, Heptanacci, and Octanacci (generalized Fibonacci-type recurrences); Fermat, Vieta–Pell, and Narayana (number-theoretic families).

- **Rational Constructions:** Padé approximants [128], explicitly adopted in the rational Jacobi network (rKAN).

- **Holomorphic Monomial Polynomials:** Simple powers $(1, z, \ldots, z^P)$, where $z = x + i\,y$ denotes the complex input, as used in PIHKAN [255].

Overall, Seydi's benchmark revealed that KAN layers can flexibly host a wide variety of polynomial structures beyond splines, broadening the design space for architectures targeting spectral, combinatorial, or rational approximation behaviors. Among these, orthogonal and number-theoretic polynomials—particularly Gottlieb—exhibited the best numerical conditioning and convergence stability. These insights motivate the deeper exploration of Jacobi-type formulations discussed below, since Jacobi, Legendre, and Chebyshev families together form the classical orthogonal polynomial hierarchy within the Askey scheme.

Fractional Jacobi Basis (fKAN). To enhance smoothness, domain flexibility, and adaptivity, Aghaei introduced the *Fractional KAN (fKAN)* [127][20], employing fractional-order Jacobi polynomials as trainable univariate maps:
$$P_n^{(\alpha,\beta)}(z_\gamma), \qquad z_\gamma = \phi_\gamma(x) = 2\,x^\gamma - 1, \quad x \in [0,1],$$

where $\alpha, \beta > -1$ are Jacobi exponents and $\gamma > 0$ is a fractional warp parameter controlling the domain stretch. The basis remains orthogonal on the canonical interval $[-1, 1]$, and different (α, β) recover classical cases: Legendre for $(0,0)$, Chebyshev of the first kind for $(-\tfrac{1}{2}, -\tfrac{1}{2})$, and Chebyshev of the second kind for $(\tfrac{1}{2}, \tfrac{1}{2})$, as illustrated in Fig. 6.

In fKAN, the univariate activation is expressed as
$$\varphi(x) = P_n^{(\alpha,\beta)}\big(\phi_\gamma(\,x(r)\,)\big),$$

where r is the raw input, $x(r) \in [0,1]$ denotes a normalization map (linear, sigmoid, or $\tfrac{1}{2}(1 + \tanh r)$), and $\phi_\gamma(x) = 2x^\gamma - 1$ applies fractional warping. The parameters α, β, γ are trainable, and positivity of α, β

---

[19]https://github.com/seydi1370/Basis_Functions
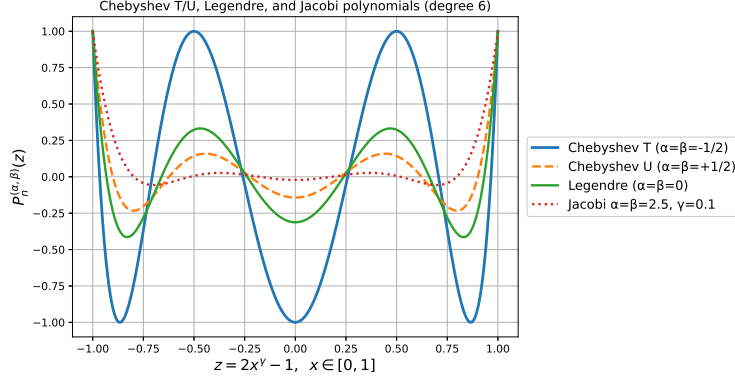[20]https://github.com/alirezaafzalaghaei/fKAN

Figure 6: Degree-$n = 6$ polynomials on $z \in [-1, 1]$: Chebyshev $T_6(z)$, Chebyshev $U_6(z)$, Legendre $P_6(z)$, and Jacobi $P_6^{(2.5, 2.5)}(z)$. The Chebyshev–T curve coincides with $T_6(z)$ in Fig. 2(a).

is enforced via ELU or sigmoid reparameterizations. This yields a globally smooth and tunable basis that performs effectively on regression and PDE benchmarks. Kashefi [70] implements fKAN using the tanh-based normalization $x(r) = \frac{1}{2}(1 + \tanh r)$ for stable input scaling.

Effect of Input Normalization. Implementations typically evaluate $P_n^{(\alpha, \beta)}(z_\gamma)$ with $z_\gamma = 2\,x(r)^\gamma - 1$. Figure 7 illustrates how the normalization choice shapes the activation. Fixing $(\alpha, \beta) = (2.5, 2.5)$, $n = 2$, and $\gamma = 0.1$, a linear mapping preserves dynamic range but produces steep edge slopes, whereas sigmoid and $\frac{1}{2}(1 + \tanh r)$ compress the tails, improving conditioning. A smaller $\gamma < 1$ increases the warp toward $+1$, further sharpening features near that end of the domain.
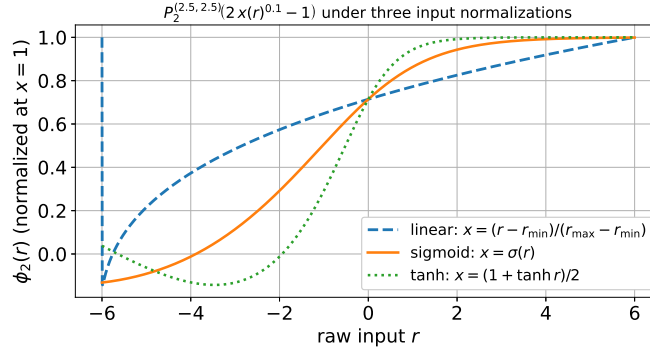

Figure 7: Degree-$n = 2$ Jacobi polynomial with $(\alpha, \beta) = (2.5, 2.5)$, $\gamma = 0.1$: $\varphi(r) = P_2^{(\alpha, \beta)}(2\,x(r)^\gamma - 1)$ under three normalizations $x(r) \in [0, 1]$: linear $x = (r - r_{\min})/(r_{\max} - r_{\min})$ (dashed), sigmoid $x = \sigma(r)$, and tanh-based $x = \frac{1}{2}(1 + \tanh r)$. All curves are rescaled by $\varphi(r{=}1)$ for comparability.

Rational Extensions (rKAN). To further expand expressivity, Aghaei proposed the *Rational KAN (rKAN)* [128][21], which generalizes fKAN by incorporating rational Jacobi compositions. Two representative variants are:

- **Padé–rKAN:** a rational quotient of Jacobi expansions,

$$\varphi(x) = \frac{\sum_{i=0}^{p} w_i^{(P)} P_i^{(\alpha_p, \beta_p)}\big(\phi(\sigma(x))\big)}{\sum_{j=0}^{q} w_j^{(Q)} P_j^{(\alpha_q, \beta_q)}\big(\phi(\sigma(x))\big)},$$

---

where $w_i^{(P)}$ and $w_j^{(Q)}$ are trainable weights, and $\sigma(x)$ is an activation function.

- **Jacobi–rKAN:** a rational domain warping approach,

$$\varphi(x) = P_n^{(\alpha,\beta)}\big(\phi(x;\iota)\big),$$

  with $\phi(x;\iota)$ representing a rational transform parameterized by $\iota > 0$ (often implemented using SoftPlus for positivity).

Both fKAN and rKAN exploit Jacobi polynomials with adaptive shape and domain parameters: fKAN emphasizes fractional-order smoothness and controlled warping, while rKAN introduces rational expressivity and sharper nonlinear transitions.

Classical Fixed-Degree Jacobi KANs. Several works retain fixed polynomial degrees ($\gamma = 1$) and use only tanh input compression into $[-1, 1]$. Each univariate activation is then represented as

$$\varphi_{ij}^{(l)}(x) = \sum_{k=0}^{K} c_{k,ij}^{(l)}\, P_k^{(\alpha,\beta)}\big(\tanh(x)\big),$$

with trainable coefficients $c_{k,ij}^{(l)}$ and often fixed (α, β). Kashefi [70][22] reported that low-degree expansions ($K = 2$) with Chebyshev-like parameters $\alpha = \beta = -0.5$ achieve an optimal balance between accuracy and numerical stability, suppressing Runge oscillations in inverse PDEs with sparse boundary data. Shukla et al. [37] applied the same formulation within a PIKAN framework for high–Reynolds cavity flow, using $(\alpha, \beta) = (1, 1)$ and degrees $K = 3$–8 depending on the regime. While higher degrees increase computational cost, their Jacobi–based PIKANs matched or exceeded conventional PINNs in accuracy.

Building upon this foundation, Xiong et al. [73] proposed the *Jacobian Orthogonal Polynomial–based KAN (J–PIKAN)*, enforcing explicit orthogonality among polynomial components to ensure stable layerwise synthesis and interpretable coefficient updates. Leveraging the three-term recurrence of Jacobi polynomials, J–PIKAN efficiently evaluates higher-degree expansions and maintains numerical stability. Using fluid-dynamics benchmarks, their study compared B-spline, Fourier, Hermite, Legendre, Chebyshev, and Jacobi bases within a unified physics-informed framework, identifying Jacobi bases with moderate parameters ($\alpha = \beta \approx 2$) as offering the best compromise between accuracy, conditioning, and convergence rate.

In parallel, Zhang et al. [74][23] examined the Legendre specialization $(\alpha, \beta) = (0, 0)$ within Jacobi-based KANs, demonstrating favorable conditioning and rapid convergence for physics-informed PDE solvers. A complementary direction is offered by the Adaptive PolyKAN [280], which treats the polynomial degree as a trainable parameter, enabling the model to adjust its functional complexity dynamically over the course of training.

Summary. Jacobi-based KANs form a versatile and mathematically rich subclass within polynomial KANs. Classical (fixed-degree) variants emphasize numerical stability and geometric fidelity, while fractional (fKAN) and rational (rKAN) extensions introduce adaptive domain warping and enhanced expressivity. Together, they provide a cohesive Jacobi toolkit—bridging spectral approximation, rational modeling, and physics-informed learning within the broader KAN framework.

6.5   Gaussian (RBF)

As researchers sought to improve the efficiency and performance of the original B–spline–based KANs, the *Gaussian radial basis function (RBF)* emerged as a powerful and computationally elegant alternative. Its smooth, localized, and infinitely differentiable nature makes it an excellent choice for representing univariate

---

[22]https://github.com/Ali-Stanford/KAN_PointNet_CFD
[23]https://github.com/zhang-zhuo001/Legend-KINN

activation functions along the edges of a KAN. Across recent studies [54, 116, 119, 120, 142, 231], Gaussian–based activations have appeared in several formulations—ranging from fixed–grid hybrids to fully learnable and reflectional variants—each striking a different balance between stability, adaptivity, and efficiency.

Foundational Gaussian Layer. The fundamental univariate Gaussian basis function is defined as

$$\varphi(x; c, \varepsilon) = \exp\left[-\left(\tfrac{x-c}{\varepsilon}\right)^2\right], \tag{14}$$

where c is the center and $\varepsilon > 0$ is the width (shape parameter). A general univariate activation is then constructed as a linear combination

$$\phi(x) = \sum_{i=0}^{G-1} w_i \, \varphi(x; g_i, \varepsilon), \tag{15}$$

with trainable coefficients w_i and equispaced grid centers $g_i \in [a, b]$. This formulation replaces the piecewise polynomial behavior of splines with globally smooth Gaussian features while retaining locality and analytical gradients.

Hybrid Gaussian–Residual Formulation (Fixed Grid).

Gaussian RBFs are a fast, smooth alternative to B–splines for KAN activations. The key observation is that cubic B–splines can be closely approximated by scaled Gaussians. Li et al. [119][24] proposed *FastKAN*, replacing the cubic B–spline $\mathcal{B}_3(x - c_i)$ with

$$\mathcal{B}_3(x - c_i) \approx \lambda \exp\left[-\left(\tfrac{x-c_i}{\sigma}\right)^2\right], \tag{16}$$

where $\lambda \in \mathbb{R}$ is a scaling constant and $\sigma \approx h$ matches the grid spacing. As shown in Figure 8, this preserves spline-like locality and smoothness while reducing computational cost.
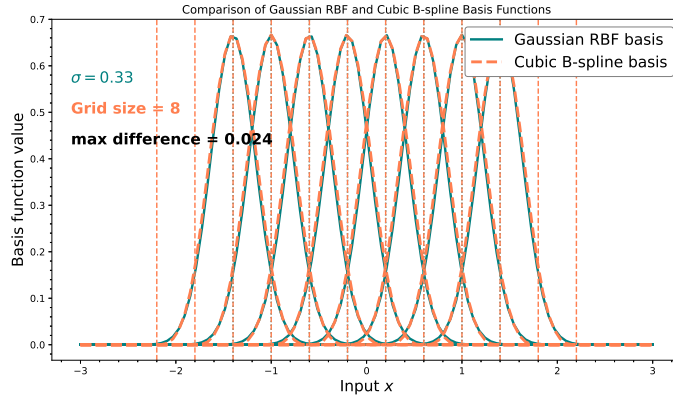

Figure 8: Comparison of cubic B–spline basis functions $\mathcal{B}_3(x)$ (non-extended) and Gaussian RBFs $\exp[-((x - c_i)/\sigma)^2]$ with matched grid spacing and width.
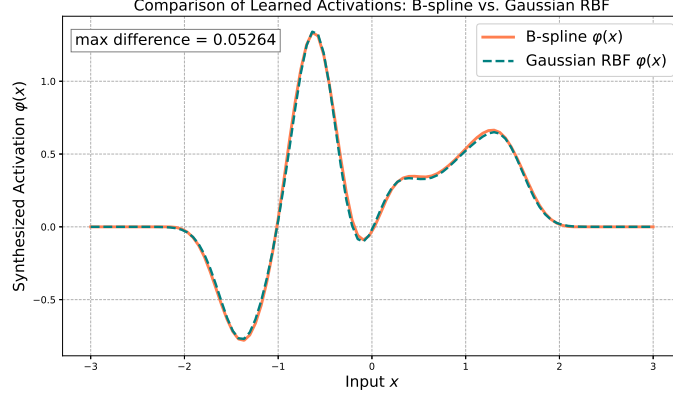
---

[24]https://github.com/ZiyaoLi/fast-kan

Figure 9: Learned univariate activation $\varphi(x)$ synthesized from Gaussian RBF and cubic B–spline bases (Figure 8) using identical random coefficients.

Figure 9 demonstrates that both bases yield nearly identical activation profiles with only minor differences near peaks. Each basis decays smoothly near the boundaries, producing flat tails where support vanishes—confirming Gaussian RBFs as faithful, efficient surrogates for B–splines in KAN layers.

Building upon this foundation, Li [119] introduced the *FastKAN* model, where Gaussian basis functions are combined with a simple residual activation such as SiLU (Swish) to form a hybrid composite activation:

$$\Phi(x) = \underbrace{\sum_{i=0}^{G-1} w_i \, \exp\left[- \left(\tfrac{x - g_i}{\varepsilon} \right)^2 \right]}_{\text{RBF component}} + w_b \, \sigma(x), \tag{17}$$

where $\sigma(x)$ is a base activation and $w_b \in \mathbb{R}$ modulates its contribution. The Gaussian component captures local variations, while the residual stabilizes optimization and accounts for global trends. Here, both the grid $\{g_i\}$ and bandwidth $\varepsilon = \frac{b-a}{G-1}$ are fixed, ensuring efficient and stable evaluation. This configuration, later adopted in LeanKAN [142] and RBFKAN [116], represents a strong, stable baseline for Gaussian–based KANs.

Pure RBF Layers with Learnable Centers. A more flexible RBF formulation appears in the DeepOKAN architecture of Abueidda et al. [54][25], where Gaussian bases are used in *both branch and trunk* networks. Each activation takes the form

$$\varphi(x) = \exp\left[-\left(\tfrac{x - g_j}{\beta}\right)^2\right], \tag{18}$$

with trainable centers g_j and width $\beta > 0$. The layer update is

$$x_{l+1} = W_l \, \varphi(x_l; G_l, \beta), \tag{19}$$

allowing the RBFs to migrate toward regions of high variation. In contrast to some later operator-learning studies, Abueidda et al. report that RBF–KANs resolve *high-frequency* sinusoidal fields with markedly higher accuracy than MLPs, confirming the strong approximation capability of Gaussian bases in mechanics problems.

A complementary conclusion arises in the recent two-step DeepOKAN for bubble dynamics [143]: while RBFs remain effective in the branch network, spline bases outperform them in the trunk for extremely high-frequency, high-amplitude oscillations. Together, these works show that RBFs are highly competitive for moderate-to-high frequency regimes, but basis choice in KAN operator networks remains problem-dependent.

---

[25]https://github.com/DiabAbu/DeepOKAN

Reflectional Gaussian Approximations (RSWAF). To further reduce computational cost, several works have replaced the exponential kernel with an algebraically similar *Reflectional Switch Activation Function (RSWAF)* proposed by Delis [120][26] and extended in Bühler et al. [231]. This activation approximates the Gaussian bell using the hyperbolic–secant squared function:

$$\varphi_{\text{RSWAF}}(x; c, h) = 1 - \tanh^2\left(\tfrac{x-c}{h}\right) = \text{sech}^2\left(\tfrac{x-c}{h}\right), \tag{20}$$

which preserves reflectional symmetry and smooth decay. Both the centers c_i and widths h_i may be fixed or trainable, controlled by configuration flags (e.g., `train_grid`, `train_inv_denominator`) in implementations such as *FasterKAN* [120]. The full activation is often expressed as

$$\phi(x) = \sum_i w_i \, s_i \left[1 - \tanh^2\left(\tfrac{x-c_i}{h_i}\right)\right], \tag{21}$$

where w_i are learnable amplitudes, s_i are reference scaling factors, and both c_i and h_i evolve during training. This formulation yields a localized, computationally efficient surrogate that mimics Gaussian curvature while offering explicit control over both shape and location.

Hybrid and Unified Gaussian Extensions. Koenig et al. [142][27] proposed a hybrid activation that mixes RBFs with a base nonlinearity:

$$\phi(x) \;=\; \sum_{i=1}^{N} w_i \, \varphi(x - c_i) \;+\; w_b \, b(x), \tag{22}$$

where $\varphi(\cdot)$ is a Gaussian RBF, $b(x)$ is a base activation (e.g., Swish or linear), and w_b modulates its contribution. Related implementations such as *RBFKAN* [116][28] also apply simple min–max normalization,

$$x_{\text{norm}} \;=\; \frac{x - x_{\text{min}}}{x_{\text{max}} - x_{\text{min}}}, \tag{23}$$

to stabilize input scaling.

The *BSRBF–KAN* model [40][29] unifies B–splines and Gaussian RBFs within a single layer:

$$\text{BSRBF}(x) \;=\; w_b \, b(x) \;+\; w_s \big(\text{BS}(x) + \text{RBF}(x)\big), \tag{24}$$

where $\text{BS}(x)$ and $\text{RBF}(x)$ are evaluated at identical grid locations, and $w_b, w_s \in \mathbb{R}$. This configuration inherits the local compactness of B–splines and the global smoothness of Gaussian functions.

Complex–Valued Gaussian Extensions. In the complex domain, Wolff et al. [129][30] introduced the *Complex–Valued KAN (CVKAN)*, extending FastKAN with concepts from complex–valued neural networks (CVNNs) [232]. The residual pathway uses a complex SiLU activation:

$$b_{\mathbb{C}}(z) = \text{CSiLU}(z) = \text{SiLU}(\text{Re}(z)) + i \, \text{SiLU}(\text{Im}(z)), \tag{25}$$

and the Gaussian RBF is generalized to complex inputs [233]:

$$\text{RBFC}(z) = \sum_{i=1}^{N} w_i \, \varphi(|z - c_i|), \qquad c_i \in \mathbb{C}, \; w_i \in \mathbb{C}. \tag{26}$$

The resulting activation combines both terms with a bias term:

$$\phi(z) = w_s \, \text{RBFC}(z) + w_b \, b_{\mathbb{C}}(z) + \beta, \qquad \beta \in \mathbb{C}. \tag{27}$$

---

[26] https://github.com/AthanasiosDelis/faster-kan
[27] https://github.com/DENG-MIT/LeanKAN
[28] https://github.com/sidhu2690/RBF-KAN
[29] https://github.com/hoangthangta/BSRBF_KAN
[30] https://github.com/M-Wolff/CVKAN

More recently, Che et al. [234] extended this formulation by introducing a *ModELU–based CVKAN*, replacing the split–type CSiLU with a modulus–preserving residual and learnable RBF shape parameters, supported by a formal complex–valued Kolmogorov–Arnold theorem.

Practical caveat: the shape parameter. Gaussian RBF performance is highly sensitive to the width parameter (ε), which governs both smoothness and conditioning [200–202]. Even small changes can strongly impact accuracy and numerical stability [203–205]. From a kernel–theoretic perspective, this sensitivity reflects an *uncertainty principle*: larger shape (width) parameters produce flatter, globally correlated kernels that improve smoothness and accuracy but worsen conditioning, whereas smaller parameters yield well–conditioned, highly localized bases at the expense of approximation power [198,199]. While heuristic tuning and learnable widths (as in FastKAN and DeepONet–RBF variants) offer partial remedies, robust and theoretically guided selection of this parameter remains an active research problem at the intersection of kernel methods and neural approximation.

Summary. Gaussian–based KANs form a versatile class of architectures bridging spline–based and kernel–theoretic perspectives. Starting from fixed equispaced Gaussian grids [119,142], through adaptive RBF layers with learnable centers [54], to reflectional Gaussian and complex–valued extensions [120,129,231,234], these models collectively demonstrate how Gaussian basis functions can serve as both efficient computational surrogates and expressive functional primitives within the KAN framework.

6.6 Fourier

Fourier features provide global, smooth, periodic expressivity that complements localized bases (e.g., B–splines, RBFs). Within the KAN family, Fourier–based KANs replace the univariate edge functions with harmonic expansions, retaining the KAN wiring while improving spectral resolution on tasks with strong periodic structure [134]. By contrast, Fourier networks such as FAN are *not* KANs: they embed cosine–sine transforms directly into each layer as a drop-in MLP replacement, targeting efficient periodicity modeling (often with reduced parameters/FLOPs) and stronger in-/out-of-domain generalization [137][31]. We mention FAN here as a related spectral approach; our focus remains on Fourier features used *inside* KANs.

Standard FourierKAN. In the baseline FourierKAN architecture [125][32], each univariate mapping is expressed as a truncated Fourier series,

$$\varphi(x) = \sum_{k=1}^{K} \big(a_k \cos(kx) + b_k \sin(kx) \big), \tag{28}$$

with learnable coefficients $a_k, b_k \in \mathbb{R}$ and cutoff frequency $K \in \mathbb{N}$. Cosines capture even–symmetric modes; sines capture odd–symmetric modes. The resulting $\varphi(x)$ is a flexible global harmonic mixture, well–suited to periodic or high–frequency structure. Guo et al. [160] adopt this classical truncated Fourier formulation, using fixed integer harmonics with trainable sine–cosine coefficients.

Random Fourier features. A limitation of (28) is the fixed set of frequencies $k = 1, \ldots, K$. Zhang et al. [71][33] propose the *Kolmogorov–Arnold–Fourier Network* (KAF), replacing fixed bases with a learnable spectral embedding via Random Fourier Features (RFF):

$$\psi_{\mathrm{RFF}}(\mathbf{x}) = \sqrt{\tfrac{2}{m}} \big[\cos(\mathbf{x}W + \mathbf{b}),\ \sin(\mathbf{x}W + \mathbf{b}) \big] \in \mathbb{R}^{2m}, \tag{29}$$

where $W \in \mathbb{R}^{d_{\mathrm{in}} \times m}$ is a trainable frequency matrix and $\mathbf{b} \in \mathbb{R}^m$ is a learnable phase vector. KAF then blends this adaptive spectral block with a smooth baseline:

$$\varphi(\mathbf{x}) = \boldsymbol{\alpha} \cdot \mathrm{GELU}(\mathbf{x})\ +\ \boldsymbol{\beta} \cdot V\, \psi_{\mathrm{RFF}}(\mathbf{x}), \tag{30}$$

---

[31] https://github.com/YihongDong/FAN
[32] https://github.com/GistNoesis/FourierKAN
[33] https://github.com/kolmogorovArnoldFourierNetwork/KAF

with $\boldsymbol{\alpha}, \boldsymbol{\beta} \in \mathbb{R}^{d_{\text{in}}}$ and $V \in \mathbb{R}^{d_{\text{in}} \times 2m}$. The GELU term captures low–frequency structure, while the RFF term adaptively models higher–frequency content throughout training. This continuous frequency control improves regression/classification where global and local patterns coexist [71].

Figure 10 compares a Gaussian (RBF) kernel slice with both random Fourier features (29) and a truncated Fourier expansion using the full cosine–sine basis. Settings match the code: one-dimensional grid $x \in [-3\varepsilon, 3\varepsilon]$ with $\varepsilon = 1.0$. The RFF map uses the unbiased scaling $1/\sqrt{m}$. With this setting, increasing m makes the RFF curve visually coincide with the Gaussian slice—clearly showing how the two are connected in practice. The Fourier expansion (28), constructed from fixed integer harmonics $\{\cos(k\gamma x), \sin(k\gamma x)\}_{k=1}^{K}$, remains strictly periodic, so its kernel slice differs structurally from the Gaussian, in contrast to RFF where frequencies are sampled from a Gaussian distribution.
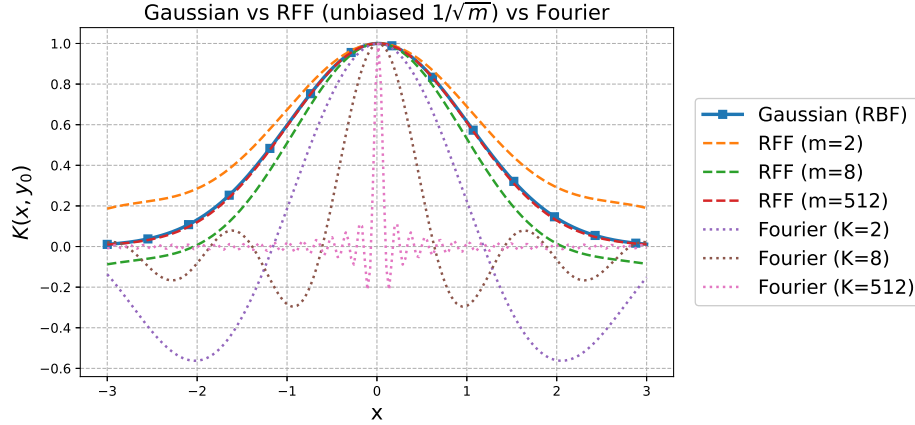

Figure 10: Gaussian (RBF) kernel slice compared with Random Fourier Features (RFF, (29)) and a truncated Fourier expansion (28). RFF uses the unbiased scaling $1/\sqrt{m}$ with both cos and sin terms, so that the diagonal kernel value is close to 1. As m increases, the RFF slice aligns with the Gaussian, while the Fourier expansion (fixed integer harmonics) retains its periodic structure.

In addition to classical Fourier-based designs, Jiang et al. [51][34] propose the quantum-inspired Kolmogorov–Arnold Network (QKAN), where each univariate map is realized by a data re-uploading variational quantum circuit. These circuits naturally generate Fourier-like expansions with exponentially scalable frequency modes, offering parameter-efficient alternatives to grid-based Fourier KANs while retaining the structured interpretability of classical KANs.

Summary. Fourier–based KANs—via deterministic truncations or randomized spectral embeddings—inject global harmonic structure into KAN layers. Compared with local polynomial bases such as B–splines, these global bases are particularly effective for smooth periodicities or problems with broad spectral support.

6.7 Wavelet

Wavelet-based KANs (Wav-KANs) extend the KAN framework by using *localized* wavelet bases, enabling multiscale representation and spatial adaptivity—especially useful for heterogeneous or hierarchical data. The architecture was introduced by Bozorgasl et al. [139][35] and draws on both the Continuous Wavelet Transform (CWT) and Discrete Wavelet Transform (DWT).

In wavelet analysis, a signal $g(t) \in L^2(\mathbb{R})$ is decomposed via scaled/translated copies of a mother wavelet $\psi(t)$. The CWT is defined [208, 209] as

$$C(s, \tau) = \int_{-\infty}^{\infty} g(t) \frac{1}{\sqrt{s}} \psi\left(\frac{t - \tau}{s}\right) dt, \tag{31}$$

---

[34]https://github.com/Jim137/qkan
[35]https://github.com/zavareh1/Wav-KAN

where $s > 0$ is the scale and $\tau \in \mathbb{R}$ is the translation. The discrete analog used in signal processing is the DWT:

$$a_j(k) \;=\; \sum_n g(n)\,\phi_{j,k}(n), \qquad d_j(k) \;=\; \sum_n g(n)\,\psi_{j,k}(n), \tag{32}$$

with $\phi_{j,k}$ and $\psi_{j,k}$ the scaling and wavelet functions at resolution level j and position k.

Wavelet activations in KAN layers. Wav-KAN embeds analytic wavelet functions directly into univariate edge functions. Each activation is parameterized by scale s and translation u:

$$\varphi(x) \;=\; \psi\!\left(\frac{x - u}{s}\right),$$

where $\psi(t)$ is chosen from canonical families:

$$\psi_{\mathrm{mex}}(t) = \tfrac{2}{\sqrt{3}\,\pi^{1/4}}(1 - t^2)\,e^{-t^2/2}, \tag{33}$$

$$\psi_{\mathrm{mor}}(t) = \cos(\omega_0 t)\,e^{-t^2/2}, \quad \omega_0 = 5, \tag{34}$$

$$\psi_{\mathrm{dog}}(t) = -t\,e^{-t^2/2}. \tag{35}$$

To compare expressivity across wavelet families, we form synchronized linear combinations

$$\varphi(t) \;=\; \sum_{j=1}^{M} c_j\,\psi(t - \mu_j),$$

using the same coefficients $\{c_j\}$ and centers $\{\mu_j\}$ for each ψ. Figure 11 shows three canonical wavelets (Mexican Hat, Morlet, DoG) centered at $t = 0$. Using these bases, Figure 12 presents the synthesized activations $\varphi(t)$ built with identical $\{c_j\}$ and $\{\mu_j\}$. The Morlet activation exhibits higher-frequency oscillations, whereas Mexican Hat and DoG yield smoother bell-shaped profiles. Since coefficients are shared, differences arise solely from the intrinsic wavelet shapes.
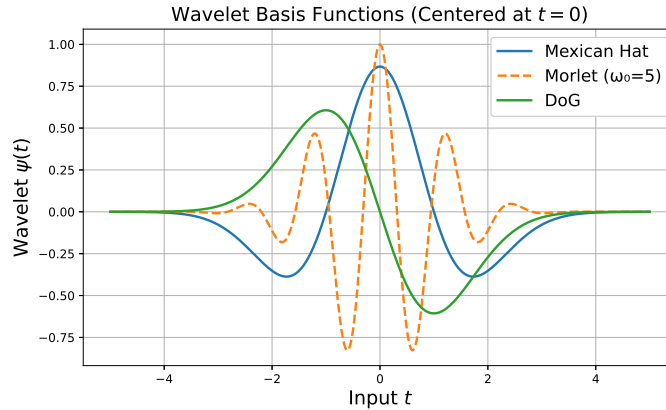

Figure 11: Three wavelet bases centered at $t = 0$: Mexican Hat, Morlet (with $\omega_0 = 5$), and Derivative of Gaussian (DoG). Each has localized support and distinct oscillatory behavior.

Learning s and u per neuron allows Wav-KAN to adapt receptive fields and frequency resolution, aiding generalization in settings with spatially varying feature scales, such as image classification [139].

Patra et al. [191] apply wavelet activations—using a sine–Gaussian basis—to physics-informed training, tuning frequency response to obtain faster data-free convergence on coupled nonlinear PDEs. Meshir et al. [270] complement this with an NTK analysis, showing that the Morlet mother-wavelet frequency (or hidden-layer width) directly controls NTK eigenvalue decay, providing explicit spectral-bias mitigation and strong gains in physics-informed settings (Poisson/Heat/Wave/Helmholtz).
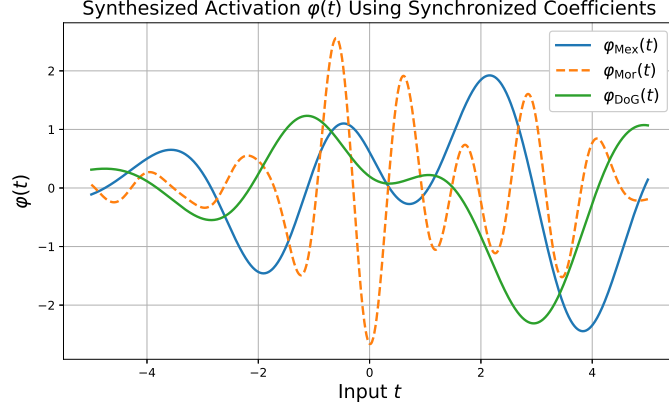
Figure 12: Synthesized activations $\varphi(t) = \sum_{j=1}^{M} c_j \psi(t - \mu_j)$ using synchronized coefficients and centers across wavelet families. Differences in frequency and amplitude follow from each wavelet's intrinsic shape.

Applications further highlight the versatility of wavelet bases: Pratyush et al. [210] employ a DoG wavelet in CaLMPhosKAN for enhanced phosphorylation-site detection, while Seydi et al. [174] combine CWT and DWT for hyperspectral imaging, outperforming spline-KANs and MLPs.

Summary. Wavelet-based KANs provide a flexible multiscale basis whose localized frequency control improves convergence and robustness across PDEs, bioinformatics, and high-dimensional imaging.

6.8   Finite-Basis (FBKANs)

Finite-Basis KANs, introduced by Howard et al. [122][36],[37], extend KANs with a domain-decomposition strategy inspired by finite-basis PINNs (FBPINNs) [211–214]. The key idea is to represent a global mapping as a sum of *local* subnetworks, each modulated by a smooth *partition-of-unity* (PoU) function. This yields scalability, robustness, and improved generalization for multiscale and physics-informed problems.

Let $\Omega \subset \mathbb{R}$ be covered by L overlapping subdomains $\{\Omega_j\}_{j=1}^{L}$. Assign a smooth PoU weight $\omega_j(x)$ to each Ω_j such that [215–217]

$$\text{supp}(\omega_j) = \Omega_j, \qquad \sum_{j=1}^{L} \omega_j(x) \equiv 1 \ \ \forall x \in \Omega.$$

Cosine windows are used to build unnormalized weights $\hat{\omega}_j$, which are then normalized:

$$\omega_j(x) \;=\; \frac{\hat{\omega}_j(x)}{\sum_{k=1}^{L} \hat{\omega}_k(x)}, \tag{36}$$

with

$$\hat{\omega}_j(x) \;=\; \begin{cases} 1, & L = 1, \\ \left[1 + \cos\left(\pi \frac{x - \mu_j}{\sigma_j}\right)\right]^2, & L > 1, \end{cases} \tag{37}$$

and

$$\mu_j \;=\; \frac{l(j-1)}{L-1}, \qquad \sigma_j \;=\; \frac{\delta\, l}{2(L-1)}, \qquad l \;=\; \max(x) - \min(x),$$

where $\delta > 1$ is the overlap ratio controlling the window width.

---

[36]https://github.com/pnnl/neuromancer/tree/feature/fbkans/examples/KANs
[37]https://github.com/pnnl/neuromancer/blob/feature/fbkans/src/neuromancer/modules

29

Each subdomain Ω_j hosts a local KAN, $K_j(x; \boldsymbol{\theta}_j)$, trained only on its region. The global predictor is a smooth PoU-weighted sum of local outputs:

$$f(x) \approx \sum_{j=1}^{L} \omega_j(x) K_j(x; \boldsymbol{\theta}_j), \tag{38}$$

where $\boldsymbol{\theta}_j$ are the local parameters. Within each local KAN, a univariate edge function φ_j is expanded in cubic B-splines:

$$\varphi_j(x) = \sum_{n=0}^{N_j-1} c_{j,n} B_n^{(3)}(x),$$

with trainable coefficients $c_{j,n} \in \mathbb{R}$. The local spline grid is initialized from the effective support of ω_j:

$$a_j = \min\{x \mid \omega_j(x) > \varepsilon\}, \quad b_j = \max\{x \mid \omega_j(x) > \varepsilon\}, \quad \varepsilon = 10^{-4}.$$

To illustrate functional flexibility, Figure 13 shows, on $[-1, 1]$, (A) the PoU weights $\{\omega_j\}_{j=1}^4$ with $\sum_j \omega_j \equiv 1$, and (B) the PoU–weighted decomposition of a single cubic B-spline basis $B_i^{(3)}(x)$. The colored curves are the localized pieces $\omega_j(x) B_i^{(3)}(x)$; their sum coincides with the original basis up to numerical precision. Only windows overlapping the spline support contribute nonzero pieces, so the PoU localizes the representation without changing the underlying spline span.
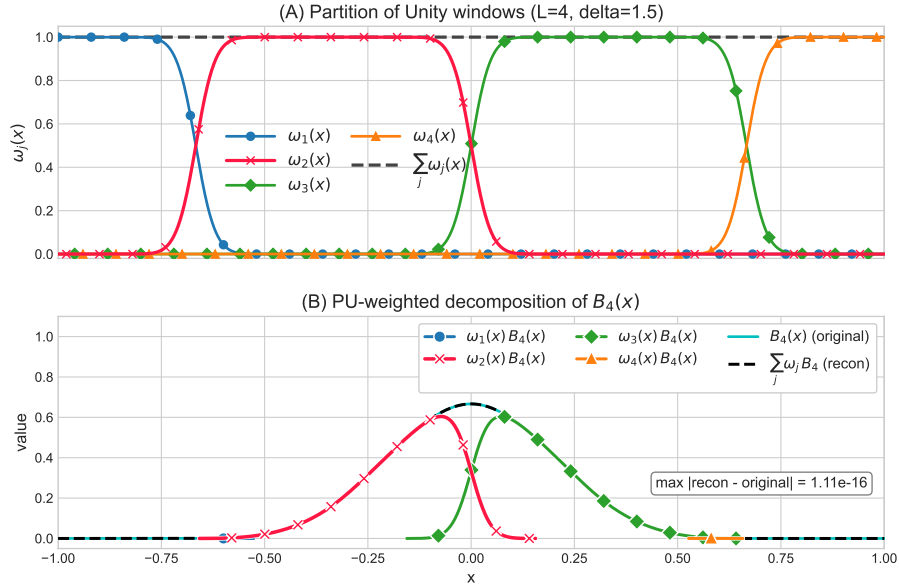

Figure 13: Two-panel illustration of PoU–weighted B-spline decomposition on $[-1, 1]$ ($L = 4$, overlap $\delta = 1.5$). (A) Cosine-based PoU windows $\{\omega_j\}$ summing to one. (B) Decomposition of a cubic B-spline basis $B_i^{(3)}(x)$ into localized pieces $\omega_j(x) B_i^{(3)}(x)$; their sum (black) matches the original basis, confirming $B_i^{(3)}(x) = \sum_{j=1}^{L} \omega_j(x) B_i^{(3)}(x)$.

Summary. FBKANs are practical because they let you model different parts of the domain with specialized sub-KANs, which can be trained independently (and in parallel) to cut memory use and wall time. They work well with physics-informed losses, handle noisy data robustly, and maintain smooth transitions between subdomains without requiring hard boundary constraints. Moreover, because sub-KANs operate on smaller supports, each local kernel matrix is better conditioned—an important advantage for large-scale PDEs.

6.9 SincKAN

To model singularities, sharp gradients, and high-frequency transitions, Yu et al. [49][38] introduced the *Sinc-based KAN* (SincKAN). The building block is the globally supported Sinc kernel

$$\text{Sinc}(x) = \frac{\sin x}{x}, \qquad \text{Sinc}(0) := 1,$$

a classical tool for bandlimited approximation.

A basic SincKAN activation expands a univariate function using uniformly shifted Sinc atoms:

$$\varphi(x) = \sum_{i=-N}^{N} c_i \, \text{Sinc}\left(\frac{\pi}{h}\left(x - ih\right)\right), \tag{39}$$

where $h > 0$ is the step size, $\{c_i\}$ are trainable c oefficients, and N controls the truncation degree (total number of atoms $2N + 1$).

Practical multi–step-size form. To avoid choosing a single "optimal" h and to improve flexibility on finite domains, SincKAN mixes several step sizes and applies a normalized coordinate transform γ^{-1}:

$$\varphi_{\text{multi}}(x) = \sum_{j=1}^{M} \sum_{i=-N}^{N} c_{i,j} \, \text{Sinc}\left(\frac{\pi}{h_j}\left(\gamma^{-1}(x) - ih_j\right)\right). \tag{40}$$

Here $\{h_j\}_{j=1}^{M}$ are (learned or preset) step sizes, M is the number of scales, $c_{i,j}$ are trainable coefficients, and γ^{-1} maps the working interval to $\mathbb{R}$ while normalizing scale. Setting $M=1$ and $\gamma^{-1}(x)=x$ recovers (39).

Figures 14 and 15 show the building blocks and a synthesized activation using a fixed truncation degree $(2N + 1 = 11)$ and spacing $h = 1.0$ over $x \in [-10, 10]$. Figure 14 displays the truncated Sinc dictionary $\{\text{Sinc}(\frac{\pi}{h}(x - kh))\}_{k=-N}^{N}$, whose elements are globally supported and oscillatory with decaying sidelobes. These atoms are linearly combined to form the learned univariate map $\varphi(x)$.
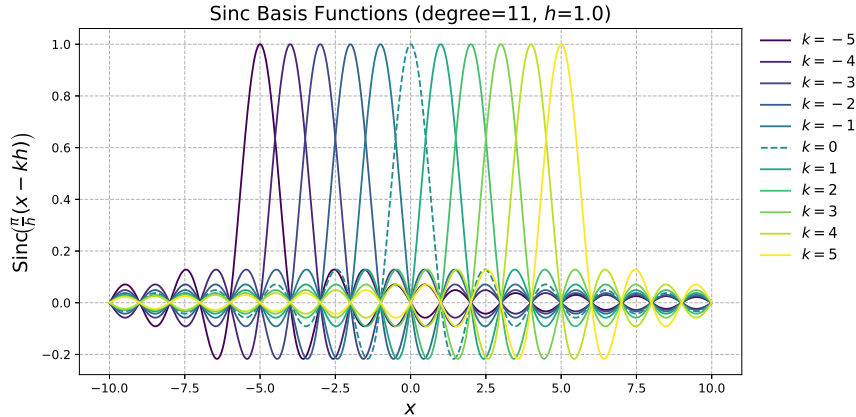

Figure 14: Truncated Sinc basis functions used in SincKAN. Each kernel is centered at $x = kh$ with spacing $h = 1.0$; the total number of shifts is $2N + 1 = 11$. This dictionary underlies the learned univariate map $\varphi(x)$.

Figure 15 plots *synchronized* learned activations

$$\varphi(x) = \sum_{i=-5}^{5} c_i \, \text{Sinc}\left(\frac{\pi}{h}(x - ih)\right)$$

with the same random coefficients $\{c_i\}$, while varying only the step size $h \in \{0.8, 1.0, 1.4\}$. The step size h sets the spacing of Sinc centers and therefore the effective bandwidth: smaller $h \Rightarrow$ denser centers, higher-frequency capacity, more oscillations; larger $h \Rightarrow$ smoother, lower-frequency behavior. Because the coefficients are synchronized, differences across curves reflect only the choice of h.
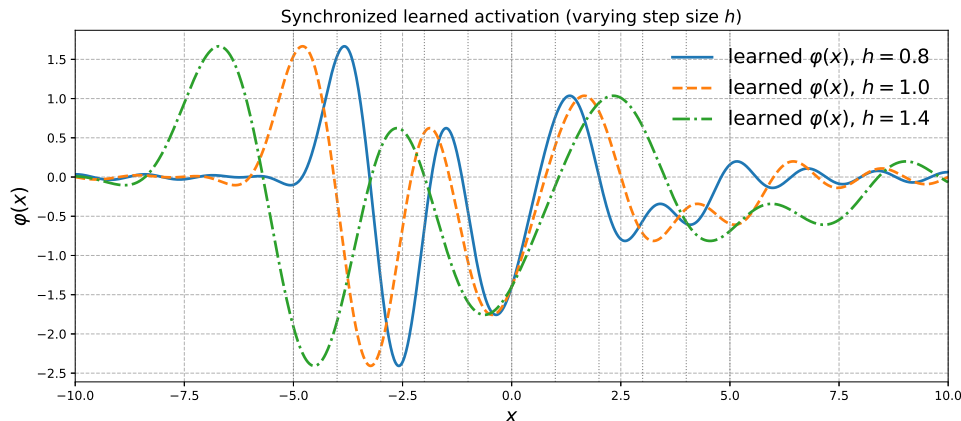

Figure 15: Synchronized learned activations with a pure (non-windowed) Sinc basis (degree $2N + 1 = 11$). The same coefficients $\{c_i\}$ are used for all curves; only the step size h changes ($h \in \{0.8, 1.0, 1.4\}$). Smaller h yields higher-frequency, more oscillatory structure, whereas larger h produces smoother responses. Vertical dotted lines mark the Sinc centers for $h = 1.0$.

For numerical stability, SincKAN applies a coordinate normalization step that maps inputs to a bounded interval (typically $[-1, 1]$) before evaluating the Sinc expansion. This preprocessing, consistent with other KAN variants, improves conditioning and convergence across layers.

7 Accuracy Improvement

We group works by *how* they improve accuracy, independent of task (regression, PINN, DeepONet), basis choice, or efficiency tricks. In most cases the same mechanism transfers across tasks.

To orient the reader, we begin with a compact summary of accuracy–improving mechanisms for KANs. The table groups methods by mechanism and lists concise technique keywords with representative references. The remainder of this section expands on each group in turn, detailing when/why they help and practical choices and caveats.

7.1 Physics Constraints & Loss Design

Physics-informed learning, introduced by Raissi et al. [1], improves accuracy by embedding governing physical laws—PDE residuals and boundary/initial conditions—directly into the training objective.

A standard PINN-style loss combines three components:

$$\mathcal{L} = w_u \underbrace{\mathcal{L}_{\text{data}}}_{\substack{\text{fit to observations} \\ \text{improves data accuracy}}} + w_f \underbrace{\mathcal{L}_{\text{phys}}}_{\substack{\text{PDE residuals} \\ \text{enforce physical laws}}} + w_b \underbrace{\mathcal{L}_{\text{bc}}}_{\substack{\text{boundary/initial} \\ \text{conditions enforcement}}}, \tag{41}$$

where $\mathcal{L}_{\text{data}}$ is the data-fidelity loss, $\mathcal{L}_{\text{phys}}$ enforces PDE residuals, and $\mathcal{L}_{\text{bc}}$ enforces boundary/initial conditions. The scalar weights $w_u, w_f, w_b > 0$ determine the balance between data fidelity and physics consistency.

Building on this foundation, a wide range of studies have extended the basic PINN loss through specialized constraints and tailored formulations in cooperation with KAN architectures [26, 49, 52, 55–63, 68, 133, 141,

165, 192, 197, 235]. Among these, several works move beyond the conventional physics-based loss in (41) by embedding more advanced physics constraints and loss designs directly into the KAN architecture:

- **Structural & Conservation Laws.** Enforce hard invariants such as Hamiltonian, quantum, or algebraic constraints. Includes *SPEL-KAN* [241], *KAN-ETS* [239], and *DAE-KAN* [254].

- **Weak-Form & Variational Constraints.** Use integral/variational formulations instead of pointwise PDE residuals. Includes *WCN* [235] and *KANtrol* [67].

- **Alternative Problem Formulations.** Modify the optimization objective or physical variables. Includes *AL-PKAN* [66], *AIVT* [221], *cPIKAN+RBA+EVM* [37], *KKAN+ssRBA* [52], *KAN-MHA* [56], and holomorphic–potential *PIHKAN* [255].

- **Physics-Guided Discovery & Design.** Physics-based losses used for inference, discovery, or design tasks. Includes *PKAN* [244] and physics-guided sensor design [236].

- **General PDE–Residual Models.** Standard PINN-style residuals without special structural constraints. Includes *KAN-PINN* [55], *Res-KAN* [57], *Anant-KAN* [256], and *PI-KAN* [269].

In all these approaches, *loss engineering*—choosing residual forms, designing constraint terms, and applying adaptive weighting strategies—serves as a powerful inductive bias. By aligning the optimization process with the underlying physics, these designs improve accuracy, stability, and extrapolation capabilities across a broad range of PDE-driven problems. Beyond modifying the loss, several works instead adapt the sampling or grid itself, yielding comparable accuracy gains through geometric rather than variational control.

7.2 Adaptive Sampling & Grids

Adaptive sampling and grid refinement focus computational effort where the solution is most difficult to capture (steep gradients, shocks, oscillations). One simple approach is multi-resolution training, where a model is trained on alternating coarse and fine point clouds to accelerate convergence and lower computational cost [72]. More advanced methods, long used in finite elements [222, 223], adapt the model's internal grid or sampling based on runtime dynamics for complex geometries [60, 69]. In stochastic systems, Chen et al. [235] introduced *adaptive collocation sampling*, selecting Gaussian test functions directly from observed data distributions.

Geometric/grid refinement with KANs. Actor et al. [46] treat spline *knots* as a learnable grid, which can be refined during training:

1. *Multilevel refinement.* Training begins on a coarse knot grid and periodically switches to finer grids. Since spline spaces are nested (coarse $\subset$ fine), the coarse solution transfers exactly to the refined grid. This preserves training progress, adds capacity only where needed, and achieves lower error at the same FLOPs compared with single-level training.

2. *Free-knot adaptation.* Knot locations are made trainable on $[a, b]$, with ordering enforced by a cumulative softmax:

$$t_i = \underbrace{a}_{\text{left endpoint}} + \underbrace{(b-a)}_{\text{interval length}} \sum_{j=1}^{i} \underbrace{\text{softmax}(s)_j}_{\text{ordered weights}}, \qquad s \in \mathbb{R}^n,$$

ensuring that endpoints remain fixed ($t_0 = a$, $t_n = b$). This naturally places knots in regions of high variation or non-smoothness.

On both regression and physics-informed tasks, multilevel schedules and free-knot adaptation consistently reduced errors relative to fixed grids and MLP baselines [46].

Grid–adaptive PIKANs. Rigas et al. [118, 259] extend this idea by adapting not only the spline grid but also the collocation points, so resolution follows the PDE residual:

1. *Grid extension with smooth state transition.* Start with few spline intervals (G) and periodically increase G. At each extension, an adaptive optimizer state transition preserves momentum and avoids loss spikes, while the finer grid captures unresolved structure (Fig. 16(a)).

2. *Residual-based adaptive resampling (RAD).* Compute residuals on a dense probe set S and convert them into sampling probabilities: larger residuals $\Rightarrow$ higher sampling chance. A new collocation set is then drawn accordingly (Fig. 16(b)).

Since KAN basis functions are tied to the knot grid, jointly adapting the grid and collocation points reduces projection error and concentrates model capacity in residual hotspots.

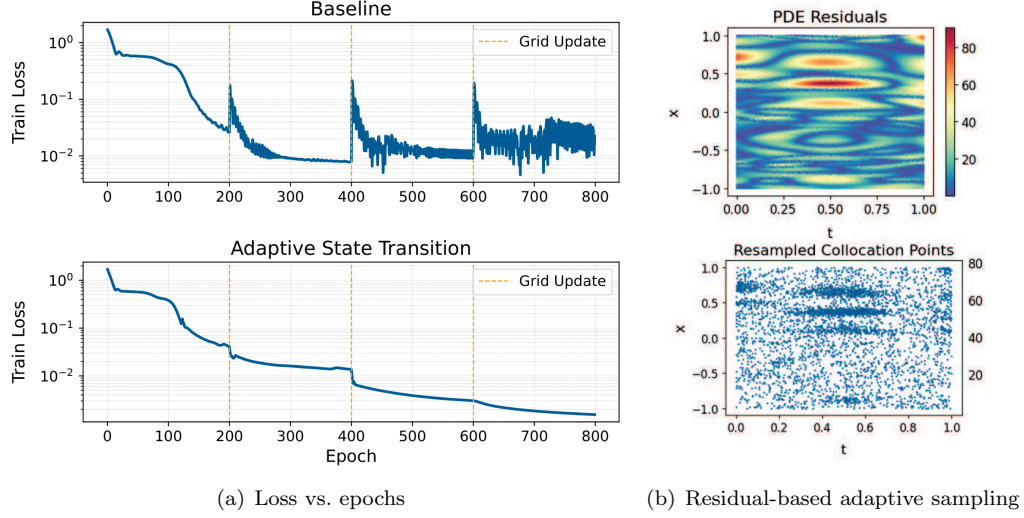| (a) Loss vs. epochs | (b) Residual-based adaptive sampling |

Figure 16: Adaptive PIKAN training after [118]. (a) Loss vs. epochs: adaptive state transition smooths grid updates. (b) RAD concentrates collocation points where PDE residuals are largest.

7.3 Domain decomposition

Splitting a difficult global map into easier local ones and blending them smoothly often improves accuracy. For example, temporal subdomaining can sharpen NTK conditioning and convergence [64]. Finite-basis KANs [122], as discussed in Sec. 6.8, achieve this by decomposing Ω (or $\Omega \times [0, T]$) into L overlapping subdomains $\{\Omega_j\}_{j=1}^{L}$ with a smooth partition of unity (PoU) $\{\omega_j\}_{j=1}^{L}$ such that

$$\underbrace{\mathrm{supp}(\omega_j)}_{\text{support of local weight}} = \Omega_j, \qquad \underbrace{\sum_{j=1}^{L} \omega_j(x) \equiv 1}_{\text{partition of unity}}.$$

A schematic is shown in Fig. 17.

A convenient 1D choice uses normalized "cosine bumps." With domain length l and overlap ratio $\delta > 1$:

$$\hat{\omega}_j(x) = \left[1 + \cos\big(\pi(x - \mu_j)/\sigma_j\big)\right]^2, \quad \mu_j = \underbrace{\frac{l(j-1)}{L-1}}_{\text{center of bump}}, \quad \sigma_j = \underbrace{\frac{\delta\, l/2}{L-1}}_{\text{width/overlap}},$$

$$\omega_j(x) = \underbrace{\frac{\hat{\omega}_j(x)}{\sum_{k=1}^{L} \hat{\omega}_k(x)}}_{\text{normalized local weight}}.$$

34

In d dimensions, the construction extends by taking products across coordinates.

The global surrogate is then the PoU blend of local KANs:

$$f_\Theta(x) = \sum_{j=1}^{L} \underbrace{\omega_j(x)}_{\text{local weight}} \underbrace{K_j(x; \boldsymbol{\theta}_j)}_{\text{local KAN}},$$

where each K_j is trained only on Ω_j, using its *own* knot grid induced by ω_j (basis/grid choices per Sec. 6.8). A basic error estimate illustrates the benefit:

$$\|u - f_\Theta\| \leq \sum_{j=1}^{L} \underbrace{\|\omega_j\|_\infty}_{\text{PoU weight}} \underbrace{\|u - K_j\|_{\Omega_j}}_{\text{local error}},$$

showing that reducing each local error reduces the global error. Increasing L or the tunable overlap δ concentrates resolution where it is most needed. Each local KAN operates on a smaller, better-conditioned subproblem, allowing parallel training with improved numerical stability. In practice, per-subdomain grids adapt to local scales and consistently yield lower relative L_2 errors than single-domain KANs at the same model capacity [122].
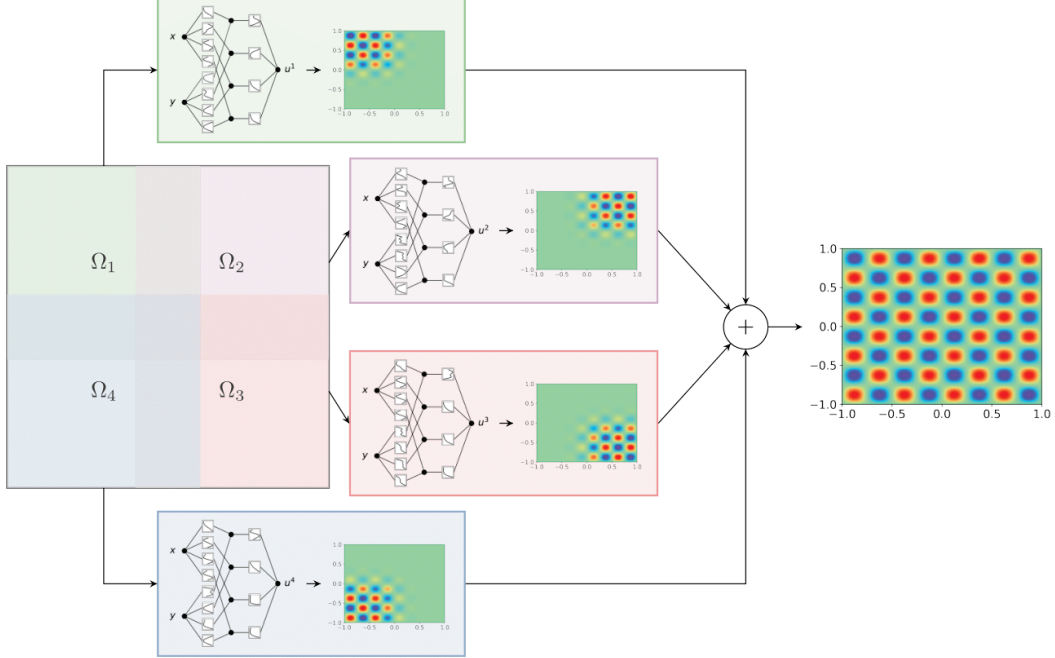

Figure 17: Schematic of FBKAN domain decomposition and PoU blending. Overlapping subdomains Ω_j host lightweight local KANs K_j, smoothly combined via PoU weights $\omega_j(x)$. This enables parallel training and per-subdomain knot/hyperparameter choices (adapted from [122]).

7.4 Function decomposition

Howard et al. [189] introduce a simple but effective fidelity–space split. A low-fidelity surrogate K_L is first trained on a large LF dataset $\{(x_i, f_L(x_i))\}_{i=1}^{N_{LF}}$ and then frozen. A high-fidelity model K_H is trained on a much smaller HF dataset $\{(x_j, f_H(x_j))\}_{j=1}^{N_{HF}}$, using both x and $K_L(x)$ as inputs. The HF predictor blends a linear LF→HF trend with a nonlinear correction:

$$K_H(x) = (1 - \alpha) K_\ell\big(x, K_L(x)\big) + \alpha K_{nl}\big(x, K_L(x)\big),$$

where $\alpha \in [0,1]$ is trainable, K_ℓ is the linear head, and K_{nl} the nonlinear correction.

The HF loss balances accuracy, linearity preference, and regularization:

$$\mathcal{L}_{HF} = \frac{1}{N_{HF}} \sum_{j=1}^{N_{HF}} \left(K_H(x_j) - f_H(x_j) \right)^2 + \lambda_\alpha \, \alpha^n + w \, \|\Phi_{nl}\|_2^2.$$

Here $\lambda_\alpha > 0$ and $n \in \mathbb{N}$ control the preference for the linear block, while $w > 0$ regularizes the nonlinear one.

The intuition is that the LF model captures the dominant structure, while the HF nonlinear head corrects only the residual. This reduces overfitting and stabilizes training when HF data are scarce. MFKAN achieved lower relative L_2 errors than single-fidelity KANs under the same HF budget [189]. The same fidelity split also benefits PIKANs, where K_L serves as a coarse physics surrogate and the HF head is trained only on residual or boundary losses, making fidelity decomposition complementary to spatial domain decomposition (Sec. 7.3).

In a related direction, Jacob et al. [190][39] propose a *separable* PIKAN (SPIKAN), expressing the solution as a sum of products of 1D KAN factors—one per coordinate—before combining them into a global field. Bühler et al. [231] propose KAN-SR, a symbolic regression framework inspired by Udrescu et al. [230]. The method checks for separability or symmetry before modeling. If such structure exists, the function is decomposed into smaller subproblems, each fit with a compact KAN, and then recomposed into a closed-form symbolic expression. This divide–and–conquer strategy improves interpretability and robustness in noisy or high-dimensional settings.
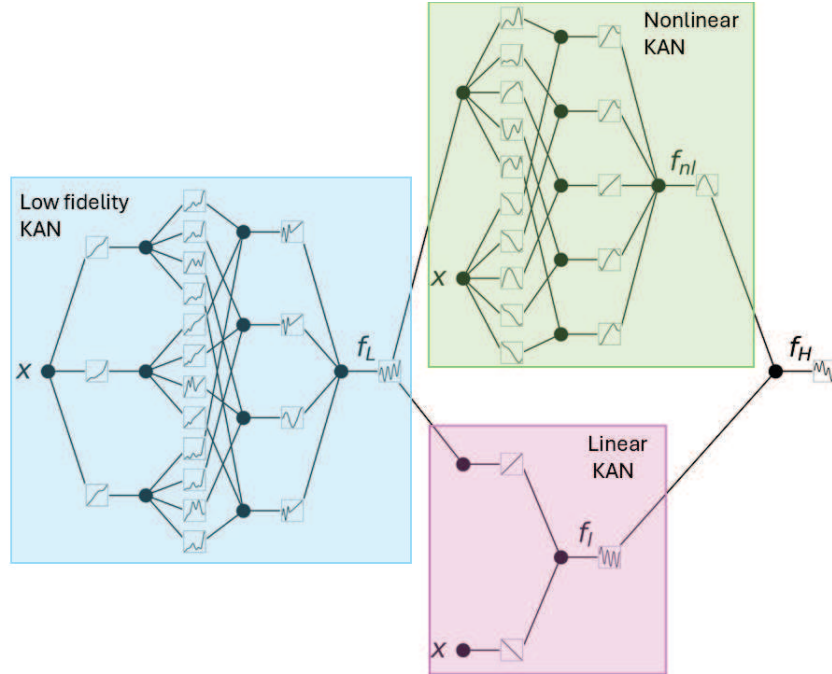

Figure 18: Multifidelity KAN (MFKAN) (adapted from [26, 189]). A low-fidelity KAN K_L is trained and then frozen. Linear and nonlinear heads K_ℓ and K_{nl} learn LF→HF correlations and residual corrections, which are blended to form K_H.

7.5 Hybrid, Ensemble, and Data-Integrated Models

A complementary line of work boosts accuracy not by modifying KAN bases, but by *combining KAN modules with other neural components*—MLPs, attention blocks, or ensemble mechanisms. These hybrids exploit

---

[39]

KAN's structured 1D functional mappings while leveraging the expressive power of deep networks.

- **MLP–KAN hybrids.** These architectures use MLPs for broad feature extraction and KANs for structured refinement. Examples include the MLP–KAN mixture-of-experts of He et al. [41] and the HPKM-PINN parallel fusion model of Xu et al. [58].

- **Task-specific KAN replacements.** Kundu et al. [257] (KANQAS)[40] replace the MLP in a Double Deep Q-Network with a KAN module for quantum architecture search.

- **Structured functional hybrids.** KKAN [52] inserts small per-dimension MLPs to generate learned one-dimensional features $\Psi_{p,q}(x_p)$, sums them across dimensions, and applies a simple outer basis expansion (Chebyshev, Legendre, sinusoidal, or RBF). This yields a pipeline

$$\text{inputs} \rightarrow \text{inner MLPs} \rightarrow \text{dimensionwise sum} \rightarrow \text{basis expansion} \rightarrow \text{output},$$

combining expressive learned features with a stable, low-bias basis. KKAN reports consistent gains over vanilla KANs and MLPs across regression, operator learning, and PDE benchmarks (Fig 19).
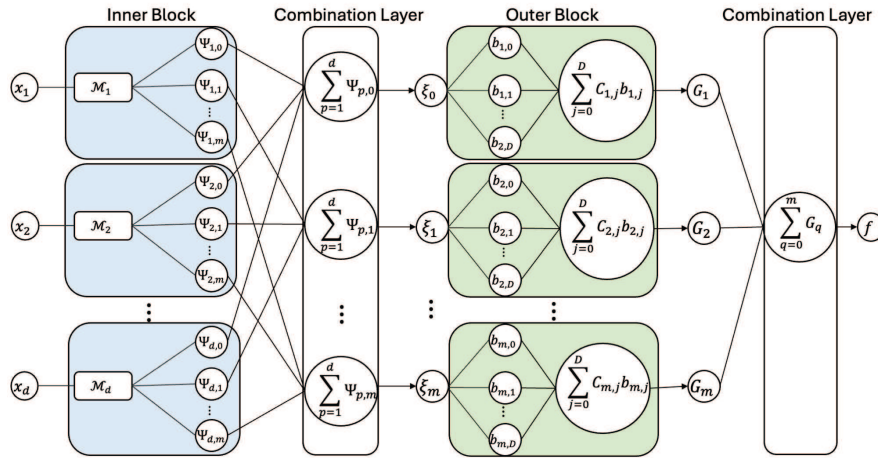

Figure 19: KKAN architecture (adapted from [52]). Each input coordinate x_p These are summed across dimensions to form ξ_m, which are expanded via basis functions in the outer block. A final summation yields the output. Bases may include Chebyshev/Legendre polynomials, sine series, or RBFs. This "MLP inside + basis outside" layout mirrors the Kolmogorov–Arnold recipe.

7.6 Sequence and Attention Hybrids

KANs are increasingly combined with sequence encoders and attention mechanisms to capture long-range temporal structure, global context, or multi-scale interactions. Most architectures fall into three categories: (i) attention-enhanced KANs, (ii) sequence-to-field encoder–decoder hybrids, and (iii) generative or data-augmentation models that stabilize training.

- **Attention-enhanced KANs.** These models insert KAN blocks into attention layers to improve multi-scale representation. Includes *KAN–MHA* [56], *FlashKAT* (Group-Rational KAN in Transformers) [193], and *Attention-KAN-PINN* for battery SOH forecasting [207].

---

[40]https://github.com/Aqasch/KANQAS_code

- **Sequence encoders and encoder–decoder hybrids.** These pair temporal encoders with KAN decoders to map sequences into spatial or field outputs. Includes *AL-PKAN* (GRU→KAN) [66], *GINN-KAN* [192], and *KAN-ODE* for continuous-time modeling [44].

- **Generative / data-augmentation hybrids.** These integrate KANs with GAN or adaptive-activation mechanisms to improve learning from sparse or noisy data. Includes *AAKAN–WGAN* [195], which uses a Wasserstein GAN to augment training data.

Across all designs, the auxiliary module supplies memory, context, or synthetic data, while the KAN block provides a compact and interpretable functional mapping at the output stage.

7.7 Discontinuities and Sharp Gradients

KAN variants approach discontinuities, shocks, and steep gradients through three main mechanisms: (i) using bases that naturally represent non-smooth features, (ii) attention or residual reweighting that concentrates learning where gradients are large, and (iii) physics-driven stabilization for shock-dominated PDEs.

- **Non-smooth or localized bases.** Designed to capture kinks, singularities, or asymptotic regimes. Includes *SincKAN* [49], *rKAN* [128], and *KINN* for stress singularities [69].

- **Attention and adaptive residuals.** Focuses computational effort on regions with steep gradients. Includes *KAN–MHA* [56], *KKAN+ssRBA* [52], and *AIVT* [221].

- **Physics-driven shock stabilization.** Embeds stabilization mechanisms from numerical PDEs directly into the loss. Includes *cPIKAN+EVM/RBA* [37], *Buckley–Leverett KANs* [61], and *EPi–cKAN* for elasto-plastic transitions [62].

Overall, these approaches mitigate non-smoothness by introducing localized bases (Sinc, rational), adaptive residual focusing, or physics-aware stabilization that controls oscillations near shocks.

Edge-aware KANs. Lei et al. [60] embed an explicit *edge activation* inside each KAN layer, enabling sharp jumps while keeping the rest of the representation smooth:

$$\psi(x) = w_t \tanh\big(\alpha(x - \beta)\big) + w_s \sum_i c_i \, S_i(x),$$

where $\alpha, \beta, w_t, w_s, c_i \in \mathbb{R}$ and $S_i(\cdot)$ are B-spline basis functions.

The tanh term places and sharpens the discontinuity, while the spline component fits the surrounding smooth regions. Incorporated into a PIKAN framework, this mechanism reduces spectral bias and yields more stable representations of steep fronts, a persistent difficulty for both MLPs and classical spline-based KANs.

7.8 Optimization & Adaptive Training

Training KANs—especially in physics-informed or data-scarce settings—relies heavily on optimization choices. Two themes dominate: (i) hybrid optimization schedules and (ii) Bayesian/probabilistic methods.

Hybrid and staged optimizers. A recurring finding is that optimizer choice strongly influences KAN convergence. Kalesh [61] showed that Adam→L-BFGS schedules improve sharp-front resolution in two-phase flow PINNs. Mostajeran [63] reported similar gains on large-domain PDEs, while Faroughi and Mostajeran [64] linked these improvements to better NTK conditioning. Daryakenari [65] benchmarked several first/second-order combinations (e.g., RAdam→BFGS) with warm-up and mixed precision, noting improved stability for both PINNs and PIKANs. Zeng et al. [47] refined these results by identifying regimes where Adam alone or L-BFGS alone is preferable. Overall, staged optimizers—early Adam-type exploration followed by quasi-Newton refinement—consistently yield more reliable KAN training.

Bayesian and probabilistic methods. Probabilistic formulations are increasingly used to calibrate KANs or quantify prediction uncertainty. Lin [188] employed Bayesian optimization to tune RBF–KAN hyperparameters. Giroux and Fanelli [141][41] introduced variational Bayesian inference for Higher–Order ReLU–KANs, placing priors on both weights and basis parameters; KL regularization improved robustness on stochastic Poisson and Helmholtz problems. Hassan [161] proposed a spline-based *Bayesian–KAN*, assigning Gaussian priors $c_n \sim \mathcal{N}(\mu_n, \sigma_n^2)$ to the activation coefficients for uncertainty quantification across layers.

A complementary direction is the probabilistic KAN of Polar and Poluektov [258][42], which replaces Bayesian priors with an ensemble built by *divisive data re-sorting*. This approach learns multiple KANs over recursively refined subsets of the data, capturing full input-dependent output distributions—including multi-modality—while remaining computationally lightweight and highly parallelizable.

Initialization and depth-stabilized training. Beyond optimizer choice and probabilistic tuning, Rigas et al. [262][43] show that deep Chebyshev-based KANs (cPIKANs) fail primarily due to variance blow-up across layers. They introduce a *basis-agnostic Glorot-like initialization* that preserves forward/backward variance and a *Residual–Gated Adaptive* block that stabilizes deep gradient flow. For spline KANs, Rigas et al. [276][44] demonstrate that Glorot-style and power-law initializations substantially improve NTK conditioning and convergence across regression and PDE benchmarks, underscoring initialization as a key design lever for scalable KAN depth.

Advanced quasi-Newton methods. Kiyani et al. [263] show that self-scaled BFGS/Broyden optimizers markedly outperform Adam and standard BFGS on stiff PDEs. Their results reveal two effects: the PDE residual creates a highly "crinkled" loss landscape where first-order methods stall, and stronger optimizers cut this optimization error so effectively that *smaller networks* reach equal or better accuracy. *One-liner: self-scaled quasi-Newton methods tame the PDE landscape and enable accurate, compact PIKANs.* A related line of work by Poluektov and Polar [264][45] replaces gradient training entirely with a Newton–Kaczmarz update on the spline/Gaussian coefficients, yielding a solver that is less sensitive to initialization and efficient for large datasets.

These works highlight the role of probabilistic reasoning for calibration, interpretability, and reliable prediction in settings with randomness or limited data.

8 Efficiency Improvement

Efficiency gains in KANs arise from two complementary directions: (i) exploiting hardware parallelism and compiler support, and (ii) reducing algebraic and basis-level complexity.

8.1 Parallelism, GPU, and JAX engineering

A major line of work accelerates KANs by making their core operations GPU-friendly. Iterative B-spline evaluations are replaced by non-iterative ReLU-power activations [48] or reformulated as CUDA-optimized matrix kernels [123, 133]. Model-level restructuring further boosts throughput: dual-matrix compression with Random Fourier Features [71], custom backward kernels to reduce memory stalls [193], and GPU-accelerated B-spline evaluation [124]. Architectural parallelism also plays a role, including multi-branch KAN–MLP hybrids [58] and domain-decomposition designs for PINNs [37, 122, 190]. At the framework level, JAX implementations [65, 118] leverage `jit`/XLA and optimized autodiff to deliver substantial end-to-end speedups.

---

[41] https://github.com/wmdataphys/Bayesian-HR-KAN
[42] https://github.com/andrewpolar/pkan
[43] https://github.com/srigas/RGA-KANs
[44] https://github.com/srigas/KAN_Initialization_Schemes
[45] https://github.com/andrewpolar/det5

8.2 Matrix optimization and parameter-efficient bases

A second strategy reduces computational cost by simplifying basis functions and matrix operations. Replacing spline bases with faster alternatives—ReLU-power [48, 123, 133], Chebyshev/Jacobi/Legendre polynomials [37, 62, 63, 69, 197], RBFs [44, 188], or wavelets [191]—lowers FLOPs and parameter counts while maintaining approximation quality. Additional savings come from structural compression: dual-matrix fusion with RFFs [71], sparsity-promoting regularizers [57], hierarchical knot refinement [46], and topology search via Differential Evolution [43]. Operator-aware designs further reduce cost by mixing spectral and spatial representations to keep matvecs near-diagonal [237], limiting mode mixing and memory traffic on variable-coefficient PDEs. Anant-Net [256][46] extends these ideas with dimension-wise tensor-product sweeps and selective differentiation, both of which reduce high-dimensional autodiff complexity and are readily transferable to KANs. In a related direction, lookup multivariate KANs (lmKANs) replace univariate inner functions with multivariate spline lookup tables and CUDA-efficient evaluation, providing a parameter-rich yet computationally light alternative to linear layers [268][47].

Together, these techniques make KANs increasingly competitive in large- and high-dimensional settings by aligning basis, algebra, and implementation with modern hardware.

9 Sparsity & Regularization

Regularization plays a central role in improving the stability and generalization of KANs, especially in noisy, high-dimensional, or ill-posed regimes. Existing approaches fall into four broad families: sparsity penalties, Lipschitz/complexity control, weight decay, and implicit or dropout-style regularizers.

L1 sparsity and entropy balancing. Liu et al. [26] introduce an activation-level ℓ_1 penalty,

$$\|\varphi_{ij}\|_1 = \frac{1}{N_p}\sum_{s=1}^{N_p}|\varphi_{ij}(x^{(s)})|, \qquad \|\Phi\|_1 = \sum_{i,j}\|\varphi_{ij}\|_1, \tag{42}$$

supplemented by an entropy balancing term,

$$S(\Phi) = -\sum_{i,j}\frac{\|\varphi_{ij}\|_1}{\|\Phi\|_1}\log\Big(\frac{\|\varphi_{ij}\|_1}{\|\Phi\|_1}\Big), \tag{43}$$

leading to the regularized objective

$$\mathcal{L}_{\text{total}} = \mathcal{L}_{\text{pred}} + \lambda\big(\mu_1\sum_\ell\|\Phi_\ell\|_1 + \mu_2\sum_\ell S(\Phi_\ell)\big). \tag{44}$$

Variants such as *EfficientKAN* [117][48] and *DeepKAN* [115][49] apply ℓ_1 directly to weights; the same scheme appears in symbolic regression [53] and PDE learning [57]. For Neural ODEs, Koenig et al. [44] use a layerwise ℓ_1 followed by pruning,

$$\mathcal{L}_{\text{total}} = \mathcal{L}_{\text{fit}} + \lambda_{\text{L1}}\|\theta\|_1, \tag{45}$$

eliminating redundant connections without accuracy loss.

Structured sparsity for symbolic regression. Bühler et al. [231] propose a composite regularizer for KAN-SR combining: (i) a magnitude penalty to suppress unused inputs, (ii) row/column entropies to localize attention, and (iii) an ℓ_1 penalty on linear weights. This promotes compact, interpretable expressions while preventing the overspecification typical of symbolic regression networks.

---

[46] https://github.com/ParamIntelligence/Anant-Net
[47] https://github.com/schwallergroup/lmkan
[48] https://github.com/Blealtan/efficient-kan
[49] https://github.com/sidhu2690/Deep-KAN

Bayesian sparsity. Zou and Yan [243] introduce *Probabilistic KANs (PKAN)* and their sparse counterpart *SSKAN*, using Gaussian-process priors and spike–and–slab priors, respectively. These provide principled sparsity and uncertainty quantification, forming a Bayesian alternative to ℓ_1-based pruning.

Lipschitz-driven regularization. Li et al. [274] show that KAN generalization is governed by a *Lipschitz complexity* depending on per-layer Lipschitz constants and mixed tensor norms. Their *LipKAN* architecture inserts 1-Lipschitz layers and replaces ℓ_1 with a theoretically motivated $\ell_{1.5}$ penalty, providing tighter complexity control and improved generalization on complex distributions.

Low-rank RKHS regularization. Zhang and Zhou [273] establish generalization bounds for KANs whose activations lie in a *low-rank* RKHS (e.g., Wendland functions [275]), with complexity scaling in the activation *rank* rather than width. This motivates LoRA-style rank-constrained fine-tuning of pre-trained KAN activations: maintaining expressivity while regularizing model capacity.

L2 weight decay and extensions. Shen et al. [195] incorporate ℓ_2 weight decay,

$$\mathcal{L}_{\text{base}} = \mathcal{L}_{\text{pred}} + \lambda_1 \mathcal{L}_{\text{L2}}, \tag{46}$$

along with temporal smoothness and mutual-information terms,

$$\mathcal{L}_{\text{AAKAN}} = \mathcal{L}_{\text{base}} + \lambda_2 \mathcal{L}_{\text{time}} + \lambda_3 \mathcal{L}_{\text{MI}}, \tag{47}$$

to stabilize dynamics. Small ℓ_2 penalties are similarly used in physics-informed KANs [37, 221] to prevent overfitting while preserving optimization stability.

Implicit and dropout-style regularizers. Implicit regularization arises when activations themselves bound outputs. Daryakenari et al. [65] show that nested activations such as $\tanh(\tanh(x))$ naturally confine outputs, smoothing gradients in Chebyshev-based KANs. Altarabichi et al. [224] propose *DropKAN*, which masks post-activation outputs rather than inputs, injecting noise directly into spline evaluations and offering more stable regularization than standard dropout.

10 Convergence and Scaling Laws

Classical approximation theorems guarantee that neural networks can approximate any continuous function, but provide little insight into convergence *rates*. Recent KAN studies fill this gap by deriving Sobolev-space error bounds, analyzing gradient-flow dynamics via NTK theory [8, 225], and documenting empirical scaling laws [187].

10.1 Theoretical Approximation Rates and Empirical Scaling Laws

Sobolev and Besov rates. Wang [53] proved that for $f \in W^s(\Omega)$, a KAN with depth L and spline order k satisfies

$$\|f - g\|_{L^p(\Omega)} \leq C\, L^{-2s/d},$$

corresponding to a parameter-rate $\mathcal{O}(P^{-2s/d})$, doubling the classical $\mathcal{O}(P^{-s/d})$ rate of standard neural and kernel approximators [226, 227]. Kratsios et al. [271] extend this to *Besov* spaces [272], showing that spline-based Res-KANs achieve the optimal Besov approximation rate on Lipschitz and fractal sets with dimension-free sample complexity. Complementing these approximation-centric results, Liu et al. [140] establish the first minimax *statistical* rates for KAN regression: spline-based additive and hybrid KANs achieve the optimal

$$O\left(n^{-2r/(2r+1)}\right)$$

for Sobolev-r functions, together with an optimal knot-scaling rule $k_n \asymp n^{1/(2r+1)}$. These three perspectives jointly show that KANs match the best-known approximation and estimation rates of classical spline and sieve methods while retaining neural-network–style compositional structure.

Empirical scaling. Liu [26] observed that KAN RMSE follows a power law

$$\ell \propto N^{-\alpha},$$

with task-dependent $\alpha > 0$. Increasing basis resolution (e.g., spline grid size G) consistently improves accuracy more than widening layers, echoing the theoretical depth benefit in [53] and the statistical spline-resolution rule in [140]. Together, these findings indicate that KANs achieve fast decay in both theory (Sobolev/Besov/minimax rates) and practice (empirical power laws), though [271] emphasizes that many of these gains reflect favorable optimization dynamics rather than asymptotic expressivity alone.

10.2   Spectral Bias and Frequency Learning Behavior

A model has *spectral bias* if low frequencies are learned before high ones [247, 248, 251]. In NTK terms, this corresponds to steep eigenvalue decay. Flatter spectra indicate more uniform frequency learning.

Reduced spectral bias in KANs. Wang [53] showed via Hessian–eigenvalue analysis that shallow KANs possess a well-conditioned landscape, enabling fast learning of oscillatory modes. Grid extension further widens the representable frequency band. Their experiments show KANs capturing high-frequency signals in a few iterations, unlike MLPs.

Farea [39] confirmed this in PDE settings: KANs and learnable-basis PINNs (e.g., Fourier/Jacobi) maintain flatter NTK eigenvalue spectra, indicating weaker spectral bias [252, 253]. However, they also showed that broader spectra can increase curvature, worsen conditioning, and destabilize training [250]. Wang [53] similarly noted that overly fine spline grids may amplify noise sensitivity, whereas modest coarsening can improve generalization.

Together, these results show that KANs learn high-frequency features more uniformly [39, 53], but at the cost of sharper loss landscapes—consistent with kernel-theoretic ill-conditioning phenomena [198, 199]. Basis choice must therefore balance spectral reach (e.g., Fourier-like) and stability (e.g., splines).

10.3   NTK-Based Convergence and Physics-Informed Extensions

Gradient-flow convergence. Gao [165] analyzed two-layer KANs under gradient flow, showing that the residual $s(t)$ evolves via

$$\frac{d}{dt}s(t) = -G\,s(t),$$

with $G = D^\top D$ the NTK Gram matrix. If $G \succ 0$, the loss decays exponentially:

$$\mathcal{L}(t) \leq \left(1 - \eta\tfrac{\lambda_{\min}}{2}\right)^t \mathcal{L}(0),$$

giving a rigorous rate under appropriate learning rates. The same holds in expectation for SGD.

Physics-informed settings. For PDE residual losses,

$$\mathcal{L}_{\mathrm{PDE}}(t) \ \leq \ \left(1 - \eta\,\tfrac{\lambda_{\min}}{2}\right)^t \mathcal{L}_{\mathrm{PDE}}(0),$$

but $\lambda_{\min}$ depends strongly on operator stiffness [64, 165]. Faroughi [64] showed that Chebyshev-based cKAN/cPIKAN models maintain better NTK conditioning and converge faster on diffusion, Helmholtz, Allen–Cahn, and beam PDEs. They also demonstrated that temporal decomposition and hybrid Adam–BFGS schedules improve conditioning, aligning with multi-stage results in [62, 63]. *Initialization can also influence NTK conditioning*: Rigas et al. [276][50] show that variance-preserving Glorot-style and power-law schemes produce more stable initial NTKs for spline-KANs, leading to faster convergence.

---

[50]https://github.com/srigas/KAN_Initialization_Schemes

10.4 Practical Trade-offs and Convergence Guarantees

KAN convergence is tightly controlled by the conditioning of the NTK Gram matrix: structured bases often enlarge the smallest eigenvalue $\lambda_{\min}$ relative to MLPs [53,165], accelerating early optimization. Yet the same expressivity that broadens spectral coverage also increases curvature in the loss landscape, making training sensitive to basis resolution and learning-rate choices [39]. Effective practice therefore requires moderating basis richness to preserve numerical stability.

Physics-informed models highlight this balance. Chebyshev-KAN and cPIKAN architectures benefit from well-spread NTK spectra, producing faster PDE residual decay and more stable training [62–64]. But these gains diminish when grids are refined too aggressively or dimensionality grows, where operators become both costly to evaluate and harder to condition [42]. The result is a gradual trade-off between spectral reach and computational/numerical stability.

Generalization theory reaches the same conclusion from a different angle. Zhang and Zhou [273] show that KAN complexity is governed by ℓ_1 coefficient norms and per-layer Lipschitz constants—precisely the terms that inflate when bases become overly sharp or high-frequency. Li et al. [274] formalize this perspective through *Lipschitz complexity*, deriving complexity-dependent generalization bounds and introducing LipKANs, which reduce Lipschitz growth via Lipschitz-controlled layers and $L^{1.5}$ regularization. Their results empirically demonstrate that controlling Lipschitz complexity mirrors the conditioning behavior seen in NTK dynamics: sharper bases yield higher curvature and poorer generalization.

Taken together, NTK convergence guarantees [165], approximation-rate theory [53,273], Lipschitz-based generalization analyses [274], and empirical scaling laws [26] support a unified conclusion: KANs are expressive and parameter-efficient, but their practical performance depends on managing the expressivity–stability trade-off. The most effective models achieve wide spectral coverage while keeping curvature, conditioning, and coefficient growth under control [39,53,64].

11 Practical "Choose–Your–KAN" Guide

KANs offer a modular design space. The correct configuration depends on (i) the structure of the target function (smooth, oscillatory, discontinuous, periodic, multi-scale), (ii) computational constraints (time, memory, precision), and (iii) desired properties (accuracy, interpretability). Below is a clear, seven-step recipe synthesizing Sections 6–10.

Step 1 — Begin with a stable default. For general regression/classification, start with a **cubic B-spline KAN** on a uniform grid. This setup is mature, stable, and well-conditioned [26,113]. For PDE or boundary-sensitive tasks, enable *grid extension* and, if needed, apply *post-training refinement* (Sec. 6.1; Fig. 1; [113]).

Step 2 — Select a basis, matched to the problem structure. Choose the basis family whose functional properties align with the anticipated solution:

- **Globally smooth / oscillatory:** Chebyshev (ChebyKAN) with per-layer tanh normalization [49,64, 130,196].

- **Controllable smoothness or boundary shaping:** Jacobi (fKAN, Jacobi-KAN) with fractional/domain parameters [70,127].

- **Discontinuities, fronts, boundary layers:** SincKAN (bandlimited) [49], rational rKAN [128], or DKAN (tanh-jump + smooth background) [60].

- **Periodic structure:** FourierKAN or KAF (learnable RFF) [71,134].

- **Local, multi-scale, or bursty features:** Wavelets (Wav-KAN) [139,191].

Step 3 — If speed matters, replace heavy components. For wall-clock efficiency, modify the basis or architecture:

- **Fast local bases:** ReLU-KAN/HRKAN ($ReLU^m$) [123, 133]; or Gaussian RBF variants (FastKAN) [119].

- **Parallelism and compilers:** JAX `jit`/XLA, fused CUDA kernels, multi-branch or domain-decomposition architectures [65, 118, 122].

- **Parameter economy:** Prefer orthogonal polynomials or RBFs; prune using ℓ_1+entropy penalties [26, 37, 57].

Step 4 — Stabilize via normalization, grid design, and Lipschitz control. Choose conditioning mechanisms suited to the basis, and reduce Lipschitz complexity where possible:

- Chebyshev/Jacobi $\rightarrow$ apply tanh normalization to prevent blow-up of high-order modes [49, 65].

- RBF/Wavelet $\rightarrow$ use min–max or sigmoid/tanh scaling to keep oscillatory activations bounded [209, 231].

- Splines $\rightarrow$ employ extended grids or free-knot refinement near sharp gradients [46, 118].

- **All bases** optionally insert 1-Lipschitz "Lip" layers (tanh/sigmoid/ReLU) between Σ and linear maps to reduce Lipschitz complexity and improve generalization [274].

Step 5 — Add physics and adaptive sampling only when needed. For PINNs/PIKANs, form

$$\mathcal{L} = w_u \mathcal{L}_{\text{data}} + w_f \mathcal{L}_{\text{phys}} + w_b \mathcal{L}_{\text{bc}},$$

and enhance only when necessary:

- Augmented Lagrangian or residual-based attention for conflicting constraints [1, 52, 66].

- Residual-adaptive sampling (RAD) for error concentration [118].

- Coarse$\rightarrow$fine grid updates as residuals localize [46].

Step 6 — Use the standard optimizer progression. Warm up with Adam/RAdam, then refine with (L)BFGS. Activate mixed precision and gradient clipping for stiff PDEs [47, 63–65].

Step 7 — Increase capacity *targetedly*, not uniformly. KAN error typically follows $\ell \propto P^{-\alpha}$, $\alpha > 0$ (Sec. 10; [26, 53]). The most effective scaling strategies are:

- Local refinement (free knots) [46],

- Subdomain PoU decomposition (FBKAN) [122],

- Selective basis enrichment (not uniform widening).

This seven-step procedure consolidates the full review into a single, consistent decision pipeline, with one basis-selection step and all relevant citations preserved.

12 Current Gaps and Path Forward

Despite rapid growth in publications and open-source implementations (Tables 2, 3), the KAN ecosystem remains fragmented. Most studies show strong empirical potential in regression, operator learning, and PDE solving, yet comparisons are inconsistent and rarely grounded in theory. The field now requires principled foundations rather than isolated "KAN vs. MLP" or "basis-vs.-basis" experiments.

Limits of Current Comparative Frameworks

(1) KAN vs. MLP benchmarks. These comparisons often match parameter counts but ignore essential differences: functional roles of parameters, basis-induced inductive bias, and normalization/grid constraints. Outcomes range from clear KAN advantages to near parity [36–38], offering little predictive insight into when KANs should win.

(2) Basis-vs.-basis races. Comparisons of splines, Chebyshev, Gaussians, etc. [39] highlight problem dependence but mask deeper structure. Each basis involves choices of normalization, grids, and regularization—too many degrees of freedom for a single benchmark to be conclusive.

Overall, KANs are not a single architecture but a *framework* whose performance depends on principled design choices rooted in approximation theory, numerical conditioning, and optimization geometry.

Case Study: The Many Faces of a Chebyshev KAN: A plain Chebyshev KAN can be unstable, but targeted refinements substantially improve behavior:

- **Domain stabilization**: `tanh` normalization confines inputs to $[-1, 1]$ for numerically stable Chebyshev evaluation (Section 6.2).

- **Architectural hybrids**: Linear heads reduce overfitting in inverse/PDE tasks [65].

- **Grid-informed adaptivity**: Learnable `tanh`-based grids add local adaptivity [52].

- **Principled optimization**: Hybrid Adam–L-BFGS schedules improve spectral conditioning [63, 64].

- **Adaptive polynomial degree**: Making the polynomial degree itself trainable, as in Adaptive PolyKAN [280].

Similar refinements benefit other bases: adaptive centers for Gaussian KANs [54], free-knot updates for spline KANs [46, 113], and domain decomposition for finite-basis KANs [122].

A Multi-Pillar Framework for Future KAN Research

Pillar 1: Robust component library. Canonical, stable implementations for Chebyshev, spline, Gaussian/RBF, Fourier, and wavelet bases with standardized normalization and initialization.

Pillar 2: Basis selection theory. Principles linking problem structure to basis choice, including spectral alignment, NTK conditioning, and approximation–regularization trade-offs.

Pillar 3: Finite-width optimization theory. Beyond NTK predictions [64, 165]; characterize finite-width loss geometry, adaptive basis movement, and optimization dynamics. Include Extreme Learning Machine–style regimes [278] as an alternative training strategy for KANs.

Pillar 4: Generalization and regularization. Joint treatment of parameter count, basis complexity, smoothness, and explicit ℓ_1/ℓ_2 penalties for improved generalization bounds.

Pillar 5: Composition and hierarchy. Depth in KANs currently has no formal interpretation. Open problems include understanding the functional role of layer composition, the interactions among heterogeneous bases, and the trade-off between expressivity and stability under deep compositions (see also the theoretical results of [53, 273] and the empirical observations of [267][51]).

---

[51] https://github.com/geoelements-dev/mlp-kan

Pillar 6: Interpretability and identifiability. Uniqueness of learned univariate functions, robustness, and symbolic identifiability.

Pillar 7: RKHS-based formulation. Develop RKHS-guided KAN theory using recent formulations [273] and earlier functional-analytic perspectives on KST [100].

Pillar 8: New basis functions. Introduce and test new basis families in KANs, including Newton basis functions [277, 279], low-order Wendland functions, and Matérn/Sobolev kernels [275].

Outlook A unified framework combining stable components, principled basis selection, finite-width theory, RKHS insights, and exploration of new bases can guide future KAN development.

13   Conclusion

Kolmogorov–Arnold Networks shift the locus of learning from linear weights to univariate basis functions placed on edges, offering a flexible alternative to conventional MLPs. This review has consolidated the rapidly expanding KAN literature, with emphasis on applications in function approximation, regression, and PDE solving. Our central observation is that the key question is not *whether* KANs outperform MLPs, but rather *which KAN* is appropriate for a given task.

A clear pattern emerges across studies: well-designed KAN variants often exceed vanilla MLP and PINN baselines in accuracy and convergence, albeit with higher per-epoch computational cost. Unlocking this performance hinges on navigating KANs' large design space. We organized this space through the lens of basis families—local B-splines and Gaussians, global Chebyshev and Fourier series—and highlighted how normalization, grid layout, and initialization shape stability and expressivity.

We also outlined the ecosystem of techniques for enhancing KAN performance. Accuracy gains arise from physics-informed losses, adaptive sampling, domain decomposition, and hybrid sequence/attention modules. Efficiency gains are enabled by GPU-aware engineering, matrix-level optimizations, and lighter bases such as ReLU-powers. These developments, combined with emerging theory on approximation and convergence, signal a transition from exploratory experimentation to principled model design.

The practical "Choose–Your–KAN" guide in Section 11 distills these insights into a decision framework linking problem characteristics to architectural and training choices. Ultimately, the strength of the KAN framework lies in its modularity: basis families, normalization schemes, and optimization strategies can be selected and composed to encode problem-specific inductive biases. Continued progress will require deeper basis-specific analysis and standardized benchmarks, but KANs have clearly established themselves as a versatile and promising direction in neural network architecture.

14   Acknowledgments

References

[1] M. Raissi, P. Perdikaris, and G. E. Karniadakis, "Physics-informed neural networks: A deep learning framework for solving forward and inverse problems involving nonlinear partial differential equations," *Journal of Computational Physics*, vol. 378, pp. 686–707, 2019.

[2] G. Pang, L. Lu, and G. E. Karniadakis, "fPINNs: Fractional physics-informed neural networks," *SIAM Journal on Scientific Computing*, vol. 41, no. 4, pp. A2603–A2626, 2019.

[3] D. Zhang, L. Lu, L. Guo, and G. E. Karniadakis, "Quantifying total uncertainty in physics-informed neural networks for solving forward and inverse stochastic problems," *Journal of Computational Physics*, vol. 397, p. 108850, 2019.

[4] E. Kharazmi, Z. Zhang, and G. E. Karniadakis, "Variational physics-informed neural networks for solving partial differential equations," *arXiv preprint* arXiv:1912.00873, 2019.

[5] A. D. Jagtap and G. E. Karniadakis, "Extended physics-informed neural networks (XPINNs): A generalized space–time domain decomposition based deep learning framework for nonlinear partial differential equations," *Communications in Computational Physics*, vol. 28, no. 5, 2020.

[6] X. Meng and G. E. Karniadakis, "A composite neural network that learns from multi-fidelity data: Application to function approximation and inverse PDE problems," *Journal of Computational Physics*, vol. 401, p. 109020, 2020.

[7] Y. Shin, J. Darbon, and G. E. Karniadakis, "On the convergence of physics-informed neural networks for linear second-order elliptic and parabolic type PDEs," *arXiv preprint* arXiv:2004.01806, 2020.

[8] S. Wang, P. Yu, and P. Perdikaris, "When and why PINNs fail to train: A neural tangent kernel perspective," *Journal of Computational Physics*, vol. 449, p. 110768, 2022.

[9] L. Lu, X. Meng, Z. Mao, and G. E. Karniadakis, "DeepXDE: A deep learning library for solving differential equations," *SIAM Review*, vol. 63, no. 1, pp. 208–228, 2021.

[10] Y. Wang and C.-Y. Lai, "Multi-stage neural networks: Function approximator of machine precision," *arXiv preprint* arXiv:2307.08934, 2023.

[11] L. McClenny and U. Braga-Neto, "Self-adaptive physics-informed neural networks using a soft attention mechanism," *arXiv preprint* arXiv:2009.04544, 2020.

[12] K. Shukla, A. D. Jagtap, and G. E. Karniadakis, "Parallel physics-informed neural networks via domain decomposition," *Journal of Computational Physics*, vol. 447, p. 110683, 2021.

[13] Z. Hu, K. Shukla, G. E. Karniadakis, and K. Kawaguchi, "Tackling the curse of dimensionality with physics-informed neural networks," *Neural Networks*, vol. 176, p. 106369, 2024.

[14] S. Wang, S. Sankaran, P. Stinis, and P. Perdikaris, "Simulating three-dimensional turbulence with physics-informed neural networks," *arXiv preprint* arXiv:2507.08972, 2025.

[15] S. Wang, B. Li, Y. Chen, and P. Perdikaris, "Piratenets: Physics-informed deep learning with residual adaptive networks," *Journal of Machine Learning Research*, vol. 25, no. 402, pp. 1–51, 2024.

[16] F. Rossi and B. Conan-Guez, "Functional multi-layer perceptron: A non-linear tool for functional data analysis," *Neural Networks*, vol. 18, no. 1, pp. 45–60, 2005.

[17] M. Cranmer, "Interpretable machine learning for science with PySR and SymbolicRegression.jl," *arXiv preprint* arXiv:2305.01582, 2023.

[18] H. Cunningham, A. Ewart, L. Riggs, R. Huben, and L. Sharkey, "Sparse autoencoders find highly interpretable features in language models," *arXiv preprint* arXiv:2309.08600, 2023.

[19] A. Noorizadegan, R. Cavoretto, D. L. Young, and C. S. Chen, "Stable weight updating: A key to reliable PDE solutions using deep learning," *Engineering Analysis with Boundary Elements*, vol. 168, p. 105933, 2024.

[20] A. Noorizadegan, D. L. Young, Y. C. Hon, and C. S. Chen, "Power-enhanced residual network for function approximation and physics-informed inverse problems," *Applied Mathematics and Computation*, vol. 480, p. 128910, 2024.

[21] S. Wang, A. K. Bhartari, B. Li, and P. Perdikaris, "Gradient alignment in physics-informed neural networks: A second-order optimization perspective," *arXiv preprint* arXiv:2502.00604, 2025.

[22] S. Wang, Y. Teng, and P. Perdikaris, "Understanding and mitigating gradient flow pathologies in physics-informed neural networks," *SIAM Journal on Scientific Computing*, vol. 43, no. 5, pp. A3055–A3081, 2021.

[23] N. Rahaman, A. Baratin, D. Arpit, F. Draxler, M. Lin, F. Hamprecht, Y. Bengio, and A. Courville, "On the spectral bias of neural networks," in *Proceedings of the 36th International Conference on Machine Learning (ICML)*, vol. 97, Proceedings of Machine Learning Research (PMLR), pp. 5301–5310, 2019.

[24] Z. Q. J. Xu, Y. Zhang, T. Luo, Y. Xiao, and Z. Ma, "Frequency principle: Fourier analysis sheds light on deep neural networks," *Communications in Computational Physics*, vol. 28, no. 5, pp. 1746–1767, 2020.

[25] W. Cai and Z. Q. J. Xu, "Multi-scale deep neural networks for solving high-dimensional PDEs," *arXiv preprint* arXiv:1910.11710, 2019.

[26] Z. Liu, Y. Wang, S. Vaidya, F. Ruehle, J. Halverson, M. Soljačić, T. Y. Hou, and M. Tegmark, "KAN: Kolmogorov-Arnold networks," *arXiv preprint* arXiv:2404.19756, 2024.

[27] M. Andrade, L. Freitas, and J. Beatrize, "Kolmogorov–Arnold Networks for interpretable and efficient function approximation," *Preprints*, 2025.

[28] D. Basina, J.R. Vishal, A. Choudhary, and B. Chakravarthi, "KAT to KANs: A review of Kolmogorov–Arnold Networks and the neural leap forward," *arXiv preprint* arXiv:2411.10622, 2024.

[29] J. Beatrize, "Scalable and interpretable function-based architectures: A survey of Kolmogorov–Arnold Networks," *engrXiv preprint*, doi:10.31224/4515, 2025. [Online]. Available: https://engrxiv.org/preprint/view/4515/version/6148

[30] S.A. Faroughi, F. Mostajeran, A.H. Mashhadzadeh, and S. Faroughi, "Scientific machine learning with Kolmogorov–Arnold Networks," *arXiv preprint* arXiv:2507.22959, 2025.

[31] B.H. Kilani, "Convolutional Kolmogorov–Arnold Networks: A survey," *HAL preprint* hal-05177765, 2025.

[32] Y. Hou, T. Ji, and D. Zhang, A. Stefanidis "Kolmogorov-Arnold Networks: A Critical Assessment of Claims, Performance, and Practical Viability," *arXiv preprint* arXiv:2407.11075, 2024.

[33] A. Dutta, B. Maheswari, N. Punitha, *et al.*, "The first two months of Kolmogorov-Arnold Networks (KANs): A survey of the state-of-the-art," *Arch. Computat. Methods Eng.*, 2025. doi: 10.1007/s11831-025-10328-2

[34] S. Essahraui, I. Lamaakal, K. E. Makkaoui, I. Ouahbi, M. F. Bouami, and Y. Maleh, "Kolmogorov-Arnold Networks: Overview of Architectures and Use Cases," *Proc. Int. Conf. Circuit, Systems and Communication (ICCSC)*, Fez, Morocco, 2025, pp. 1–6. doi: 10.1109/ICCSC66714.2025.11135248

[35] S. Somvanshi, S.A. Javed, M.M. Islam, D. Pandit, and S. Das, "A survey on Kolmogorov–Arnold Networks," *ACM Computing Surveys*, 2025.

[36] R. Yu, W. Yu, and X. Wang, "KAN or MLP: A fairer comparison," *arXiv preprint* arXiv:2407.16674, 2024. [Online]. Available: https://github.com/yu-rp/KANbeFair

[37] K. Shukla, J. D. Toscano, Z. Wang, Z. Zou, and G. E. Karniadakis, "A comprehensive and fair comparison between MLP and KAN representations for differential equations and operator networks," *Computer Methods in Applied Mechanics and Engineering*, vol. 431, 2024.

[38] Z. Yang, J. Zhang, X. Luo, Z. Lu, and L. Shen, "Activation Space Selectable Kolmogorov-Arnold Networks," *arXiv preprint* arXiv:2408.08338, 2024.

[39] A. Farea and M. S. Celebi, "Learnable activation functions in physics-informed neural networks for solving partial differential equations," *Computer Physics Communications*, vol. 315, p. 109753, 2025. GitHub: https://github.com/afrah/pinn_learnable_activation

[40] H.-T. Ta, "BSRBF-KAN: A combination of B-splines and radial basis functions in Kolmogorov-Arnold networks," *arXiv preprint* arXiv:2406.11173, 2024. [Online]. Available: https://github.com/hoangthangta/BSRBF_KAN

[41] Y. He, Y. Xie, Z. Yuan, and L. Sun, "MLP-KAN: Unifying deep representation and function learning," *arXiv preprint* arXiv:2410.03027, 2024.

[42] A. Pal and D. Das, "Understanding the limitations of B-spline KANs: Convergence dynamics and computational efficiency," in *NeurIPS 2024 Workshop on Scientific Methods for Understanding Deep Learning*, 2024.

[43] D. Li, B. Yan, Q. Long, and B. Wang, "DE-KAN: A differential evolution-based optimization framework for enhancing Kolmogorov-Arnold networks in complex nonlinear modeling," in *IEEE Congress on Evolutionary Computation (CEC)*, pp. 1–8, 2025.

[44] B. C. Koenig, S. Kim, and S. Deng, "KAN-ODEs: Kolmogorov-Arnold Network ordinary differential equations for learning dynamical systems and hidden physics," *Computer Methods in Applied Mechanics and Engineering*, vol. 432, p. 117397, 2024.

[45] S. Mallick, S. Ghosh, and T. Roy, "KAN-Therm: A lightweight battery thermal model using Kolmogorov-Arnold Network," *arXiv preprint* arXiv:2509.09145, 2025.

[46] J. A. Actor, G. Harper, B. Southworth, and E. C. Cyr, "Leveraging KANs for expedient training of multichannel MLPs via preconditioning and geometric refinement," *arXiv preprint* arXiv:2505.18131, 2025.

[47] C. Zeng, J. Wang, H. Shen, and Q. Wang, "KAN versus MLP on irregular or noisy functions," *arXiv preprint* arXiv:2408.07906, 2024.

[48] R. Qiu, Y. Miao, S. Wang, Y. Zhu, L. Yu, and X.-S. Gao, "PowerMLP: An efficient version of KAN," *Proceedings of the AAAI Conference on Artificial Intelligence*, vol. 39, no. 19, pp. 20069–20076, 2025. [Online]. Available: https://github.com/Iri-sated/PowerMLP

[49] T. Yu, J. Qiu, J. Yang, and I. Oseledets, "Sinc Kolmogorov-Arnold network and its applications on physics-informed neural networks," *arXiv preprint* arXiv:2410.04096, 2024. [Online]. Available: https://github.com/DUCH714/SincKAN

[50] A.A. Mahmoud, A. Pester, M.M. Muttardi, F. Andres, S. Tanabe, N. Greneche, and H.H. Ali, "Cheby-KANs: Advanced Kolmogorov–Arnold Networks for Applying Geometric Deep Learning in Quantum Chemistry Applications," *IEEE Access*, vol. 13, pp. 130525–130534, 2025.

[51] J.-C. Jiang, Y.-C. Huang, T. Chen, and H.-S. Goan, "Quantum variational activation functions empower Kolmogorov–Arnold networks," *arXiv preprint* arXiv:2509.14026, 2025. [Online]. Available: https://github.com/Jim137/qkan

[52] J. D. Toscano, L.-L. Wang, and G. E. Karniadakis, "KKANs: Kurkova-Kolmogorov-Arnold networks and their learning dynamics," *Neural Networks*, vol. 191, p. 107831, 2025.

[53] Y. Wang, J. W. Siegel, Z. Liu, and T. Y. Hou, "On the expressiveness and spectral bias of KANs," *arXiv preprint* arXiv:2410.01803, 2024.

[54] D. W. Abueidda, P. Pantidis, and M. E. Mobasher, "DeepOKAN: Deep operator network based on Kolmogorov-Arnold networks for mechanics problems," *Computer Methods in Applied Mechanics and Engineering*, vol. 436, p. 117699, 2025. GitHub: https://github.com/DiabAbu/Dee

[55] L. Zhang, L. Chen, F. An, Z. Peng, Y. Yang, T. Peng, Y. Song, and Y. Zhao, "A physics-informed neural network for nonlinear deflection prediction of ionic polymer-metal composite based on Kolmogorov-Arnold networks," *Engineering Applications of Artificial Intelligence*, vol. 144, p. 110126, 2025.

[56] S. Yang, K. Lin, and A. Zhou, "The KAN-MHA model: A novel physical knowledge based multi-source data-driven adaptive method for airfoil flow field prediction," *Journal of Computational Physics*, vol. 528, p. 113846, 2025.

[57] M.-H. Guo, X. Lü, and Y.-X. Jin, "Extraction and reconstruction of variable-coefficient governing equations using Res-KAN integrating sparse regression," *Physica D: Nonlinear Phenomena*, vol. 481, p. 134689, 2025.

[58] Z. Xu and B. Lv, "Enhancing physics-informed neural networks with a hybrid parallel Kolmogorov-Arnold and MLP architecture," *arXiv preprint* arXiv:2503.23289, 2025.

[59] O. Khedr, A. Al-Oufy, A. Saleh, et al., "Physics-informed Kolmogorov-Arnold networks: A superior approach to fluid simulation," *Research Square* (preprint), 2025. doi:10.21203/rs.3.rs-6743344/v1.

[60] G. Lei, D. Exposito, and X. Mao, "Discontinuity-aware KAN-based physics-informed neural networks," *arXiv preprint* arXiv:2507.08338, 2025.

[61] D. Kalesh, T. Merembayev, S. Omirbekov, and Y. Amanbek, "Physics-informed Kolmogorov-Arnold network for two-phase flow model with experimental data," in *ICCSA 2025 Workshops*, LNCS 15888, Springer, 2026.

[62] F. Mostajeran and S. A. Faroughi, "EPi-cKANs: Elasto-plasticity informed Kolmogorov–Arnold networks using Chebyshev polynomials," *arXiv preprint* arXiv:2410.10897, 2024.

[63] F. Mostajeran and S. A. Faroughi, "Scaled-cPIKANs: Domain scaling in Chebyshev-based physics-informed Kolmogorov–Arnold networks," *arXiv preprint* arXiv:2501.02762, 2025.

[64] S. A. Faroughi and F. Mostajeran, "Neural tangent kernel analysis to probe convergence in physics-informed neural solvers: PIKANs vs. PINNs," *arXiv preprint* arXiv:2506.07958, 2025.

[65] N. A. Daryakenari, K. Shukla, and G. E. Karniadakis, "Representation meets optimization: Training PINNs and PIKANs for gray-box discovery in systems pharmacology," *arXiv preprint* arXiv:2504.07379, 2025.

[66] Z. Zhang, Q. Wang, Y. Zhang, et al., "Physics-informed neural networks with hybrid Kolmogorov-Arnold network and augmented Lagrangian function for solving partial differential equations," *Scientific Reports*, vol. 15, p. 10523, 2025.

[67] A. A. Aghaei, "KANtrol: A physics-informed Kolmogorov-Arnold network framework for solving multi-dimensional and fractional optimal control problems," *arXiv preprint* arXiv:2409.06649, 2024.

[68] H. Shuai and F. Li, "Physics-informed Kolmogorov-Arnold networks for power system dynamics," *arXiv preprint* arXiv:2408.06650, 2024.

[69] Y. Wang, J. Sun, J. Bai, C. Anitescu, M. S. Eshaghi, X. Zhuang, T. Rabczuk, and Y. Liu, "Kolmogorov–Arnold-informed neural network: A physics-informed deep learning framework for solving forward and inverse problems based on Kolmogorov–Arnold networks," *Computer Methods in Applied Mechanics and Engineering*, vol. 433, p. 117518, 2025.

[70] A. Kashefi, "Kolmogorov–Arnold PointNet: Deep learning for prediction of fluid fields on irregular geometries," *Computer Methods in Applied Mechanics and Engineering*, vol. 439, p. 117888, 2025. [Online]. Available: https://github.com/Ali-Stanford/KAN_PointNet_CFD

[71] J. Zhang, Y. Fan, K. Cai, and K. Wang, "Kolmogorov-Arnold Fourier networks," *arXiv preprint* arXiv:2502.06018, 2025. [Online]. Available: https://github.com/kolmogorovArnoldFourierNetwork/KAF

[72] Y.-S. Yang, L. Guo, and X. Ren, "Multi-Resolution Training-Enhanced Kolmogorov–Arnold Networks for Multi-Scale PDE Problems," *arXiv preprint* arXiv:2507.19888, 2025.

[73] X. Xiong, K. Lu, Z. Zhang, Z. Zeng, S. Zhou, Z. Deng, and R. Hu, "J-PIKAN: A physics-informed KAN network based on Jacobi orthogonal polynomials for solving fluid dynamics," *Communications in Nonlinear Science and Numerical Simulation*, vol. 152, p. 109414, 2026.

[74] Z. Zhang, X. Xiong, S. Zhang, W. Wang, Y. Zhong, C. Yang, and X. Yang, "Legend-KINN: A Legendre polynomial-based Kolmogorov–Arnold-informed neural network for efficient PDE solving," *Expert Systems with Applications*, vol. 298, p. 129839, 2026. [Online]. Available: https://github.com/zhang-zhuo001/Legend-KINN

[75] mintisan, "awesome-kan," GitHub repository, 2024. [Online]. Available: https://github.com/mintisan/awesome-kan

[76] D. Hilbert, "Mathematical problems," *Bull. Amer. Math. Soc.*, vol. 8, pp. 437–479, 1902.

[77] A. N. Kolmogorov, "On the representation of continuous functions of several variables as superpositions of continuous functions of a smaller number of variables," *Dokl. Akad. Nauk SSSR*, vol. 108, no. 2, pp. 179–182, 1956. (In Russian.)

[78] V. I. Arnol'd, "On functions of three variables," *Dokl. Akad. Nauk SSSR*, vol. 114, pp. 679–681, 1957. (In Russian.)

[79] A. N. Kolmogorov, "On the representation of continuous functions of many variables by superposition of continuous functions of one variable and addition," *Doklady Akademii Nauk*, vol. 114, pp. 953–956, 1957.

[80] J.-P. Kahane, "Sur le théorème de superposition de Kolmogorov," *J. Approx. Theory*, vol. 13, no. 3, pp. 229–234, 1975.

[81] T. Hedberg, "The Kolmogorov Superposition Theorem," in *Topics in Approximation Theory*, Lecture Notes in Mathematics, vol. 187, Springer, 1971, Appendix II.

[82] G. G. Lorentz, "Metric entropy, width, and superpositions of functions," *Amer. Math. Monthly*, vol. 69, pp. 469–485, 1962.

[83] D. A. Sprecher, "On the structure of representations of continuous functions of several variables," *Trans. Amer. Math. Soc.*, vol. 115, pp. 340–355, 1965.

[84] V. I. Arnol'd, "The representation of functions of several variables," *Mat. Prosvesch.*, vol. 3, pp. 41–61, 1958. (In Russian.)

[85] Y. Sternfeld, "Superpositions of continuous functions," *J. Approx. Theory*, vol. 25, pp. 360–368, 1979.

[86] A. G. Vitushkin, "On Hilbert's thirteenth problem," *Dokl. Akad. Nauk SSSR*, vol. 95, pp. 701–704, 1954.

[87] A. G. Vitushkin, "On representation of functions by means of superpositions and related topics," *L'Enseignement Mathématique*, 1977.

[88] G. M. Henkin, "Linear superpositions of continuously differentiable functions," *Dokl. Akad. Nauk SSSR*, vol. 157, pp. 288–290, 1964. (In Russian.)

[89] F. Girosi and T. Poggio, "Representation properties of networks: Kolmogorov's theorem is irrelevant," *Neural Comput.*, vol. 1, pp. 465–469, 1989.

[90] V. Kůrková, "Kolmogorov's theorem is relevant," *Neural Comput.*, vol. 3, pp. 617–622, 1991.

[91] V. Kůrková, "Kolmogorov's theorem and multilayer neural networks," *Neural Networks*, vol. 5, no. 3, pp. 501–506, 1992.

[92] B. L. Fridman, "Improvement in the smoothness of functions in the Kolmogorov superposition theorem," *Dokl. Akad. Nauk SSSR*, vol. 177, pp. 1019–1022, 1967. English transl.: *Soviet Math. Dokl.*, vol. 8, pp. 1550–1553, 1967.

[93] D. A. Sprecher, "An improvement in the superposition theorem of Kolmogorov," *J. Math. Anal. Appl.*, vol. 38, no. 1, pp. 208–213, 1972.

[94] J. Actor, *Computation for the Kolmogorov Superposition Theorem*, PhD Dissertation, 2018.

[95] J. Actor and M. G. Knepley, "An algorithm for computing Lipschitz inner functions in Kolmogorov's superposition theorem," *arXiv preprint* arXiv:1712.08286, 2017.

[96] D. A. Sprecher, "A numerical implementation of Kolmogorov's superpositions," *Neural Networks*, vol. 9, pp. 765–772, 1996.

[97] D. A. Sprecher, "A numerical implementation of Kolmogorov's superpositions II," *Neural Networks*, vol. 10, no. 3, pp. 447–457, 1997.

[98] M. Köppen, "On the training of a Kolmogorov network," in *Lecture Notes in Computer Science*, vol. 2415, ICANN 2002, pp. 474–479.

[99] J. Braun and M. Griebel, "On a constructive proof of Kolmogorov's superposition theorem," *Constr. Approx.*, vol. 30, pp. 653–675, 2009. doi: 10.1007/s00365-009-9054-2

[100] J. Braun, *An Application of Kolmogorov's Superposition Theorem to Function Reconstruction in Higher Dimensions*, PhD Dissertation, University of Bonn, 2009.

[101] M. Nakamura, R. Mines, and V. Kreinovich, "Guaranteed intervals for Kolmogorov's theorem (and their possible relation to neural networks)," *Interval Comput.*, vol. 3, pp. 183–199, 1993.

[102] M. Nees, "Approximative versions of Kolmogorov's superposition theorem, proved constructively," *J. Comput. Appl. Math.*, vol. 54, no. 2, pp. 239–250, 1994.

[103] M. Nees, "Chebyshev approximation by discrete superposition: Application to neural networks," *Adv. Comput. Math.*, vol. 5, no. 1, pp. 137–151, 1996.

[104] R. D. Figueiredo, "Implications and applications of Kolmogorov's superposition theorem," *IEEE Trans. Autom. Control*, vol. 25, pp. 1227–1231, 1980.

[105] R. Hecht-Nielsen, "Kolmogorov's mapping neural network existence theorem," in *Proc. IEEE Int. Conf. Neural Networks*, 1987, pp. 11–13.

[106] B. Igelnik and N. Parikh, "Kolmogorov's spline network," *IEEE Trans. Neural Netw.*, vol. 14, no. 4, pp. 725–733, 2003.

[107] M. Coppejans, "On Kolmogorov's representation of functions of several variables by functions of one variable," *J. Econometrics*, vol. 123, pp. 1–31, 2004.

[108] D. Fakhoury, E. Fakhoury, and H. Speleers, "ExSpliNet: An interpretable and expressive spline-based neural network," *Neural Networks*, vol. 152, pp. 332–346, 2022.

[109] H. van Deventer, P. J. van Rensburg, and A. Bosman, "KASAM: Spline additive models for function approximation," *arXiv preprint*, arXiv:2205.06376, 2022.

[110] A. Polar and M. Poluektov, "A deep machine learning algorithm for construction of the Kolmogorov–Arnold representation," *Eng. Appl. Artif. Intell.*, vol. 99, 104137, 2021.

[111] H. L. Frisch, C. Borzi, G. Ord, J. K. Percus, and G. O. Williams, "Approximate representation of functions of several variables in terms of functions of one variable," *Phys. Rev. Lett.*, vol. 63, no. 9, pp. 927–929, 1989.

[112] D. A. Sprecher, "A universal mapping for Kolmogorov superposition theorem," *Neural Networks*, vol. 6, pp. 1089–1094, 1993.

[113] Z. Liu, P. Ma, Y. Wang, W. Matusik, and M. Tegmark, "KAN 2.0: Kolmogorov-Arnold networks meet science," *arXiv preprint* arXiv:2408.10205, 2024. [Online]. Available: https://github.com/KindXiaoming/pykan

[114] S. S. Bhattacharjee, "TorchKAN: Simplified KAN Model with Variations," 2024. [Online]. Available: https://github.com/1ssb/torchkan/

[115] S. Sidharth, "Deep-KAN," GitHub repository, 2024–2025. [Online]. Available: https://github.com/sidhu2690/Deep-KAN

[116] S. Sidharth, "RBF-KAN," GitHub repository, 2024–2025. [Online]. Available: https://github.com/sidhu2690/RBF-KAN

[117] Blealtan, "Efficient-KAN: Efficient Kolmogorov-Arnold networks," GitHub repository, 2024. [Online]. Available: https://github.com/Blealtan/efficient-kan

[118] S. Rigas, M. Papachristou, T. Papadopoulos, F. Anagnostopoulos, and G. Alexandridis, "Adaptive training of grid-dependent physics-informed Kolmogorov-Arnold networks," *arXiv preprint* arXiv:2407.17611, 2024. [Online]. Available: https://github.com/srigas/jaxKAN

[119] Z. Li, "Kolmogorov-Arnold networks are radial basis function networks," *arXiv preprint* arXiv:2405.06721, 2024. [Online]. Available: https://github.com/ZiyaoLi/fast-kan

[120] A. Delis, "FasterKAN," GitHub repository, 2024. [Online]. Available: https://github.com/AthanasiosDelis/faster-kan

[121] Indoxer, "LKAN," GitHub repository, 2024. Available at: https://github.com/Indoxer/LKAN

[122] A. A. Howard, B. Jacob, S. H. Murphy, A. Heinlein, and P. Stinis, "Finite basis Kolmogorov-Arnold networks: Domain decomposition for data-driven and physics-informed problems," *arXiv preprint* arXiv:2406.19662, 2024. [Online]. Available: https://github.com/pnnl/neuromancer/tree/feature/fbkans/examples/KANs

[123] Q. Qiu, T. Zhu, H. Gong, L. Chen, and H. Ning, "ReLU-KAN: New Kolmogorov-Arnold networks that only need matrix addition, dot multiplication, and ReLU," *arXiv preprint* arXiv:2406.02075, 2024. [Online]. Available: https://github.com/quiqi/relu_kan

[124] C. Coffman and L. Chen, "MatrixKAN: Parallelized Kolmogorov-Arnold network," *arXiv preprint* arXiv:2502.07176, 2025.

[125] GistNoesis, "FourierKAN," GitHub repository, 2024. [Online]. Available: https://github.com/GistNoesis/FourierKAN

[126] GistNoesis, "FusedFourierKAN," GitHub repository, 2024. [Online]. Available: https://github.com/GistNoesis/FusedFourierKAN

[127] A. A. Aghaei, "fKAN: Fractional Kolmogorov-Arnold networks with trainable Jacobi basis functions," *arXiv preprint* arXiv:2406.07456, 2024. [Online]. Available: https://github.com/alirezaafzalaghaei/fKAN

[128] A. A. Aghaei, "rKAN: Rational Kolmogorov-Arnold networks," *arXiv preprint* arXiv:2406.14495, 2024. [Online]. Available: https://github.com/alirezaafzalaghaei/rKAN

[129] M. Wolff, F. Eilers, and X. Jiang, "CVKAN: Complex-valued Kolmogorov-Arnold networks," *arXiv preprint* arXiv:2502.02417, 2025. [Online]. Available: https://github.com/M-Wolff/CVKAN

[130] SynodicMonth, "ChebyKAN," GitHub repository. [Online]. Available: https://github.com/SynodicMonth/ChebyKAN

[131] Boris-73-TA, "OrthogPolyKANs," GitHub repository, 2024. [Online]. Available: https://github.com/Boris-73-TA/OrthogPolyKANs

[132] kolmogorovArnoldFourierNetwork, "kaf_act," GitHub repository, 2024. [Online]. Available: https://github.com/kolmogorovArnoldFourierNetwork/kaf_act

[133] C. C. So and S. P. Yung, "Higher-order ReLU-KANs (HRKANs) for solving physics-informed neural networks (PINNs) more accurately, robustly, and faster," *arXiv preprint* arXiv:2409.14248, 2024.

[134] J. Xu, Z. Chen, J. Li, S. Yang, W. Wang, X. Hu, and E. C. H. Ngai, "FourierKAN-GCF: Fourier Kolmogorov-Arnold network—An effective and efficient feature transformation for graph collaborative filtering," *arXiv preprint* arXiv:2406.01034, 2024. [Online]. Available: https://github.com/Jinfeng-Xu/FKAN-GCF

[135] Zhangyanbo, "MLP-KAN," GitHub repository, 2024. [Online]. Available: https://github.com/Zhangyanbo/MLP-KAN

[136] X. Yang and X. Wang, "Kolmogorov-Arnold transformer," *arXiv preprint* arXiv:2409.10594, 2024. [Online]. Available: https://github.com/Adamdad/kat

[137] Y. Dong, "FAN: Fourier analysis network," GitHub repository, 2024. [Online]. Available: https://github.com/YihongDong/FAN

[138] S. T. Seydi, "Exploring the potential of polynomial basis functions in Kolmogorov-Arnold networks: A comparative study of different groups of polynomials," *arXiv preprint* arXiv:2406.02583, 2024.

[139] Z. Bozorgasl and H. Chen, "Wav-KAN: Wavelet Kolmogorov-Arnold networks," *arXiv preprint* arXiv:2405.12832, 2024. [Online]. Available: https://github.com/zavareh1/Wav-KAN

[140] W. Liu, E. Chatzi, and Z. Lai, "On the rate of convergence of Kolmogorov-Arnold Network regression estimators," *arXiv preprint* arXiv:2509.19830, 2025. [Online]. Available: https://github.com/liouvill/KAN-Converge

[141] J. Giroux and C. Fanelli, "Uncertainty quantification with Bayesian higher order ReLU-KANs," *arXiv preprint* arXiv:2410.01687, 2024. [Online]. Available: *GitHub repository:* https://github.com/wmdataphys/Bayesian-HR-KAN,

[142] B. C. Koenig, S. Kim, and S. Deng, "LeanKAN: A parameter-lean Kolmogorov-Arnold network layer with improved memory efficiency and convergence behavior," *arXiv preprint* arXiv:2502.17844, 2025. [Online]. Available: https://github.com/DENG-MIT/LeanKAN

[143] Y. Zhang, L. Cheng, A. Gnanaskandan, and A. D. Jagtap, "BubbleONet: A Physics-Informed Neural Operator for High-Frequency Bubble Dynamics," *arXiv preprint* arXiv:2508.03965, 2025.

[144] S. Wang, J. H. Seidman, S. Sankaran, H. Wang, G. J. Pappas, and P. Perdikaris, "CViT: Continuous vision transformer for operator learning," *arXiv preprint* arXiv:2405.13998, 2024.

[145] J. D. Toscano, V. Oommen, A. J. Varghese, Z. Zou, N. A. Daryakenari, C. Wu, and G. E. Karniadakis, "From PINNs to PIKANs: Recent advances in physics-informed machine learning," *arXiv preprint* arXiv:2410.13228, 2024.

[146] S. Cuomo, V. S. Di Cola, F. Giampaolo, G. Rozza, M. Raissi, and F. Piccialli, "Scientific machine learning through physics-informed neural networks: Where we are and what's next," *Journal of Scientific Computing*, vol. 92, no. 3, p. 88, 2022.

[147] M. Raissi, A. Yazdani, and G. E. Karniadakis, "Hidden fluid mechanics: A Navier–Stokes informed deep learning framework for assimilating flow visualization data," *arXiv preprint* arXiv:1808.04327, 2018.

[148] W. Cai and Z. Q. J. Xu, "Multi-scale deep neural networks for solving high dimensional PDEs," *arXiv preprint* arXiv:1910.11710, 2019.

[149] L. Lu, P. Jin, and G. E. Karniadakis, "DeepONet: Learning nonlinear operators for identifying differential equations based on the universal approximation theorem of operators," *arXiv preprint* arXiv:1910.03193, 2019.

[150] A. D. Jagtap, K. Kawaguchi, and G. E. Karniadakis, "Locally adaptive activation functions with slope recovery for deep and physics-informed neural networks," *Proceedings of the Royal Society A*, vol. 476, no. 2239, p. 20200334, 2020.

[151] L. Yang, X. Meng, and G. E. Karniadakis, "B-PINNs: Bayesian physics-informed neural networks for forward and inverse PDE problems with noisy data," *Journal of Computational Physics*, vol. 425, p. 109913, 2021.

[152] S. Wang, H. Wang, and P. Perdikaris, "On the eigenvector bias of Fourier feature networks: From regression to solving multi-scale PDEs with physics-informed neural networks," *arXiv preprint* arXiv:2012.10047, 2020.

[153] R. Mattey and S. Ghosh, "A novel sequential method to train physics-informed neural networks for Allen–Cahn and Cahn–Hilliard equations," *Computer Methods in Applied Mechanics and Engineering*, vol. 390, p. 114474, 2022.

[154] J. Cho, S. Nam, H. Yang, S.-B. Yun, Y. Hong, and E. Park, "Separable physics-informed neural networks," *arXiv preprint* arXiv:2306.15969, 2023.

[155] Q. Zhang, C. Wu, A. Kahana, Y. Kim, Y. Li, G. E. Karniadakis, and P. Panda, "Artificial to spiking neural networks conversion for scientific machine learning," *arXiv preprint* arXiv:2308.16372, 2023.

[156] S. J. Anagnostopoulos, J. D. Toscano, N. Stergiopulos, and G. E. Karniadakis, "Residual-based attention and connection to information bottleneck theory in PINNs," *arXiv preprint* arXiv:2307.00379, 2023.

[157] A. A. Howard, S. H. Murphy, S. E. Ahmed, and P. Stinis, "Stacked networks improve physics-informed training: Applications to neural networks and deep operator networks," *arXiv preprint* arXiv:2311.06483, 2023.

[158] J. Hou, Y. Li, and S. Ying, "Enhancing PINNs for solving PDEs via adaptive collocation point movement and adaptive loss weighting," *Nonlinear Dynamics*, vol. 111, no. 16, pp. 15233–15261, 2023.

[159] D. Bar-Natan, "Dessert: Hilbert's 13th problem, in full colour," [Online].

[160] H. Guo, L. Zheng, S. Lin, M. Dong, X. Cao, and H. Zheng, "A novel and robust Fourier-based Kolmogorov–Arnold Network in early warning of rockbursts from microseismic data," *Stochastic Environmental Research and Risk Assessment*, 2025.

[161] M. M. Hassan, "Bayesian Kolmogorov–Arnold Networks: Uncertainty-aware interpretable modeling through probabilistic spline decomposition," *Physica A: Statistical Mechanics and its Applications*, vol. 680, p. 131041, 2025.

[162] M.-J. Lai and Z. Shen, "The Kolmogorov superposition theorem can break the curse of dimensionality when approximating high dimensional functions," *arXiv preprint* arXiv:2112.09963, 2021.

[163] P.-E. Leni, Y. D. Fougerolle, and F. Truchetet, "The Kolmogorov spline network for image processing," in *Image Processing: Concepts, Methodologies, Tools, and Applications*, pp. 54–78, IGI Global, 2013.

[164] N. Schoots and M. J. Villani, "Relating piecewise linear Kolmogorov-Arnold networks to ReLU networks," *arXiv preprint* arXiv:2503.01702, 2025.

[165] Y. Gao and V. Y. Tan, "On the convergence of (stochastic) gradient descent for Kolmogorov–Arnold networks," *IEEE Transactions on Information Theory*, 2025 (early access).

[166] A. D. Bodner, A. S. Tepsich, J. N. Spolski, and S. Pourteau, "Convolutional Kolmogorov-Arnold Networks," *arXiv preprint* arXiv:2406.13155, 2024.

[167] Y. Sun, U. Sengupta, and M. Juniper, "Physics-informed deep learning for simultaneous surrogate modeling and PDE-constrained optimization of an airfoil geometry," *Computer Methods in Applied Mechanics and Engineering*, vol. 411, p. 116042, 2023.

[168] R. T. Q. Chen, Y. Rubanova, J. Bettencourt, and D. Duvenaud, "Neural Ordinary Differential Equations," *arXiv preprint* arXiv:1806.07366, 2019.

[169] M. Eghbalian, M. Pouragha, and R. Wan, "A physics-informed deep neural network for surrogate modeling in classical elasto-plasticity," *Computers and Geotechnics*, vol. 159, p. 105472, 2023.

[170] S. Song, T. Mukerji, and D. Zhang, "Physics-informed multigrid neural operator: Theory and an application to porous flow simulation," *Journal of Computational Physics*, vol. 520, p. 113438, 2025.

[171] R. C. Yu, S. Wu, and J. Gui, "Residual Kolmogorov-Arnold network for enhanced deep learning," *arXiv preprint* arXiv:2410.05500, 2024. GitHub: https://github.com/withray/residualKAN

[172] SekiroRong, "KAN-AutoEncoder," GitHub repository, 2024. Available at: https://github.com/SekiroRong/KAN-AutoEncoder

[173] C. Li, X. Liu, W. Li, C. Wang, H. Liu, and Y. Yuan, "U-KAN makes strong backbone for medical image segmentation and generation," *arXiv preprint* arXiv:2406.02918, 2024.

[174] S. T. Seydi, "Unveiling the power of wavelets: A wavelet-based Kolmogorov-Arnold network for hyperspectral image classification," *arXiv preprint* arXiv:2406.07869, 2024.

[175] M. Cheon, "Kolmogorov-Arnold Network for satellite image classification in remote sensing," *arXiv preprint* arXiv:2406.00600, 2024.

[176] Y. Chen, Z. Zhu, S. Zhu, L. Qiu, B. Zou, F. Jia, Y. Zhu, C. Zhang, Z. Fang, F. Qin, *et al.*, "SCKansformer: Fine-grained classification of bone marrow cells via Kansformer backbone and hierarchical attention mechanisms," *arXiv preprint* arXiv:2406.09931, 2024.

[177] Q. Zhou, C. Pei, F. Sun, J. Han, Z. Gao, D. Pei, H. Zhang, G. Xie, and J. Li, "KAN-AD: Time series anomaly detection with Kolmogorov-Arnold Networks," *arXiv preprint* arXiv:2411.00278, 2024.

[178] C. J. Vaca-Rubio, L. Blanco, R. Pereira, and M. Caus, "Kolmogorov-Arnold Networks (KANs) for time series analysis," *arXiv preprint* arXiv:2405.08790, 2024.

[179] K. Xu, L. Chen, and S. Wang, "Kolmogorov-Arnold Networks for time series: Bridging predictive power and interpretability," *arXiv preprint* arXiv:2406.02496, 2024.

[180] R. Genet and H. Inzirillo, "TKAN: Temporal Kolmogorov-Arnold Networks," *arXiv preprint* arXiv:2405.07344, 2024.

[181] R. Genet and H. Inzirillo, "A temporal Kolmogorov-Arnold transformer for time series forecasting," *arXiv preprint* arXiv:2406.02486, 2024.

[182] W. Hua, "GraphKAN: Graph Kolmogorov–Arnold Networks," GitHub repository, 2024. Available at: https://github.com/WillHua127/GraphKAN-Graph-Kolmogorov-Arnold-Networks

[183] Y. Liu, "KAN4Graph," GitHub repository, 2023. Available at: https://github.com/yueliu1999/KAN4Graph

[184] M. Kiamari, M. Kiamari, and B. Krishnamachari, "GKAN: Graph Kolmogorov-Arnold Networks," *arXiv preprint* arXiv:2406.06470, 2024.

[185] B. Azam and N. Akhtar, "Suitability of Kolmogorov-Arnold Networks for computer vision: A preliminary investigation," *arXiv preprint* arXiv:2406.09087, 2024.

[186] M. Cheon, "Demonstrating the efficacy of Kolmogorov-Arnold Networks in vision tasks," *arXiv preprint* arXiv:2406.14916, 2024.

[187] D. Basina, J. R. Vishal, A. Choudhary, and B. Chakravarthi, "KAT to KANs: A review of Kolmogorov-Arnold networks and the neural leap forward," *arXiv preprint* arXiv:2411.10622, 2024.

[188] S. Lin, M. Dong, H. Guo, L. Zheng, K. Zhao, and H. Zheng, "Early warning system for risk assessment in geotechnical engineering using Kolmogorov-Arnold networks," *Journal of Rock Mechanics and Geotechnical Engineering*, 2025 (in press).

[189] A. A. Howard, B. Jacob, and P. Stinis, "Multifidelity Kolmogorov-Arnold networks," *Machine Learning: Science and Technology*, 6(3):035038, 2025.

[190] B. Jacob, A. A. Howard, and P. Stinis, "SPIKANs: Separable physics-informed Kolmogorov-Arnold networks," *arXiv preprint* arXiv:2411.06286, 2024. Available at: https://github.com/pnnl/spikans

[191] S. Patra, S. Panda, B. K. Parida, M. Arya, K. Jacobs, D. I. Bondar, and A. Sen, "Physics-informed Kolmogorov-Arnold neural networks for dynamical analysis via Efficient-KAN and Wav-KAN," *arXiv preprint* arXiv:2407.18373, 2024.

[192] N. Ranasinghe, Y. Xia, S. Seneviratne, and S. Halgamuge, "GINN-KAN: Interpretability pipelining with applications in physics-informed neural networks," *arXiv preprint* arXiv:2408.14780, 2024.

[193] M. Raffel and L. Chen, "FlashKAT: Understanding and addressing performance bottlenecks in the Kolmogorov-Arnold transformer," *arXiv preprint* arXiv:2505.13813, 2025.

[194] Y. Wang, C. Zhu, S. Zhang, C. Xiang, Z. Gao, G. Zhu, ... and X. Shen, "Accurately models the relationship between physical response and structure using Kolmogorov–Arnold network," *Advanced Science*, vol. 12, no. 12, p. 2413805, 2025.

[195] Y. Shen, J. Du, Y. He, Y. Wang, T. Hao, X. Niu, and Q. Jiang, "AAKAN-WGAN: Predicting mechanical properties of magnesium alloys based on generative design and adaptive activation of Kolmogorov-Arnold networks," *Materials Today Communications*, vol. 47, p. 113198, 2025.

[196] SS, Sidharth, Keerthana AR, and Anas KP "Chebyshev polynomial-based Kolmogorov-Arnold networks: An efficient architecture for nonlinear function approximation," *arXiv preprint* arXiv:2405.07200, 2024.

[197] C. Guo, L. Sun, S. Li, and Z. Yuan, C. Wang, "Physics-informed Kolmogorov-Arnold network with Chebyshev polynomials for fluid mechanics," *arXiv preprint* arXiv:2411.04516, 2024.

[198] R. Schaback, "Error estimates and condition numbers for radial basis function interpolation," *Advances in Computational Mathematics*, vol. 3, no. 3, pp. 251–264, 1995.

[199] R. Schaback, "Small errors imply large evaluation instabilities," *Advances in Computational Mathematics*, vol. 49, no. 2, p. 25, 2023.

[200] A. Noorizadegan, C.-S. Chen, D. L. Young, and C. S. Chen, "Effective condition number for the selection of the RBF shape parameter with the fictitious point method," *Applied Numerical Mathematics*, vol. 178, pp. 280–295, 2022.

[201] C.-S. Chen, A. Noorizadegan, D. L. Young, and C. S. Chen, "On the selection of a better radial basis function and its shape parameter in interpolation problems," *Applied Mathematics and Computation*, vol. 442, p. 127713, 2023.

[202] E. Larsson and R. Schaback, "Scaling of radial basis functions," *IMA Journal of Numerical Analysis*, vol. 44, no. 2, pp. 1130–1152, 2024.

[203] A. Noorizadegan and R. Schaback, "Introducing the evaluation condition number: A novel assessment of conditioning in radial basis function methods," *Engineering Analysis with Boundary Elements*, vol. 166, p. 105827, 2024.

[204] R. Cavoretto, A. De Rossi, M. S. Mukhametzhanov, and Y. D. Sergeyev, "On the search of the shape parameter in radial basis functions using univariate global optimization methods," *Journal of Global Optimization*, vol. 79, no. 2, pp. 305–327, 2021.

[205] G. E. Fasshauer and J. G. Zhang, "On choosing 'optimal' shape parameters for RBF approximation," *Numerical Algorithms*, vol. 45, no. 1, pp. 345–368, 2007.

[206] Y. Gong, Y. He, Y. Mei, X. Zhuang, F. Qin, and T. Rabczuk, "Physics-Informed Kolmogorov–Arnold Networks for multi-material elasticity problems in electronic packaging," *arXiv preprint* arXiv:2508.16999, 2025.

[207] C. Wei, H. Pang, T. Huang, Z. Quan, and Z. Qian, "Predicting lithium-ion battery health using attention mechanism with Kolmogorov–Arnold and physics-informed neural networks," *Expert Systems with Applications*, vol. 296, p. 128969, 2026.

[208] A. Grossmann and J. Morlet, "Decomposition of Hardy functions into square integrable wavelets of constant shape," *SIAM Journal on Mathematical Analysis*, vol. 15, no. 4, pp. 723–736, 1984.

[209] A. Calderón, "Intermediate spaces and interpolation, the complex method," *Studia Mathematica*, vol. 24, no. 2, pp. 113–190, 1964.

[210] P. Pratyush, C. Carrier, S. Pokharel, H. D. Ismail, M. Chaudhari, and D. B. KC, "CaLMPhosKAN: Prediction of general phosphorylation sites in proteins via fusion of codon aware embeddings with amino acid aware embeddings and wavelet-based Kolmogorov-Arnold network," *bioRxiv*, 2024.

[211] B. Moseley, A. Markham, and T. Nissen-Meyer, "Finite basis physics-informed neural networks (FBPINNs): A scalable domain decomposition approach for solving differential equations," *Advances in Computational Mathematics*, vol. 49, no. 4, p. 62, 2023.

[212] V. Dolean, A. Heinlein, S. Mishra, and B. Moseley, "Finite basis physics-informed neural networks as a Schwarz domain decomposition method," in *DDM in Science and Engineering XXVII*, pp. 165–172, Springer, 2024.

[213] V. Dolean, A. Heinlein, S. Mishra, and B. Moseley, "Multilevel domain decomposition-based architectures for physics-informed neural networks," *Computer Methods in Applied Mechanics and Engineering*, vol. 429, p. 117116, 2024.

[214] A. Heinlein, A. A. Howard, D. Beecroft, and P. Stinis, "Multifidelity domain decomposition–based physics-informed neural networks for time-dependent problems," *arXiv preprint* arXiv:2401.07888, 2024.

[215] R. Cavoretto, A. De Rossi, and E. Perracchione, "Efficient computation of partition of unity interpolants through a block-based searching technique," *Computers & Mathematics with Applications*, vol. 71, no. 12, pp. 2568–2581, 2016.

[216] G. Garmanjani, R. Cavoretto, and M. Esmaeilbeigi, "A RBF partition of unity collocation method based on finite difference for initial–boundary value problems," *Computers & Mathematics with Applications*, vol. 75, no. 11, pp. 4066–4090, 2018.

[217] R. Cavoretto, S. De Marchi, A. De Rossi, E. Perracchione, and G. Santin, "Partition of unity interpolation using stable kernel-based techniques," *Applied Numerical Mathematics*, vol. 116, pp. 95–107, 2017.

[218] S. J. Anagnostopoulos, J. D. Toscano, N. Stergiopulos, and G. E. Karniadakis, "Residual-based attention in physics-informed neural networks," *Computer Methods in Applied Mechanics and Engineering*, vol. 421, p. 116805, 2024.

[219] Z. Wang, M. S. Triantafyllou, Y. Constantinides, and G. E. Karniadakis, "An entropy-viscosity large eddy simulation study of turbulent flow in a flexible pipe," *Journal of Fluid Mechanics*, vol. 859, pp. 691–730, 2019.

[220] J.-L. Guermond, R. Pasquetti, and B. Popov, "Entropy viscosity method for nonlinear conservation law," *Journal of Computational Physics*, vol. 230, no. 11, pp. 4248–4267, 2011.

[221] J. D. Toscano, et al., "AIVT: Inference of turbulent thermal convection from measured 3D velocity data by physics-informed Kolmogorov-Arnold networks," *Science Advances*, vol. 11, p. eads5236, 2025.

[222] O. Zienkiewicz, J. Zhu, and N. Gong, "Effective and practical h–p-version adaptive analysis procedures for the finite element method," *International Journal for Numerical Methods in Engineering*, vol. 28, no. 4, pp. 879–891, 1989.

[223] V. M. Nguyen-Thanh, C. Anitescu, N. Alajlan, T. Rabczuk, and X. Zhuang, "Parametric deep energy approach for elasticity accounting for strain gradient effects," *Computer Methods in Applied Mechanics and Engineering*, vol. 386, p. 114096, 2021.

[224] M. G. Altarabichi, "DropKAN: Regularizing KANs by masking post-activations," *arXiv preprint* arXiv:2407.13044, 2024.

[225] A. Jacot, F. Gabriel, and C. Hongler, "Neural tangent kernel: Convergence and generalization in neural networks," in *Advances in Neural Information Processing Systems (NeurIPS)*, vol. 31, 2018. *Physics*, vol. 449, p. 110768, 2022.

[226] R. A. DeVore, "Nonlinear approximation," *Acta Numerica*, vol. 7, pp. 51–150, 1998.

[227] R. DeVore, B. Hanin, and G. Petrova, "Neural network approximation," *Acta Numerica*, vol. 30, pp. 327–444, 2021.

[228] R. T. Q. Chen, Y. Rubanova, J. Bettencourt, and D. Duvenaud, "Neural ordinary differential equations," *arXiv preprint* arXiv:1806.07366, 2019.

[229] C. Tsitouras, "Runge–Kutta pairs of order 5(4) satisfying only the first column simplifying assumption," *Computers & Mathematics with Applications*, vol. 62, no. 2, pp. 770–775, 2011.

[230] S.-M. Udrescu and M. Tegmark, "AI Feynman: A physics-inspired method for symbolic regression," *Sci. Adv.*, vol. 6, eaay2631, 2020. doi: 10.1126/sciadv.aay2631

[231] M. A. Bühler and G. Guillén-Gosálbez, "KAN-SR: A Kolmogorov-Arnold Network Guided Symbolic Regression Framework," *arXiv preprint* arXiv:2509.10089, 2025.

[232] C. Y. Lee, H. Hasegawa, and S. C. Gao, "Complex-valued neural networks: A comprehensive survey," *IEEE/CAA J. Autom. Sinica*, vol. 9, no. 8, pp. 1406–1426, Aug. 2022. doi: 10.1109/JAS.2022.105743

[233] S. Chen, S. McLaughlin, and B. Mulgrew, "Complex-valued radial basic function network, part I: network architecture and learning algorithms," *Signal Process.*, vol. 35, no. 1, pp. 19–31, 1994.

[234] R. Che, L. af Klinteberg, and M. Aryapoor, "Improved Complex-Valued Kolmogorov–Arnold Networks with Theoretical Support," in *Proc. 24th EPIA Conf. on Artificial Intelligence (EPIA)*, Faro, Portugal, Oct. 2025, Part I, pp. 439–451. Springer, Heidelberg. doi: 10.1007/978-3-032-05176-9_34

[235] Z. Chen, Z. Zeng, P. Hu, and Y. Zhu, "Weak Collocation Networks: A deep learning approach to reconstruct stochastic dynamics from aggregate data," *Commun. Nonlinear Sci. Numer. Simul.*, 2025.

[236] Y. Gong, G. Shi, J. Zhu, S. Tang, H. Liu, S. Hu, and S. Chen, "Sparse sensor measurement for indoor physical field reconstruction with physics-inspired K-means and Kolmogorov-Arnold networks," *J. Build. Eng.*, vol. 113, p. 114115, 2025.

[237] J. Lee, Z. Liu, X. Yu, Y. Wang, H. Jeong, M. Y. Niu, and Z. Zhang, "KANO: Kolmogorov-Arnold Neural Operator," *arXiv preprint* arXiv:2509.16825, 2025.

[238] Z. Li, N. Kovachki, K. Azizzadenesheli, B. Liu, K. Bhattacharya, A. Stuart, and A. Anandkumar, "Fourier neural operator for parametric partial differential equations," *arXiv preprint* arXiv:2010.08895, 2020.

[239] A. Sen, I. V. Lukin, K. Jacobs, L. Kaplan, A. G. Sotnikov, and D. I. Bondar, "Physics-informed time series analysis with Kolmogorov-Arnold Networks under Ehrenfest constraints," *arXiv preprint* arXiv:2509.18483, 2025.

[240] P. Ehrenfest, "Bemerkung über die angenäherte Gültigkeit der klassischen Mechanik innerhalb der Quantenmechanik," *Z. Phys.*, vol. 45, pp. 455–457, 1927.

[241] F. Wang, L. Chen, and J. Ding, "Symplectic physics-embedded learning via Lie groups Hamiltonian formulation for serial manipulator dynamics prediction," *Sci. Rep.*, vol. 15, p. 33179, 2025. doi: 10.1038/s41598-025-17935-w

[242] T. P. Duong, A. Altawaitan, J. Stanley, and N. Atanasov, "Port-Hamiltonian neural ODE networks on Lie groups for robot dynamics learning and control," *IEEE Trans. Rob.*, vol. 40, pp. 3695–3715, 2024.

[243] Q. Zou and H. Yan, "Probabilistic Kolmogorov-Arnold Networks via sparsified deep Gaussian processes with additive kernels," in *Proc. IEEE 21st Int. Conf. Automation Science and Engineering (CASE)*, Los Angeles, USA, Aug. 2025, pp. 2889–2894. IEEE.

[244] G. Guo, Z. Tang, Z. Cui, C. Li, H. Wang, and H. You, "Accurate analytic equation generation for compact modeling with physics-assisted Kolmogorov-Arnold networks," *ACM Trans. Des. Autom. Electron. Syst.*, Sept. 2025. doi: 10.1145/3765904

[245] A. Jacot, F. Gabriel, and C. Hongler, "Neural tangent kernel: Convergence and generalization in neural networks," *Adv. Neural Inf. Process. Syst.*, vol. 31, 2018.

[246] J. Lee, L. Xiao, S. S. Schoenholz, Y. Bahri, R. Novak, J. Sohl–Dickstein, and J. Pennington, "Wide neural networks of any depth evolve as linear models under gradient descent," *Adv. Neural Inf. Process. Syst.*, vol. 32, 2019.

[247] N. Rahaman, A. Baratin, D. Arpit, F. Draxler, M. Lin, F. Hamprecht, Y. Bengio, and A. Courville, "On the spectral bias of neural networks," in *Proc. Int. Conf. Machine Learning (ICML)*, PMLR, vol. 97, pp. 5301–5310, 2019.

[248] Z.–Q. J. Xu, Y. Zhang, T. Luo, Y. Xiao, and Z. Ma, "Frequency principle: Fourier analysis sheds light on deep neural networks," *arXiv:1901.06523*, 2019.

[249] B. Ghorbani, S. Krishnan, and Y. Xiao, "An investigation into neural net optimization via Hessian eigenvalue density," in *Proc. Int. Conf. Machine Learning (ICML)*, PMLR, vol. 97, pp. 2232–2241, 2019.

[250] P. Foret, A. Kleiner, H. Mobahi, and B. Neyshabur, "Sharpness–aware minimization for efficiently improving generalization," in *Proc. Int. Conf. Learning Representations (ICLR)*, 2021.

[251] C. Zhang, S. Bengio, M. Hardt, B. Recht, and O. Vinyals, "Understanding deep learning (still) requires rethinking generalization," *Commun. ACM*, vol. 64, no. 3, pp. 107–115, 2021.

[252] M. Tancik, P. Srinivasan, B. Mildenhall, S. Fridovich–Keil, N. Raghavan, U. Singhal, R. Ramamoorthi, J. Barron, and R. Ng, "Fourier features let networks learn high frequency functions in low dimensional domains," *Adv. Neural Inf. Process. Syst.*, vol. 33, pp. 7537–7547, 2020.

[253] Q. Hong, J. W. Siegel, Q. Tan, and J. Xu, "On the activation function dependence of the spectral bias of neural networks," *arXiv:2208.04924*, 2022.

[254] K. Luo, J. Tang, M. Cai, X. Zeng, M. Xie, and M. Yan, "DAE-KAN: A Kolmogorov–Arnold Network model for high-index differential–algebraic equations," *arXiv:2504.15806*, 2025.

[255] M. Calafà, T. Andriollo, A. P. Engsig-Karup, and C. H. Jeong, "A holomorphic Kolmogorov-Arnold network framework for solving elliptic problems on arbitrary 2D domains," *arXiv preprint* arXiv:2507.22678, 2025. GitHub: https://github.com/teocala/pihnn

[256] S. S. Menon and A. D. Jagtap, "Anant-Net: Breaking the curse of dimensionality with scalable and interpretable neural surrogate for high-dimensional PDEs," *Computer Methods in Applied Mechanics and Engineering*, vol. 447, p. 118403, 2025. GitHub: https://github.com/ParamIntelligence/Anant-Net

[257] A. Kundu, A. Sarkar, and A. Sadhu, "KANQAS: Kolmogorov-Arnold Network for Quantum Architecture Search," *EPJ Quantum Technology*, vol. 11, p. 76, 2024. GitHub: https://github.com/Aqasch/KANQAS_code

[258] A. Polar and M. Poluektov, "Probabilistic Kolmogorov–Arnold Network: An Approach for Stochastic Modelling Using Divisive Data Re-Sorting," *Modelling*, vol. 6, no. 3, p. 88, 2025. GitHub: https://github.com/andrewpolar/pkan

[259] S. Rigas, M. Papachristou, T. Papadopoulos, F. Anagnostopoulos, and G. Alexandridis, "Adaptive Training of Grid-Dependent Physics-Informed Kolmogorov-Arnold Networks," *IEEE Access*, vol. 12, pp. 176982–176998, 2024. GitHub: https://github.com/srigas/jaxKAN

[260] S. Rigas, M. Papachristou, T. Papadopoulos, F. Anagnostopoulos, and G. Alexandridis, "jaxKAN: A unified JAX framework for Kolmogorov-Arnold Networks," *Journal of Open Source Software*, vol. 10, no. 108, p. 7830, 2025. GitHub: https://github.com/srigas/jaxKAN

[261] L. F. Guilhoto and P. Perdikaris, "Deep Learning Alternatives of the Kolmogorov Superposition Theorem," *Proc. ICLR*, 2025.

[262] S. Rigas, F. Anagnostopoulos, M. Papachristou, and G. Alexandridis, "Towards deep physics-informed Kolmogorov-Arnold networks," *arXiv preprint* arXiv:2510.23501, 2025. GitHub: https://github.com/srigas/RGA-KANs

[263] E. Kiyani, K. Shukla, J. F. Urbán, J. Darbon, and G. E. Karniadakis, "Optimizing the optimizer for physics-informed neural networks and Kolmogorov-Arnold networks," *Computer Methods in Applied Mechanics and Engineering*, vol. 446, p. 118308, 2025.

[264] M. Poluektov and A. Polar, "Construction of the Kolmogorov-Arnold networks using the Newton-Kaczmarz method," *Machine Learning*, vol. 114, p. 185, 2025.

[265] M. J. Lai and Z. Shen, "Optimal linear B-spline approximation via Kolmogorov superposition theorem and its applications," *Sampling Theory, Signal Processing, and Data Analysis*, vol. 23, 11, 2025. [Online]. Available: https://doi.org/10.1007/s43670-025-00107-2

[266] M. J. Lai and Z. Shen, "The Kolmogorov superposition theorem can break the curse of dimensionality when approximating high-dimensional functions," *arXiv preprint* arXiv:2112.09963, 2021.

[267] R. Pant, S. Li, X. Li, H. Iqbal, and K. Kumar, "MLPs and KANs for data-driven learning in physical problems: A performance comparison," *arXiv preprint* arXiv:2504.11397, 2025. [Online]. Available: https://github.com/geoelements-dev/mlp-kan

[268] S. Pozdnyakov and P. Schwaller, "Lookup multivariate Kolmogorov-Arnold Networks," *arXiv preprint* arXiv:2509.07103, 2025. [Online]. Available: https://github.com/schwallergroup/lmkan

[269] S. Cui, M. Cao, Y. Liao, and J. Wu, "Physics-informed Kolmogorov–Arnold networks: Investigating architectures and hyperparameter impacts for solving Navier–Stokes equations," *Physics of Fluids*, vol. 37, no. 3, 037159, 2025. [Online]. Available: https://doi.org/10.1063/5.0257677

[270] J. D. Meshir, A. Palafox, and E. A. Guerrero, "On the study of frequency control and spectral bias in wavelet-based Kolmogorov Arnold networks: A path to physics-informed KANs," *arXiv preprint* arXiv:2502.00280, 2025.

[271] A. Kratsios and T. Furuya, "Kolmogorov-Arnold Networks: Approximation and learning guarantees for functions and their derivatives," *arXiv preprint* arXiv:2504.15110, 2025.

[272] R. A. DeVore and V. A. Popov, "Interpolation of approximation spaces," in *Constructive Theory of Functions* (Varna, 1987). Sofia: Publ. House Bulgar. Acad. Sci., 1988, pp. 110–119.

[273] X. Zhang and H. Zhou, "Generalization bounds and model complexity for Kolmogorov–Arnold networks," *arXiv preprint* arXiv:2410.08026, 2024.

[274] P. Li, L. Ding, J. Fu, G. Wang, and Y. Yuan, "Generalization Bounds for Kolmogorov-Arnold Networks (KANs) and Enhanced KANs with Lower Lipschitz Complexity," in *Advances in Neural Information Processing Systems*, NeurIPS 2025.

[275] H. Wendland, *Scattered Data Approximation*. Cambridge, UK: Cambridge University Press, 2004.

[276] S. Rigas, D. Verma, G. Alexandridis, and Y. Wang, "Initialization schemes for Kolmogorov-Arnold networks: An empirical study," *arXiv preprint* arXiv:2509.03417, 2025. [Online]. Available: https://github.com/srigas/KAN_Initialization_Schemes

[277] S. Müller and R. Schaback, "A Newton basis for kernel spaces," *Journal of Approximation Theory*, vol. 161, no. 2, pp. 645–655, 2009.

[278] F. Han and D.-S. Huang, "Improved extreme learning machine for function approximation by encoding a priori information," *Neurocomputing*, vol. 69, no. 16, pp. 2369–2373, 2006.

[279] G. Santin and R. Schaback, "Approximation of eigenfunctions in kernel-based spaces," *Advances in Computational Mathematics*, vol. 42, no. 4, pp. 973–993, 2016.

[280] K. Attouri, M. Mansouri, and A. Kouadri, "Adaptive PolyKAN-based autoencoder for fault detection and classification in wind and solar power systems," *Ain Shams Engineering Journal*, vol. 17, no. 1, 103884, 2026.